

EFFECT OF HYDRAULIC PARAMETERS ON THE FORMATION OF  
VORTICES AT INTAKE STRUCTURES

A THESIS SUBMITTED TO  
THE GRADUATE SCHOOL OF NATURAL AND APPLIED SCIENCES OF  
MIDDLE EAST TECHNICAL UNIVERSITY

BY

ALİ BAYKARA

IN PARTIAL FULFILLMENT OF THE REQUIREMENTS  
FOR  
THE DEGREE OF MASTER OF SCIENCE  
IN  
CIVIL ENGINEERING

JANUARY 2013

Approval of the thesis:

**EFFECT OF HYDRAULIC PARAMETERS ON THE FORMATION OF  
VORTICES AT INTAKE STRUCTURES**

submitted by **ALİ BAYKARA** in partial fulfillment of the requirements for the degree of **Master of Science in Civil Engineering Department, Middle East Technical University** by,

Prof. Dr. Canan ÖZGEN  
Dean, Graduate School of **Natural and Applied Sciences**

\_\_\_\_\_

Prof. Dr. Ahmet Cevdet YALÇINER  
Head of Department, **Civil Engineering**

\_\_\_\_\_

Prof. Dr. Mustafa GÖĞÜŞ  
Supervisor, **Civil Engineering Dept., METU**

\_\_\_\_\_

Assoc. Prof. Dr. Mete KÖKEN  
Co-Supervisor, **Civil Engineering Dept., METU**

\_\_\_\_\_

**Examining Committee Members**

Prof. Dr. İsmail AYDIN  
Civil Engineering Dept., METU

\_\_\_\_\_

Prof. Dr. Mustafa GÖĞÜŞ  
Civil Engineering Dept., METU

\_\_\_\_\_

Prof. Dr. Nevzat YILDIRIM  
Civil Engineering Dept., Gazi University

\_\_\_\_\_

Assoc. Prof. Dr. Burcu ALTAN SAKARYA  
Civil Engineering Dept., METU

\_\_\_\_\_

Assoc. Prof. Dr. Mete KÖKEN  
Civil Engineering Dept., METU

\_\_\_\_\_

**Date:** 17.01.2013

**I hereby declare that all information in this document has been obtained and presented in accordance with academic rules and ethical conduct. I also declare that, as required by these rules and conduct, I have fully cited and referenced all material and results that are not original to this work.**

Name, Surname: Ali BAYKARA

Signature:

## ABSTRACT

### EFFECT OF HYDRAULIC PARAMETERS ON THE FORMATION OF VORTICES AT INTAKE STRUCTURES

Baykara, Ali  
M.Sc., Department of Civil Engineering  
Supervisor: Prof. Dr. Mustafa Gögüş  
Co-Supervisor: Assoc. Prof. Dr. Mete Köken

January 2013, 157 pages

The aim of this experimental study was to investigate the hydraulic conditions at which air-entraining vortices would form in front of horizontal intakes and to determine the ways of eliminating the formation of these vortices by testing anti-vortex devices. For these reasons, a series of experiments were conducted in an experimental setup composed of a reservoir having the dimensions of 3.10 m x 3.10 m x 2.20 m and a pump connected to the intake pipe. Within the reservoir, between the concrete side walls adjustable plexiglass side walls were placed to provide the desired wall clearance for the intake pipes. Six pipes of different diameters; 5 cm, 10 cm, 14.4 cm, 19.4 cm, 25 cm and 30 cm were horizontally mounted on the front side of the reservoir one by one, and for each case, a wide range of discharges was provided from the reservoir by the pump.

Under symmetrical approach flow conditions and zero bottom wall clearance, the experiments were repeated for each intake pipe and the “critical submergence depths” for the tested discharges were determined. At some of the discharges, the effect of horizontal plates located on the top of the pipe entrance as anti-vortex devices on the elimination of the vortices was investigated. The measured critical submergence depths were related in dimensionless form to the relevant dimensionless parameters and empirical equations were derived. These equations were compared with similar ones available in the literature and it was shown that the agreement between them was quite good.

Keywords: Horizontal intakes, Vortex formation, Critical submergence, Anti-vortex plate, Scale effect.

## ÖZ

### HİDROLİK PARAMETRELERİN SU ALMA YAPILARINDA GİRDAPLARIN OLUŞUMUNA ETKİSİ

Baykara, Ali  
Yüksek Lisans, İnşaat Mühendisliği Bölümü  
Tez Yöneticisi: Prof. Dr. Mustafa Göğüş  
Ortak Tez Yöneticisi: Doç. Dr. Mete Köken

Ocak 2013, 157 Sayfa

Bu deneysel çalışmanın amacı, yatay su alma yapılarında sistemin içine hava çeken girdapların oluştuğu hidrolik şartların araştırılması ve bu tip girdapların önlenmesinde kullanılabilecek girdap önleyici düzeneklerin test edilerek belirlenmesidir. Bu sebeplerden dolayı, su alma borusuna bağlı yüksek güçte bir pompa ve 3.10 m x 3.10 m x 2.20 m boyutlarında bir rezervuarı olan deney düzeneğinde seri deneyler yapıldı. Su alma borusunun girişinde farklı değerlerde duvar aralıkları oluşturabilmek için rezervuarın içinde beton duvarlar arasında pleksiglastan yerleri değiştirilebilen hareketli duvarlar yerleştirildi. Altı farklı çapta boru; 5 cm, 10 cm, 14.4 cm, 19.4 cm, 25 cm ve 30 cm, rezervuarın ön yüzünün orta alt kısmına sıra ile yatay olarak monte edildi ve her birisi ile yapılan deneylerde gerekli olan debiler geniş bir aralıkta pompa ile rezervuardan temin edildi.

Simetrik akım şartlarında ve boru alt kotu ile rezervuar taban kotu aynı seviyede tutularak, deneyler her bir boru ile tek tek yapıldı ve gözlenen “kritik batıklık derinlikleri” ölçüldü. Bazı debilerde, su alma borusunun hemen üstüne, girdabı önlemek için yatay plakalar monte edilerek bunların performansları araştırıldı. Ölçülen kritik batıklık derinlikleri boyutsuz yapılarak ilgili boyutsuz parametrelerle ilişkilendirildi ve ampirik denklemler çıkarıldı. Bu denklemler literatürde mevcut olan benzer bağıntılarla karşılaştırıldı ve bunların birbirine uyumlu oldukları tespit edildi.

Anahtar Kelimeler: Yatay su alma yapıları, Girdap oluşumu, Kritik batıklık derinliği, Girdap önleyici plaka, Ölçek etkisi

*To my Parents...*

## ACKNOWLEDGEMENTS

Firstly, I would like to express my deepest gratitude to my supervisor Prof. Dr. Mustafa GÖĞÜŞ and co-supervisor Assoc. Prof. Dr. Mete KÖKEN for their guidance, support, encouragements and trust on me from the first day of this study to the end.

Also, I would like to thank the laboratory technicians for their help and self-sacrifice while I performed experiments.

I would like to thank Ezgi KÖKER, Ali Ersin DİNÇER and Tuğçe YILDIRIM for their support and friendship in the department. In addition, I would like to give my special thanks to Ezgi BERBEROĞLU, Utku ALBOSTAN, Muhammed BULUT, Remzi Başar ATAMAN, Aysim Damla ATALAY and Yunus AVCI for their endless friendship and encouragements for seven years.

I would like to appreciate Burcu SARI for her support for the first year.

Cansu Gece ÖĞÜT gets my thank for her support, encouragement, friendship and her well behavior towards me.

My sincere thanks goes to my beloved family for their endless support during the master study and for my entire life.

This study was supported by TUBITAK (The Scientific and Technological Research Council of Turkey) under Project No: 110M676 which is gratefully acknowledged here.

## TABLE OF CONTENTS

ABSTRACT .....	iv
ÖZ .....	v
ACKNOWLEDGEMENTS .....	vii
TABLE OF CONTENTS .....	viii
LIST OF TABLES .....	ix
LIST OF FIGURES.....	xiii
LIST OF SYMBOLS .....	xv
<b>CHAPTERS</b>	
1. INTRODUCTION .....	1
1.1 Introductory Remarks on the Formation of Vortex at Intake Structures .....	1
1.1.1 The Concept of Critical Submergence .....	1
1.1.2 The Sources of Vorticity .....	1
1.1.3 Problems Due To Vortex Formation.....	2
1.1.4 Directional and Structural Distinctions of Intakes .....	2
1.1.5 Classification of Vortices.....	4
1.1.6 Vortex Prevention .....	5
1.2 Scope of the Study.....	6
2. LITERATURE REVIEW .....	7
3. MODELLING OF AIR-ENTRAINING VORTICES.....	17
3.1 Introductory Remarks .....	17
3.2 Dimensionless Parameters .....	17
3.2.1 Influence of Kolf Number.....	18
3.2.2 Influence of Weber Number .....	18
3.2.3 Influence of Reynolds Number .....	19
3.2.4 Influence of Froude Number.....	19
4. EXPERIMENTAL EQUIPMENT AND PROCEDURE.....	21
4.1 Experimental Equipment .....	21
4.2 Experimental Procedure .....	26
4.3 Observations .....	26
5. DISCUSSION OF THE RESULTS.....	29
5.1 Introduction .....	29
5.2 The Dimensionless Critical Submergence and the Relevant Dimensionless Parameters .....	30
5.3 Empirical Equations for Dimensionless Critical Submergence .....	42
5.3.1 For Extreme Cases.....	42
5.3.1.1 The Relationship of the Maximum $S_c/D_i$ Values Measured.....	43
5.3.1.2 The Relationship of the Maximum $S_c/D_i$ Values Measured.....	43
5.3.2 For Intermediate Values of $S_c/D_i$ .....	44
5.4 Scale Effect on the Value of Dimensionless Critical Submergence .....	49
5.5 Comparison of the Proposed Empirical Equations with the Related Relationships Presented in the Literature .....	54
5.5.1 Gürbüzdal's Study (2009).....	54
5.5.2 Gordon's (1970), Reddy and Pickford's (1972) and Rindels and Gulliver's (1983) Studies .....	55
5.6 Effect of Horizontal Plates on Elimination of Vortices .....	58
6. CONCLUSION AND RECOMMENDATIONS.....	67
REFERENCES.....	68
<b>APPENDICES</b>	
A. EXPERIMENTAL RESULTS RELATED TO CRITICAL SUBMERGENCE .....	71
B. EXPERIMENTAL RESULTS RELATED TO ANTI-VORTEX PLATES .....	95

## LIST OF TABLES

### TABLES

Table 5.1 Summary of the important parameters for which the critical submergence experiments were conducted .....	29
Table 5.2 Summary of the important parameters for which the experiments related to anti-vortex plates were conducted .....	30
Table 5.3 Limit values of $2b/D_i$ above which $S_c/D_i$ is independent of $2b/D_i$ as a function of Fr, Re and $We$ for the intake pipe of diameter of $D_i$ .....	40
Table 5.4 $2b/D_i$ values of the intake pipes of $D_i$ resulted in maximum, minimum and intermediate $S_c/D_i$ .....	41
Table 5.5 Model and prototype data and related scale ratios .....	49
Table 5.6 Evaluation and summary of the data presented in Tables B.1 - B.62.....	59
Table 5.7 Evaluation and summary of the data of Table 5.6 for intermediate $S_c/D_i$ .....	62
Table 5.8 Data related to the selection of the most effective horizontal plate as an anti-vortex device	64
Table A.1 Experimental results related to critical submergence for $D_i = 30$ cm and $2b = 40$ cm .....	72
Table A.2 Experimental results related to critical submergence for $D_i = 30$ cm and $2b = 60$ cm .....	72
Table A.3 Experimental results related to critical submergence for $D_i = 30$ cm and $2b = 80$ cm .....	73
Table A.4 Experimental results related to critical submergence for $D_i = 30$ cm and $2b = 100$ cm .....	73
Table A.5 Experimental results related to critical submergence for $D_i = 30$ cm and $2b = 120$ cm .....	74
Table A.6 Experimental results related to critical submergence for $D_i = 30$ cm and $2b = 140$ cm .....	74
Table A.7 Experimental results related to critical submergence for $D_i = 25$ cm and $2b = 40$ cm .....	75
Table A.8 Experimental results related to critical submergence for $D_i = 25$ cm and $2b = 60$ cm .....	75
Table A.9 Experimental results related to critical submergence for $D_i = 25$ cm and $2b = 80$ cm .....	76
Table A.10 Experimental results related to critical submergence for $D_i = 25$ cm and $2b = 100$ cm .....	77
Table A.11 Experimental results related to critical submergence for $D_i = 25$ cm and $2b = 120$ cm .....	78
Table A.12 Experimental results related to critical submergence for $D_i = 25$ cm and $2b = 140$ cm .....	79
Table A.13 Experimental results related to critical submergence for $D_i = 19.4$ cm and $2b = 40$ cm .....	79
Table A.14 Experimental results related to critical submergence for $D_i = 19.4$ cm and $2b = 60$ cm .....	80
Table A.15 Experimental results related to critical submergence for $D_i = 19.4$ cm and $2b = 80$ cm .....	81
Table A.16 Experimental results related to critical submergence for $D_i = 19.4$ cm and $2b = 100$ cm .....	82
Table A.17 Experimental results related to critical submergence for $D_i = 19.4$ cm and $2b = 120$ cm .....	83
Table A.18 Experimental results related to critical submergence for $D_i = 19.4$ cm and $2b = 140$ cm .....	84
Table A.19 Experimental results related to critical submergence for $D_i = 14.4$ cm and $2b = 40$ cm .....	84
Table A.20 Experimental results related to critical submergence for $D_i = 14.4$ cm and $2b = 60$ cm .....	85
Table A.21 Experimental results related to critical submergence for $D_i = 14.4$ cm and $2b = 80$ cm .....	86
Table A.22 Experimental results related to critical submergence for $D_i = 14.4$ cm and $2b = 100$ cm .....	87
Table A.23 Experimental results related to critical submergence for $D_i = 14.4$ cm and $2b = 120$ cm .....	88
Table A.24 Experimental results related to critical submergence for $D_i = 14.4$ cm and $2b = 140$ cm .....	89
Table A.25 Experimental results related to critical submergence for $D_i = 10$ cm and $2b = 40$ cm .....	89
Table A.26 Experimental results related to critical submergence for $D_i = 10$ cm and $2b = 60$ cm .....	90
Table A.27 Experimental results related to critical submergence for $D_i = 10$ cm and $2b = 80$ cm .....	91
Table A.28 Experimental results related to critical submergence for $D_i = 10$ cm and $2b = 100$ cm .....	92
Table A.29 Experimental results related to critical submergence for $D_i = 10$ cm and $2b = 120$ cm .....	93
Table A.30 Experimental results related to critical submergence for $D_i = 5$ cm and $2b = 40$ cm .....	93
Table A.31 Experimental results related to critical submergence for $D_i = 5$ cm and $2b = 60$ cm .....	94
Table A.32 Experimental results related to critical submergence for $D_i = 5$ cm and $2b = 80$ cm .....	94

Table B.1 Experimental results related to the anti – vortex plate for $D_i = 25.0$ cm, $Q_i = 62.55$ lt/s and $2b = 60$ cm.....	96
Table B.2 Experimental results related to the anti – vortex plate for $D_i = 25.0$ cm, $Q_i = 45.46$ lt/s and $2b = 60$ cm.....	97
Table B.3 Experimental results related to the anti – vortex plate for $D_i = 25.0$ cm, $Q_i = 30.32$ lt/s and $2b = 60$ cm.....	98
Table B.4 Experimental results related to the anti – vortex plate for $D_i = 25.0$ cm, $Q_i = 62.55$ lt/s and $2b = 80$ cm.....	99
Table B.5 Experimental results related to the anti – vortex plate for $D_i = 25.0$ cm, $Q_i = 50.75$ lt/s and $2b = 80$ cm.....	100
Table B.6 Experimental results related to the anti – vortex plate for $D_i = 25.0$ cm, $Q_i = 27.45$ lt/s and $2b = 80$ cm.....	101
Table B.7 Experimental results related to the anti – vortex plate for $D_i = 25.0$ cm, $Q_i = 62.55$ lt/s and $2b = 100$ cm.....	102
Table B.8 Experimental results related to the anti – vortex plate for $D_i = 25.0$ cm, $Q_i = 48.08$ lt/s and $2b = 100$ cm.....	103
Table B.9 Experimental results related to the anti – vortex plate for $D_i = 25.0$ cm, $Q_i = 36.40$ lt/s and $2b = 100$ cm.....	104
Table B.10 Experimental results related to the anti – vortex plate for $D_i = 25.0$ cm, $Q_i = 62.55$ lt/s and $2b = 120$ cm.....	105
Table B.11 Experimental results related to the anti – vortex plate for $D_i = 25.0$ cm, $Q_i = 48.08$ lt/s and $2b = 120$ cm.....	106
Table B.12 Experimental results related to the anti – vortex plate for $D_i = 25.0$ cm, $Q_i = 36.40$ lt/s and $2b = 120$ cm.....	107
Table B.13 Experimental results related to the anti – vortex plate for $D_i = 25.0$ cm, $Q_i = 62.55$ lt/s and $2b = 140$ cm.....	108
Table B.14 Experimental results related to the anti – vortex plate for $D_i = 25.0$ cm, $Q_i = 48.08$ lt/s and $2b = 140$ cm.....	109
Table B.15 Experimental results related to the anti – vortex plate for $D_i = 25.0$ cm, $Q_i = 36.40$ lt/s and $2b = 140$ cm.....	110
Table B.16 Experimental results related to the anti – vortex plate for $D_i = 19.4$ cm, $Q_i = 62.55$ lt/s and $2b = 40$ cm.....	111
Table B.17 Experimental results related to the anti – vortex plate for $D_i = 19.4$ cm, $Q_i = 48.08$ lt/s and $2b = 40$ cm.....	112
Table B.18 Experimental results related to the anti – vortex plate for $D_i = 19.4$ cm, $Q_i = 62.55$ lt/s and $2b = 60$ cm.....	113
Table B.19 Experimental results related to the anti – vortex plate for $D_i = 19.4$ cm, $Q_i = 48.08$ lt/s and $2b = 60$ cm.....	114
Table B.20 Experimental results related to the anti – vortex plate for $D_i = 19.4$ cm, $Q_i = 33.69$ lt/s and $2b = 60$ cm.....	115
Table B.21 Experimental results related to the anti – vortex plate for $D_i = 19.4$ cm, $Q_i = 62.55$ lt/s and $2b = 80$ cm.....	116
Table B.22 Experimental results related to the anti – vortex plate for $D_i = 19.4$ cm, $Q_i = 48.08$ lt/s and $2b = 80$ cm.....	117
Table B.23 Experimental results related to the anti – vortex plate for $D_i = 19.4$ cm, $Q_i = 30.32$ lt/s and $2b = 80$ cm.....	118
Table B.24 Experimental results related to the anti – vortex plate for $D_i = 19.4$ cm, $Q_i = 62.55$ lt/s and $2b = 100$ cm.....	119
Table B.25 Experimental results related to the anti – vortex plate for $D_i = 19.4$ cm, $Q_i = 48.08$ lt/s and $2b = 100$ cm.....	120
Table B.26 Experimental results related to the anti – vortex plate for $D_i = 19.4$ cm, $Q_i = 33.69$ lt/s and $2b = 100$ cm.....	121
Table B.27 Experimental results related to the anti – vortex plate for $D_i = 19.4$ cm, $Q_i = 62.55$ lt/s and $2b = 120$ cm.....	122

Table B.28	Experimental results related to the anti – vortex plate for $D_i = 19.4$ cm, $Q_i = 48.08$ lt/s and $2b = 120$ cm.....	123
Table B.29	Experimental results related to the anti – vortex plate for $D_i = 19.4$ cm, $Q_i = 33.69$ lt/s and $2b = 120$ cm.....	124
Table B.30	Experimental results related to the anti – vortex plate for $D_i = 19.4$ cm, $Q_i = 62.55$ lt/s and $2b = 140$ cm.....	125
Table B.31	Experimental results related to the anti – vortex plate for $D_i = 19.4$ cm, $Q_i = 48.08$ lt/s and $2b = 140$ cm.....	126
Table B.32	Experimental results related to the anti – vortex plate for $D_i = 19.4$ cm, $Q_i = 36.40$ lt/s and $2b = 140$ cm.....	127
Table B.33	Experimental results related to the anti – vortex plate for $D_i = 14.4$ cm, $Q_i = 62.55$ lt/s and $2b = 40$ cm.....	128
Table B.34	Experimental results related to the anti – vortex plate for $D_i = 14.4$ cm, $Q_i = 62.55$ lt/s and $2b = 60$ cm.....	129
Table B.35	Experimental results related to the anti – vortex plate for $D_i = 14.4$ cm, $Q_i = 48.08$ lt/s and $2b = 60$ cm.....	130
Table B.36	Experimental results related to the anti – vortex plate for $D_i = 14.4$ cm, $Q_i = 33.69$ lt/s and $2b = 60$ cm.....	131
Table B.37	Experimental results related to the anti – vortex plate for $D_i = 14.4$ cm, $Q_i = 62.55$ lt/s and $2b = 80$ cm.....	132
Table B.38	Experimental results related to the anti – vortex plate for $D_i = 14.4$ cm, $Q_i = 48.08$ lt/s and $2b = 80$ cm.....	133
Table B.39	Experimental results related to the anti – vortex plate for $D_i = 14.4$ cm, $Q_i = 33.69$ lt/s and $2b = 80$ cm.....	134
Table B.40	Experimental results related to the anti – vortex plate for $D_i = 14.4$ cm, $Q_i = 62.55$ lt/s and $2b = 100$ cm.....	135
Table B.41	Experimental results related to the anti – vortex plate for $D_i = 14.4$ cm, $Q_i = 48.08$ lt/s and $2b = 100$ cm.....	136
Table B.42	Experimental results related to the anti – vortex plate for $D_i = 14.4$ cm, $Q_i = 30.32$ lt/s and $2b = 100$ cm.....	137
Table B.43	Experimental results related to the anti – vortex plate for $D_i = 14.4$ cm, $Q_i = 62.55$ lt/s and $2b = 120$ cm.....	138
Table B.44	Experimental results related to the anti – vortex plate for $D_i = 14.4$ cm, $Q_i = 48.08$ lt/s and $2b = 120$ cm.....	139
Table B.45	Experimental results related to the anti – vortex plate for $D_i = 14.4$ cm, $Q_i = 30.32$ lt/s and $2b = 120$ cm.....	140
Table B.46	Experimental results related to the anti – vortex plate for $D_i = 14.4$ cm, $Q_i = 62.55$ lt/s and $2b = 140$ cm.....	141
Table B.47	Experimental results related to the anti – vortex plate for $D_i = 14.4$ cm, $Q_i = 48.08$ lt/s and $2b = 140$ cm.....	142
Table B.48	Experimental results related to the anti – vortex plate for $D_i = 10.0$ cm, $Q_i = 51.65$ lt/s and $2b = 40$ cm.....	143
Table B.49	Experimental results related to the anti – vortex plate for $D_i = 10.0$ cm, $Q_i = 51.65$ lt/s and $2b = 60$ cm.....	144
Table B.50	Experimental results related to the anti – vortex plate for $D_i = 10.0$ cm, $Q_i = 38.79$ lt/s and $2b = 60$ cm.....	145
Table B.51	Experimental results related to the anti – vortex plate for $D_i = 10.0$ cm, $Q_i = 24.00$ lt/s and $2b = 60$ cm.....	146
Table B.52	Experimental results related to the anti – vortex plate for $D_i = 10.0$ cm, $Q_i = 51.65$ lt/s and $2b = 80$ cm.....	147
Table B.53	Experimental results related to the anti – vortex plate for $D_i = 10.0$ cm, $Q_i = 38.79$ lt/s and $2b = 80$ cm.....	148
Table B.54	Experimental results related to the anti – vortex plate for $D_i = 10.0$ cm, $Q_i = 24.00$ lt/s and $2b = 80$ cm.....	149

Table B.55	Experimental results related to the anti – vortex plate for $D_i = 10.0$ cm, $Q_i = 51.65$ lt/s and $2b = 100$ cm.....	150
Table B.56	Experimental results related to the anti – vortex plate for $D_i = 10.0$ cm, $Q_i = 38.79$ lt/s and $2b = 100$ cm.....	151
Table B.57	Experimental results related to the anti – vortex plate for $D_i = 10.0$ cm, $Q_i = 24.00$ lt/s and $2b = 100$ cm.....	152
Table B.58	Experimental results related to the anti – vortex plate for $D_i = 10.0$ cm, $Q_i = 51.65$ lt/s and $2b = 120$ cm.....	153
Table B.59	Experimental results related to the anti – vortex plate for $D_i = 10.0$ cm, $Q_i = 38.79$ lt/s and $2b = 120$ cm.....	154
Table B.60	Experimental results related to the anti – vortex plate for $D_i = 5.0$ cm, $Q_i = 14.69$ lt/s and $2b = 40$ cm.....	155
Table B.61	Experimental results related to the anti – vortex plate for $D_i = 5.0$ cm, $Q_i = 14.69$ lt/s and $2b = 60$ cm.....	156
Table B.62	Experimental results related to the anti – vortex plate for $D_i = 5.0$ cm, $Q_i = 14.69$ lt/s and $2b = 80$ cm.....	157

## LIST OF FIGURES

### FIGURES

Figure 1.1 Vorticity sources (a) offset introduction, (b) velocity gradients, (c) obstruction (Durgin and Hecker, 1978).....	2
Figure 1.2 Classification of intake structures (Knauss, 1987).....	3
Figure 1.3 Visual comparison of eddy/swirl, dimple and vortex tail related to their strength .....	4
Figure 1.4 ARL vortex type classification (Knauss, 1987).....	5
Figure 2.1 Dimensionless plot of data obtained from existing intakes, field installations and model studies (Rindels and Gulliver, 1983).....	11
Figure 2.2 Recommended submergence for intakes with proper approach flow conditions, but without use of special devices for vortex suppression (Knauss, 1987) .....	12
Figure 2.3 Illustration of the critical spherical sink surface (CSSS) (Yıldırım and Kocabaş, 1995).....	13
Figure 3.1 Modelling elements for the experimental intake structure.....	17
Figure 4.1 Plan (top) view and side view of the physical model (dimensions are given in cm) .....	22
Figure 4.2 General view of the experimental setup.....	23
Figure 4.3 Experimental setup with intake pipe of $D_i = 25$ cm.....	23
Figure 4.4 Experimental setup with intake pipe of $D_i = 14.4$ cm.....	24
Figure 4.5 Experimental setup with intake pipe of $D_i = 5$ cm.....	24
Figure 4.6 Anti – vortex plates with 40 cm in length.....	25
Figure 4.7 Anti – vortex plates with 50 cm in length.....	25
Figure 4.8 A picture showing an air-entraining vortex at the pipe of $D_i = 5$ cm despite of anti-vortex plate.....	27
Figure 4.9 View of an air-entraining vortex forming at higher submergence .....	28
Figure 4.10 Vortex formation at the pipe of $D_i = 25$ cm .....	28
Figure 5.1 Variation of $S_c/D_i$ with Froude number as a function of $2b/D_i$ for the pipe of $D_i = 30$ cm ..	31
Figure 5.2 Variation of $S_c/D_i$ with Reynolds number as a function of $2b/D_i$ for the pipe of $D_i = 30$ cm .....	31
Figure 5.3 Variation of $S_c/D_i$ with Weber number as a function of $2b/D_i$ for the pipe of $D_i = 30$ cm ...	32
Figure 5.4 Variation of $S_c/D_i$ with Froude number as a function of $2b/D_i$ for the pipe of $D_i = 25$ cm ..	32
Figure 5.5 Variation of $S_c/D_i$ with Reynolds number as a function of $2b/D_i$ for the pipe of $D_i = 25$ cm .....	33
Figure 5.6 Variation of $S_c/D_i$ with Weber number as a function of $2b/D_i$ for the pipe of $D_i = 25$ cm...32	33
Figure 5.7 Variation of $S_c/D_i$ with Froude number as a function of $2b/D_i$ for the pipe of $D_i = 19.4$ cm .....	34
Figure 5.8 Variation of $S_c/D_i$ with Reynolds number as a function of $2b/D_i$ for the pipe of $D_i = 19.4$ cm.....	34
Figure 5.9 Variation of $S_c/D_i$ with Weber number as a function of $2b/D_i$ for the pipe of $D_i = 19.4$ cm	35
Figure 5.10 Variation of $S_c/D_i$ with Froude number as a function of $2b/D_i$ for the pipe of $D_i = 14.4$ cm .....	35
Figure 5.11 Variation of $S_c/D_i$ with Reynolds number as a function of $2b/D_i$ for the pipe of $D_i = 14.4$ cm.....	36
Figure 5.12 Variation of $S_c/D_i$ with Weber number as a function of $2b/D_i$ for the pipe of $D_i = 14.4$ cm .....	36
Figure 5.13 Variation of $S_c/D_i$ with Froude number as a function of $2b/D_i$ for the pipe of $D_i = 10$ cm	37
Figure 5.14 Variation of $S_c/D_i$ with Reynolds number as a function of $2b/D_i$ for the pipe of $D_i = 10$ cm .....	37
Figure 5.15 Variation of $S_c/D_i$ with Weber number as a function of $2b/D_i$ for the pipe of $D_i = 10$ cm.	38
Figure 5.16 Variation of $S_c/D_i$ with Froude number as a function of $2b/D_i$ for the pipe of $D_i = 5$ cm ..	38
Figure 5.17 Variation of $S_c/D_i$ with Reynolds number as a function of $2b/D_i$ for the pipe of $D_i = 5$ cm .....	39
Figure 5.18 Variation of $S_c/D_i$ with Weber number as a function of $2b/D_i$ for the pipe of $D_i = 5$ cm...39	39

Figure 5.19 Limit values of $2b/D_i$ above which $S_c/D_i$ is independent of $2b/D_i$ and function of Fr, Re and We .....	41
Figure 5.20 Comparison of measured and calculated maximum $S_c/D_i$ values for the intake pipes tested .....	43
Figure 5.21 Comparison of measured and calculated minimum $S_c/D_i$ values for the intake pipes tested .....	44
Figure 5.22 Comparison of measured and calculated intermediate $S_c/D_i$ values for the intake pipes tested .....	45
Figure 5.23 Comparison of measured and calculated $S_c/D_i$ values from the application of Equation [5.5] to the available intermediate data .....	46
Figure 5.24 Comparison of measured and calculated $S_c/D_i$ values from the application of Equation [5.6] to the available intermediate data .....	46
Figure 5.25 Comparison of measured and calculated $S_c/D_i$ values from the application of Equation [5.7] to the available intermediate data .....	47
Figure 5.26 Comparison of measured and calculated $S_c/D_i$ values from the application of Equation [5.8] to the available intermediate data .....	48
Figure 5.27 Comparison of measured and calculated $S_c/D_i$ values from the application of Equation [5.9] to the available intermediate data .....	48
Figure 5.28 Variation of $(S_c/D_i)_r$ with Froude number .....	52
Figure 5.29 Variation of $(S_c/D_i)_r$ with $L_r$ .....	52
Figure 5.30 Variation of $(S_c/D_i)_r$ with $(Re)_r$ .....	53
Figure 5.31 Variation of $(S_c/D_i)_r$ with $(We)_r$ .....	53
Figure 5.32 For present and Gürbüzdal (2009) study, limit values of $2b/D_i$ above which $S_c/D_i$ is independent of $2b/D_i$ and function of Fr, Re and We .....	54
Figure 5.33 Comparison of measured and calculated (from Eq. 5.4) intermediate $S_c/D_i$ values of Gürbüzdal (2009) .....	55
Figure 5.34 Dimensionless plot of data obtained from existing intakes, field installations and model studies (Rindels and Gulliver, 1983) with the relationships proposed by Gordon (1970), Reddy and Pickford (1972), Eq. 5.9 and corrected Eq 5.9 for $L_r = 1/10$ .....	57
Figure 5.35 Variation of $(W_p/D_i)_1$ with Fr for $2.00 \leq L_p/W_p \leq 8.00$ .....	65
Figure 5.36 Variation of $(W_p/D_i)_2$ with Fr for $L_p/W_p = 2.5$ .....	65
Figure A.1 Simple illustration of the critical submergence concept.....	71
Figure B.1 Plan View of Vortex Zones .....	95

## LIST OF SYMBOLS

a	Intake gate height
b	Horizontal distance from the center of the intake to a side wall of the reservoir
$b_1$	Horizontal distance from the center of the intake to the right side plexiglass wall
$b_2$	Horizontal distance from the center of the intake to the left side plexiglass wall
c	Vertical distance between the lowest point of the intake pipe and reservoir bottom
$C_d$	Discharge coefficient of the intake in a uniform canal flow
c1	Regression variable
c2	Regression variable
c3	Regression variable
c4	Regression variable
$D_i$	Intake diameter
$D_i^*$	Orifice diameter
Fr	Intake Froude number
g	Gravity acceleration
h	The depth of water above centerline of the intake
H	Submergence for vertical intakes
$H_c$	Critical submergence for vertical intakes
H'	Distance between bottom of the tank and free water surface
K	Viscous correction factor
$K_o$	Intake Kolf number
$L_p$	Plate length
$L_r$	Model length scale ratio
$N_v$	Ratio of intake Froude number to intake Reynolds number
$N_\Gamma$	Circulation number
$Q_i$	Intake discharge
R	Correlation coefficient
Re	Intake Reynolds number
$Re_R$	Radial Reynolds number
$r_0$	Shadow radius of vortex at the bottom of canal
$s_a$	Depth of approach flow to sump
S	Submergence for horizontal intakes
$S_c$	Critical submergence measured from the summit point of horizontal intakes
$S_c^*$	Critical submergence measured from the center of horizontal intakes
T	The cross-sectional trash rack opening percentage
$u_a$	Velocity of approach to sump
$U_\infty$	Velocity of uniform canal flow at the upstream of the intake
$V_i$	Intake velocity
We	Intake Weber number
$W_p$	Plate width
Z	Intake wall slope
$\Gamma$	Circulation
$\mu$	Viscosity
$\nu$	Kinematic viscosity
$\rho$	Density of the fluid
$\sigma$	Surface tension



## CHAPTER 1

### INTRODUCTION

#### 1.1 Introductory Remarks on the Formation of Vortex at Intake Structures

In modern world, water demand increases more and more due to exhausting of natural water resources. Consequently, they should be used more carefully and efficiently due to the possibility of facing with problems in the future. Since water is transmitted from seas, lakes, rivers or simply reservoirs through intakes to be used in power generation, irrigation, domestic and industrial supply, improvements in the design criteria of the intakes have a great importance to minimize cost and to use water efficiently. It is obvious that the formation of air-entraining vortices at intake structures has a definite effect on the design criteria. The location and direction of the intake should be so arranged that the water level should be well above the intake to prevent the occurrence of air-entraining vortices under the most critical scenarios (when the reservoir is at dead or minimum storage level.). However, to reduce the cost of construction, the intake must be placed close to the water surface as much as possible. Therefore, a design problem arises between reducing the cost and increasing the usable water capacity at the reservoir. Consequently, vortex formation at intakes should be researched continuously to obtain better optimization between them.

##### 1.1.1 The Concept of Critical Submergence

Vertical distance between the free surface and the intake is known as submergence. Moreover, in literature, some researchers measure this distance from the center of the intake, and others measure it from the top of the intake. If the water level decreases up to a level where air-entraining vortex starts to occur at the free surface, this level is called as “critical submergence”. At an effective intake structure, submergence should be large enough to prevent the occurrence of air-entraining vortices extending from the free surface, down to the intake entrance while the available water potential can be used freely.

##### 1.1.2 The Sources of Vorticity

In literature, many vorticity sources have been defined by researchers for different geometrical flow conditions. According to them, an eccentricity of the approach flow relative to intake structure and asymmetric approach flow caused by geometrical conditions are two most effective vortex formation triggers. Moreover, Durgin & Hecker (1978) defined three fundamental vorticity sources as shown in Figure 1.1. They emphasized that vortices are mainly initiated by: eccentric orientation of the intake relative to a symmetric approach flow, existence of shear layers of high velocity gradients, rotational wakes created by obstructions.

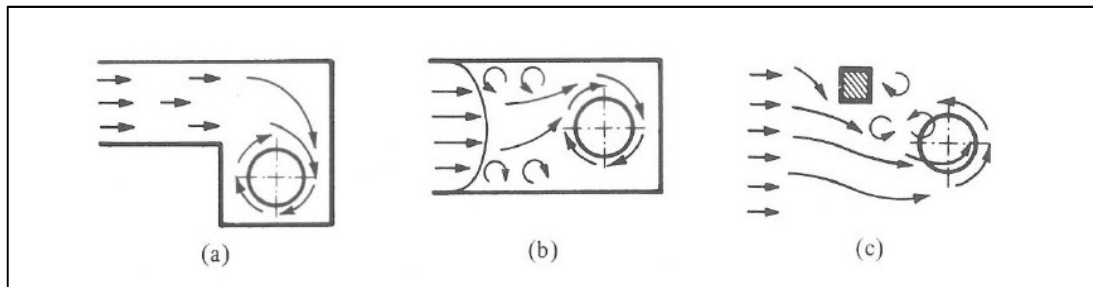


Figure 1.1 Vorticity sources (a) offset introduction, (b) velocity gradients, (c) obstruction (Durgin and Hecker, 1978)

### 1.1.3 Problems Due To Vortex Formation

Knauss (1987) mentioned that air-entraining vortex formation causes two main hydraulic problems at intakes: unfavorable vibrations on the hydraulic machines and serious problems on the closed channel system due to air ingestion. In other words, the difficulties can be listed as the following subtitles:

- Increase of head loss,
- Reduction of intake discharge,
- Reduction of efficiency of hydraulic machines due to lower discharge,
- Problems at the operational stage of hydraulic machines due to disturbed flow pattern,
- Vibrations and cavitation problems at hydraulic machines due to air ingestion.

### 1.1.4 Directional and Structural Distinctions of Intakes

Since air-entraining vortex formation starts from the free surface of the water and ends inside of the intake, the classification of intakes gains a great importance on it. In literature, intakes may be classified under two subtitles, namely, distinction related to intake direction or orientation and structural distinction. In structural distinction, the location of the intake is considered as whether it is placed in the floor or walls of the basin or is projecting into the reservoir or the sump. Figure 1.2 shows this classification based on directional and structural differences.

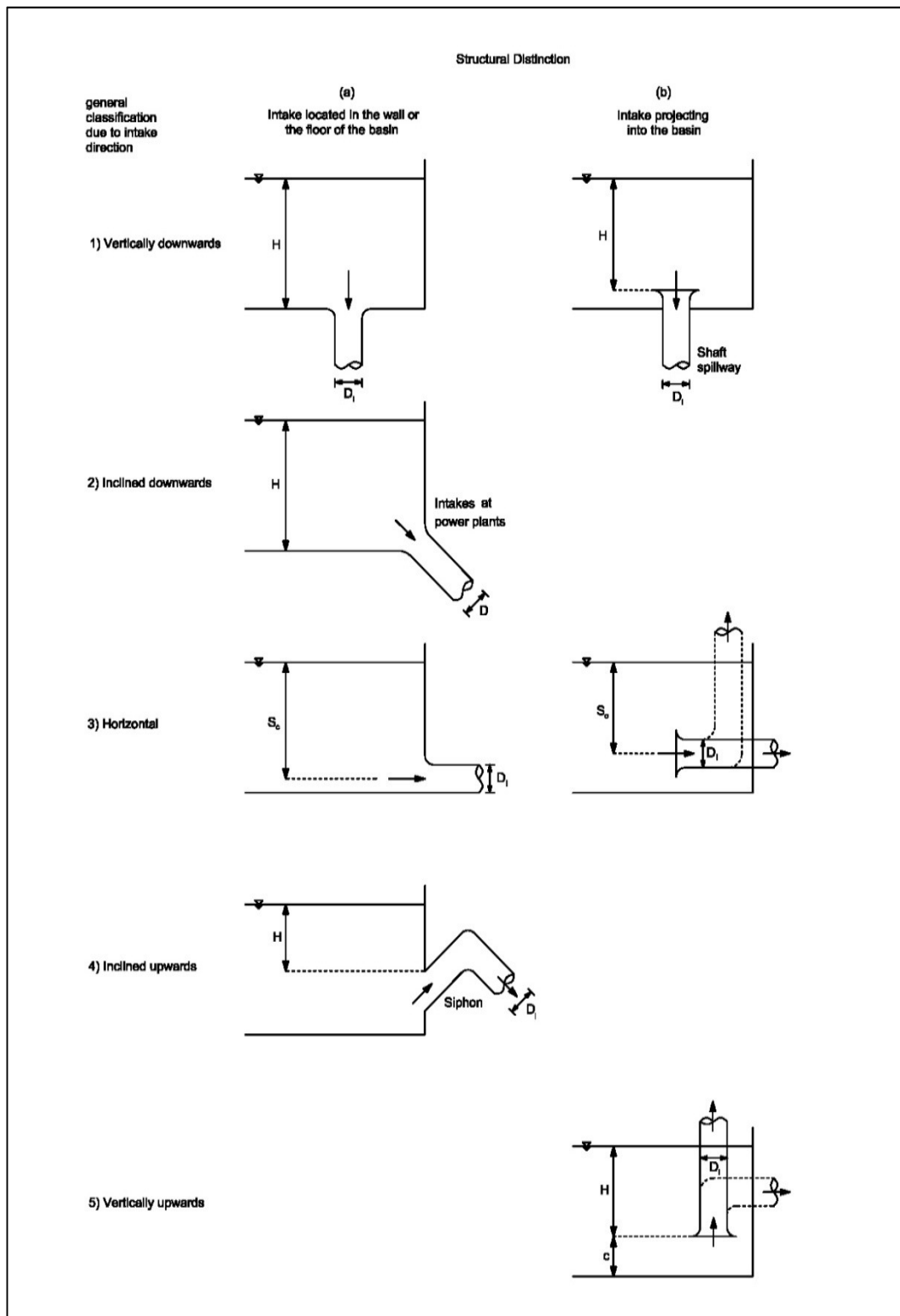


Figure 1.2 Classification of intake structures (Knauss, 1987)

### 1.1.5 Classification of Vortices

Vortices can be classified according to their location, namely, surface vortices and subsurface vortices. Surface vortices occur at the free surface of the water and are responsible from air entrainment and swirl. Subsurface vortices start from the floor and/ or the walls of upstream basin and cause swirl intrusion. However, a useful classification is made related to vortex strength. Next, to make this classification, visual techniques are used and some quantities related to vortex strength are measured directly or indirectly. Discharge coefficient of the intake entrance, the magnitude of inlet pipe flow swirl, or the amount of ingested air into the intake can be used for the latter case. Nevertheless, there are two main problems about it. The first one is that if the vortex size is too small compared to the inlet, it may not produce reliably measurable effects even though vortex has an air core, and the second one is that vortices and the selected dependent parameters may have a weak correlation between them and may be variable with some other parameters. Therefore, visual observation is the most common way to classify vortex types although it is a subjective technique. Alden Research Laboratory, ARL, has made a visual classification of vortex types related to their formation (Knauss, 1987). Before examining the formation steps, some useful words about visual observation should be explained, namely, swirl or eddy, dimple and vortex tail.

Eddy or swirl, dimple and vortex tail, shown in Figure 1.3, are used to describe the appearance of water surface according to the vortex strength in this order. Vortex formation starts with a small swirl which is observed only by reflection of the light from the water surface and with gaining strength, it turns to dimple and then, it extends to downward direction and becomes a vortex tail.

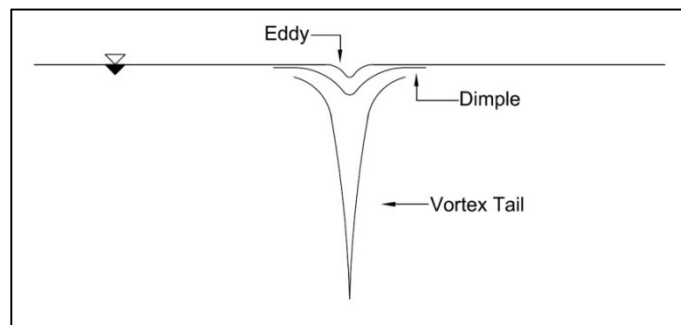


Figure 1.3 Visual comparison of eddy/swirl, dimple and vortex tail related to their strength

Stages of the vortex classification related to ARL vortex classification are explained below (Figure 1.4):

1. Only a weak swirl is observed at the free surface of the water.
2. By gaining strength and increasing rotational velocity, weak swirl turns to a surface dimple.
3. In type 3 vortex, a vortex tail appears without air entrainment. However, a dye is added into the water to see a filament which shows location of the vortex axis.
4. Vortex strength becomes so strong that some floating objects such as trash but no air is sucked due to vortex into the inside of the intake.
5. Vortex tail almost reaches to the intake and vortex strength increases as air bubbles are taken from the water surface and pulled into the inside of the intake.

6. A continuous air entrainment starts due to vortex from the free surface up to entrance of the intake. Near the free surface, it has a funnel shape and it extends up to the intake like a rope.

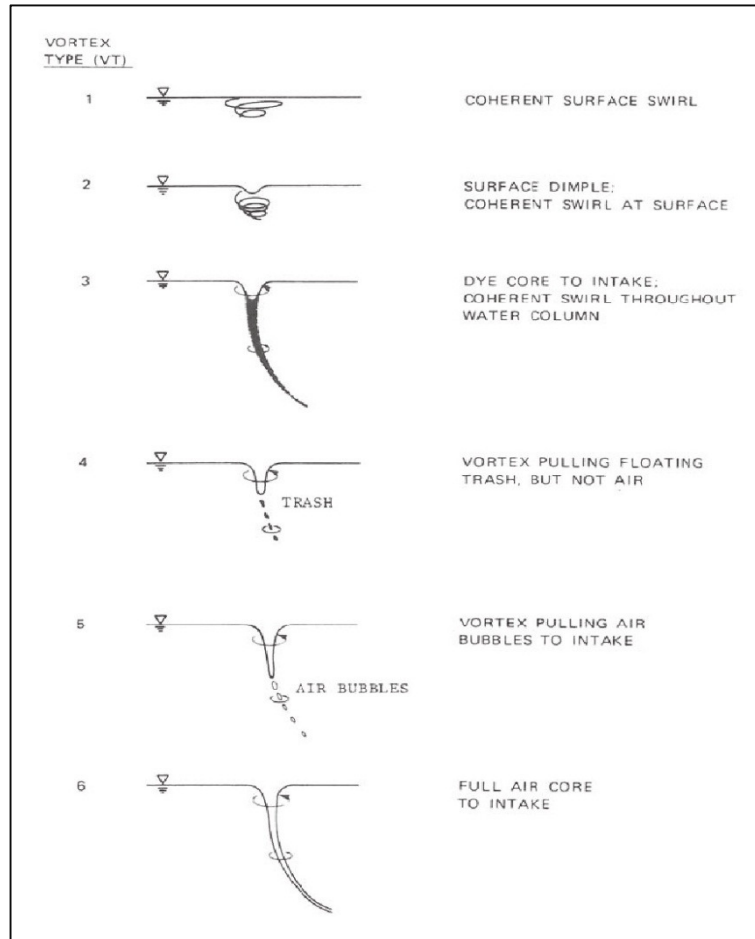


Figure 1.4 ARL vortex type classification (Knauss, 1987)

### 1.1.6 Vortex Prevention

As it is mentioned before, vortices are mainly triggered by eccentric orientation of the intake and asymmetric approach flow conditions due to geometry. Although hydraulic design of the intake structure is made by considering prevention of vortex formation, in some cases, the formation of vortices cannot be suppressed because design requirements cannot be satisfied due to extreme approach flow conditions, submergence requirements or economic reasons. Therefore, some structural measures can be applied to eliminate vortex formation at intake structures. Rutschmann et al. (1987) proposed that air ingestion can be removed or the effect of swirl can be lowered by increasing the distance of streamlines between the intake structure and the free water surface, improving approach flow condition to remove non – uniformities, and applying some anti-vortex devices. Many different applications of anti-vortex devices in real and laboratory cases are illustrated by Rutschmann et al. (Knauss, 1987).

## **1.2 Scope of the Study**

The aim of this study is to investigate effects of the hydraulic parameters on the formation of air-entraining vortices at horizontal intakes and the use of anti-vortex plates to eliminate the formation of vortices. This was achieved by conducting experiments and comparing these experimental results with the theoretical analysis of air-entraining vortices and with previous data.

To succeed in this purpose, a hydraulic model was constructed in the laboratory to observe the initiation formation conditions of air-entraining vortices (Type 6) at horizontal intakes with pipes of different diameters. In Chapter 2, a literature review which consists of the summaries of previous studies of several researchers is presented. The governing non-dimensional parameters of the flow where air-entraining vortex initiates and the relation between the critical submergence ratio and the determined dimensionless parameters are given in Chapter 3. Chapter 4 includes the description of the experimental setup, experimental procedure and observations of the study. Evaluation of the experimental results of air-entraining vortex formation with sets of curves, empirical formulas for the critical submergence ratio, comparison of the present study with the past studies, and usability of the anti-vortex plates are expressed in Chapter 5. A conclusion of the study and recommendations are given in Chapter 6.

## CHAPTER 2

### LITERATURE REVIEW

In literature, many researchers have worked to solve vortex formation problems at intakes by comprehensive analytical and numerical methods. In analytical model applications, different intake arrangements, boundary and approach flow conditions were tested and some parameters were eliminated when it was considered that there are no effects of them on vortex formation. However, applications of these analytical models to real cases are very difficult since each case has a unique flow geometry and each behavior is different from others. In theoretical case, vortex formation problem is found very difficult to deal with due to its complexity. Consequently, some assumptions are made to simplify the theoretical analysis. However applications of theoretical solutions to real cases are problematic too and also, theoretical results and experimental results may not coincide because of the eliminated effects of some parameters on the formation of vortices. By considering above argumentation, model studies for real cases are strongly suggested by researchers.

Iversen (1953) made a research about submergence requirements of high-specific-speed pumps. In experiments, a vertically downward intake was used in a simple rectangular sump and also, a model test was applied based on Froude similitude. Experimental results shows that side wall and end wall clearance in the range of  $D_i/2$  to  $D_i/4$ , where  $D_i$  is the diameter of the intake pipe, have no effect on the pump efficiency. In addition, the same situation is valid for bottom clearance which is equal to  $D_i/2$ . Moreover, at the end of model tests, it was observed that a similitude based on Froude number is not enough to obtain acceptable results due to friction effects.

Blaisdell and Donnelly (1958) carried out a study in order to investigate the use of hood inlet since this type inlet is simple, economical, and can be easily installed for agricultural purposes. The hood inlet is formed by cutting a pipe at an angle and it is placed such that the longer part is at the top. During experiments on the hood inlet, a number of different types of vortex inhibitors were tested in order to prevent vortex formation at the inlet. In the test program, as an anti-vortex device, first, a splitter wall mounted on the outside crown of the inlet and it gave satisfactory results although sometimes vortices are formed at the inlet. In the case of larger splitter wall, a little additional benefit was obtained. The headwall type of anti-vortex device is also tested but this type of anti-vortex device could not prevent much stronger vortices and caused more air ingestion into the inlet. On the other hand, the entrance loss is less with headwall type anti-vortex device. Finally, vortex plates which are placed at the top of the inlet entrance were tested and the results were found satisfactory when it is compared with splitter wall but it should be noted that head loss increases with this kind of anti-vortex device.

Anwar (1965, 1967 and 1968) worked experimentally and theoretically on a steady vortex with an air core at the entrance of an outlet pipe and also on solutions to suppress vortex formation. Experiments conducted with a cylindrical tank and by placing a vertical intake pipe centrally on the bottom of the tank. Experiments showed that if the radial Reynolds number,  $Re_R = Q_i/vH$ , where  $Q_i$  is the volumetric flow rate,  $H$  is the vertical intake submergence and  $v$  is the kinematic viscosity of water, is greater than  $10^3$ , effect of viscosity can be neglected; therefore, circulation and submergence become the primary parameters affecting the vortex formation. Based on these conditions, it was concluded that the vortex formation can be prevented by three ways: increasing roughness in the rigid boundaries, designing the geometry of the intake zone as streamlined approach to the inlet with small curvature and sloping the floor gradually from the base to the level of the inlet for the case of projection of inlet from the base. In addition, a floating raft above the inlet and baffle wall was suggested to prevent vortex formation because these kinds of vortex suppressor devices dissipate the energy necessary to maintain the vortex by increasing roughness.

Moreover, it was mentioned that performance of a pump depends very much on the side wall and floor clearances.

Zielinski and Villemonte (1968) performed experiments in a cylindrical vortex tank by using five different orifice diameters and oil with various viscosities to obtain information about the viscous effects on vortex formation. The physical effects of viscosity on the vortex-orifice flow were found that the circulation decreases with the rise of viscosity due to increase in the viscous shear and decrease of circulation causes decrease of the dropdown; consequently, air core reduction occurs with the augmentation of the area of the jet and thereby, the coefficient of contraction and the overall coefficient of discharge rises too. Thus, head must decrease to maintain a constant amount of discharge. Moreover, the experiments showed that the effects of viscosity become negligible when Reynolds number,  $Re = V_i D_i^* / \nu$ , where  $V_i$  is the average flow velocity through the orifice opening and  $D_i^*$  is the orifice diameter, is greater than  $1 \times 10^4$ .

Gordon (1970) examined 29 existing hydroelectric intakes to develop design criteria to avoid vortices at low – head intakes. At the end of his study, it was decided that the geometry of the approach flow to the intake, the velocity at the intake, the size of the intake and the submergence are the main factors which affect formation of vortices. However, since each geometry of the intake approach channel is unique, it is hard to investigate the effect of the geometry on formation of vortices. Therefore, it was decided to focus on other parameters which affect the vortex formation. According to the available data, the following formulas were derived to find the critical submergence ratio:

$$\frac{S_c}{D_i} = 1.70Fr \quad [2.1]$$

for symmetrical approach flow conditions and,

$$\frac{S_c}{D_i} = 2.27Fr \quad [2.2]$$

for asymmetrical approach flow conditions, where  $S_c$  is the critical submergence depth which is measured from the summit point of the intake and the above formulas are altered to be used in the SI unit system.

Reddy and Pickford (1972) tried to describe design criteria to prevent vortices in pump sumps and at horizontal intakes. In their study, the critical submergence was defined as a function of Froude number, Reynolds number and wave parameter. However, since vortex formation was considered as a free surface phenomenon and wave length is so small compared to total water depth in a conventional hydroelectric power plant, both Reynolds number and wave parameter were removed from the field of the vortex formation and Froude number became the only parameter affecting vortex formation. It was suggested that for the cases of anti-vortex device usage,  $S_c/D_i = Fr$  (otherwise  $S_c/D_i = 1 + Fr$ ) gives sufficient submergence without vortices either in hydroelectric practice and pump sumps. However, it should be stated that they have plotted data for both horizontal and vertically inverted intakes. This implies that the flow field approaching a vertically inverted intake is the same as that for a horizontal intake, and the submergence required for a vertical intake is the same as that required for a horizontal intake. The critical submergence for the intake types cannot be equated because of the great differences in the flow field created by the different types of intakes.

Daggett and Keulegan (1974) worked on effects of surface tension and viscosity on vortex formation to clarify similarity conditions between prototypes of hydraulic structures and their related models in terms of the incipient condition for vortex formation, the vortex shape, the vortex size and the efficiency of the outlet structure. Experiments were conducted in two different scaled similar cylindrical tanks with various diameters of vertical outlet pipes, liquids and vane angles. It was found that for the values of  $Re > 5 \times 10^4$ , viscosity parameter loses its effect and the circulation number becomes the only important parameter. During the experiments, no significant effects of

surface tension and vane angles were determined. Based on the study results, critical depth ratio was found as the formula below

$$\left(\frac{H'}{D_i}\right)_c = 7 \times 10^{-2} N_\Gamma \text{Re}; \text{Re} < 5 \times 10^4 \quad [2.3]$$

$$\left(\frac{H'}{D_i}\right)_c = 300 N_\Gamma; \text{Re} \geq 5 \times 10^4 \quad [2.4]$$

where  $H'$  = distance from the bottom of the tank to the free surface and  $(H'/D_i)_c$  is the smallest value of  $H'/D_i$  for which air core vortex does not occur,  $N_\Gamma$  = circulation number =  $\Gamma D_i / Q_i$ , where  $\Gamma$  = circulation and  $Q_i$  = intake discharge.

Zeigler (1976) studied on a hydraulic model of Grand Coulee Third Powerplant in order to determine whether air-entraining vortices will occur near the penstock of Grand Coulee Third Powerplant and to investigate the use of rafts to prevent formation of air-entraining vortices. In the hydraulic model, the tests were carried out with and without trashracks. According to the tests without trashracks, the vortex formation becomes more severe for higher discharges. In addition, when the operating units are increased in the smaller discharges, the vortex severity increases either. The results of the tests with the trashracks implied that trashracks has a definite suppressive effect on vortex severity. In the experiments three different screen sizes were used as trashracks and it was observed that more suppressive effect on the vortex severity obtained with smaller grid sizes. In the raft tests, different sizes of rafts were tested as floating or submerged and it was found that they prevented intakes from vortex formation successfully. The rafts were not cover the whole area and consequently, it is placed near the center of the vortex formation area. According to the results of the experiments, it was seen that submerged rafts are more effective on the prevention of the vortex. However, although the vortex formation was prevented by using rafts, swirl formation continued to occur. Also, the grid size of the rafts was found to be effective on the formation of these swirls.

An experimental study was undertaken by Anwar et al. (1978) on the onset of air-entraining vortices at horizontal intakes. Experiments conducted with and without bellmouthed entry and intake was projected into the flume or mounted flush with the side wall. Experimental results showed that viscous and surface tension effects can be eliminated from the formation process when radial Reynolds number and Weber number, where  $We = \rho V_i^2 D_i / \sigma$ , are greater than  $3 \times 10^4$  and  $1 \times 10^4$ , respectively. Therefore, other parameters such as circulation number and Froude number gain more importance. It was noted that bellmouth entry does not improve intake performance about vortices. However, intake mounted flush with the side wall of the flume, boundary wall reduces circulation and free surface almost reached the intake lip before air-entraining vortices occur. Consequently, an intake can be placed closer to the water surface if there would be a boundary wall.

Jain et al. (1978) conducted experiments with two geometrically similar cylindrical tanks by placing vertically oriented intake pipe at the center of the bottom boundary of the tanks. They performed experiments with three intake pipes of different diameter, adjustable guide vanes to ensure radial flow and three different liquids to research effects of surface tension and viscosity of these liquids on the vortex formation. Experiments implied that critical submergence is independent of viscosity and surface tension within the range of  $(2.5 \times 10^3 \leq Re \leq 6.5 \times 10^5$  and  $1.2 \times 10^2 \leq We \leq 3.4 \times 10^4)$ . The critical submergence ratio was found to be a function of the Froude number in the following form from the experimental data which are valid for the range of Froude number;  $1.1 \leq Fr \leq 20$ .

$$\frac{H_c}{D_i} = 0.47 Fr^{0.50} \quad [2.5]$$

Jain et al. (1978) repeated their previous study with a very similar experimental setup to the previous one but by using different liquids to introduce the similarity conditions for the onset of air-entraining vortices at vertical pipe intakes. Effects of surface tension was found to be negligible when Weber number is in the range of  $1.2 \times 10^2 \leq We \leq 3.4 \times 10^4$  which has the same range of the previous results. Moreover, it was observed that the critical submergence decreases with increase of

kinematic viscosity due to the reduction in the strength of circulation. By plotting  $S_c/D_i$  versus  $Fr$  on a double log paper, a formula was produced and by arranging it with circulation, it took the final form as follows:

$$K \frac{H_c}{D_i} = 5.6 N_\Gamma^{0.42} Fr^{0.50} \quad [2.6]$$

where  $K$  is the correction factor related to viscosity parameter,  $N_v = g^{1/2} D_i^{3/2} / \nu$ , and attains a constant value for  $N_v \geq 5 \times 10^4$ ,  $N_\Gamma = \Gamma S_c / Q_i$  is the circulation parameter.

As a result of experiments, it was determined that Reynolds number has limit values for each Froude number and beyond it, viscous effects become negligible and these limits increase with rise of Froude number. At the end of their study, they proposed an equation of computing  $K$  value to predict the critical submergence of the prototype:

$$\frac{\frac{H_c}{D_i} \text{ for zero viscous influence}}{\frac{H_c}{D_i} \text{ for any Reynolds number}} = K \quad [2.7]$$

Anwar and Amphlett (1980) made experiments with a vertically inverted intake to investigate the variables responsible for the formation of air-entraining vortices. To measure these variables; different intake heights, side and back wall clearances, guide vane settings and the circulation intensities were tested. Three different pipe sizes were used with and without bellmouth entry and the results were compared with horizontal intake arrangement results. It was found that bellmouth entry did not improve critical submergence heads as compared with single pipe intake while it did improve entry flow conditions to the intake. By drawing circulation number,  $\Gamma r_0 / Q_i$ , versus radial Reynolds number,  $Re_R = Q_i / \nu H$ , graph, it was concluded that circulation number decreases rapidly while  $Re_R$  increases from 1 to  $3 \times 10^4$  and it becomes almost independent when  $Re_R > 4 \times 10^4$ , where  $r_0$  is the shadow radius of the vortex at the bottom of the canal. By plotting the circulation number versus coefficient of discharge, it was shown that  $H/D_i$  and  $D_i$  are dependent variables whereas  $b/D_i$  is independent, where  $b$  is the side wall clearance. According to these graphs, a model can be designed with less influence of the circulation number on the viscous effect, and coefficient of discharge became a function of  $D_i$  and  $H$ . By plotting side wall clearance versus critical submergence graph, it was observed that  $H/D_i$  becomes independent of  $b/D_i$  when  $b/D_i > 8$  for high value of circulation and when  $b/D_i > 4$  for non-swirl flow.

Rindels and Gulliver (1983) compiled all the available data, together with Gordon's data, on existing installations and model studies of proposed installations and presented it in Figure 2.1 to obtain the most accurate values of submergence for the available discharge. Two envelope curves which result from Gordon's (1970) criteria are also given in Figure 2.1. From this figure, it is seen that neither Gordon's nor Reddy and Pickford's (1972) design criteria are sufficient to avoid vortex problems. There is a region, however, in Figure 2.1 where free-surface vortices are less likely to occur, that is the region segmented by a dimensionless submergence,  $S/D_i$ , greater than 0.7 and an intake Froude number,  $V_i/\sqrt{gD_i}$ , less than 0.5. However, if a given intake installation has extremely poor approach flow conditions, vortices are still possible in this "safe" region.

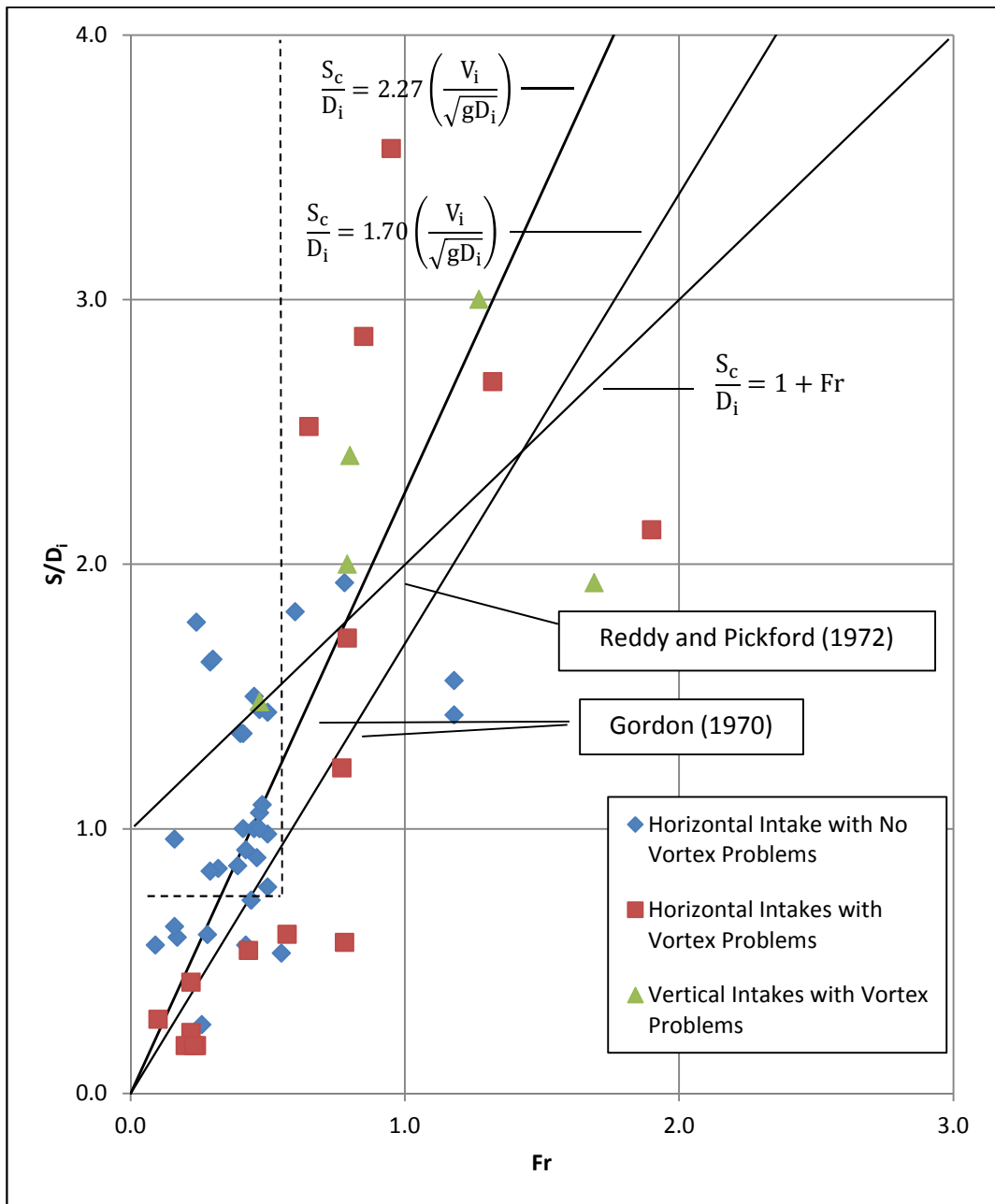


Figure 2.1 Dimensionless plot of data obtained from existing intakes, field installations and model studies (Rindels and Gulliver, 1983)

Padmanabhan and Hecker (1984) performed experiments on one full-sized and two scaled models of a pump sump to geometric scales of 1:2 and 1:4 to search possible scale effects on the surface and subsurface vortexing based on Froude similitude. Possible scale effects were examined in terms of vortex formation, pipe swirl, inlet losses and air ingestion by conducting experiments with two pipe operation, one pipe operation and screen blockage tests. At the end of the tests, it was determined that viscous and surface tension effects become negligible, if  $Re_R$ ,  $Re$  and  $We$  are greater than  $1.5 \times 10^4$ ,  $7.7 \times 10^4$  and 600, respectively. In addition, if approach flow Reynolds number,  $u_a s_a / \nu$  where  $u_a$  = velocity of approach flow to sump and  $s_a$  = depth of approach flow to sump, is below about  $3 \times 10^4$ , some scale effects were observed in scaled sump models. Another result is that inlet losses can be predicted well for circumstances where  $Re > 1 \times 10^5$ . As a result of the experiments, no important scale effects were observed on modeling free-surface vortexing and reduced scale models gave reasonable prediction of vortex types and air ingestion.

Knauss (1987) analyzed the minimum design submergences of well operating prototypes and presented the curves given in Figure 2.2. For large size intakes at powerplants, especially at pumped storage systems ( $Fr \leq 1/3$ ), a submergence depth of 1 up to 1.5 times the intake height (or diameter) is recommended. For medium and small size installations ( $Fr \geq 1/3$ ), especially at pumps sumps, submergence requirements may be calculated using the formula given in Figure 2.2. The recommendations are valid for intakes with proper approach flow conditions. In Figure 2.2,  $h$  is the depth of water above centerline of the intake, and  $Fr = V_i / \sqrt{gD_i}$ .

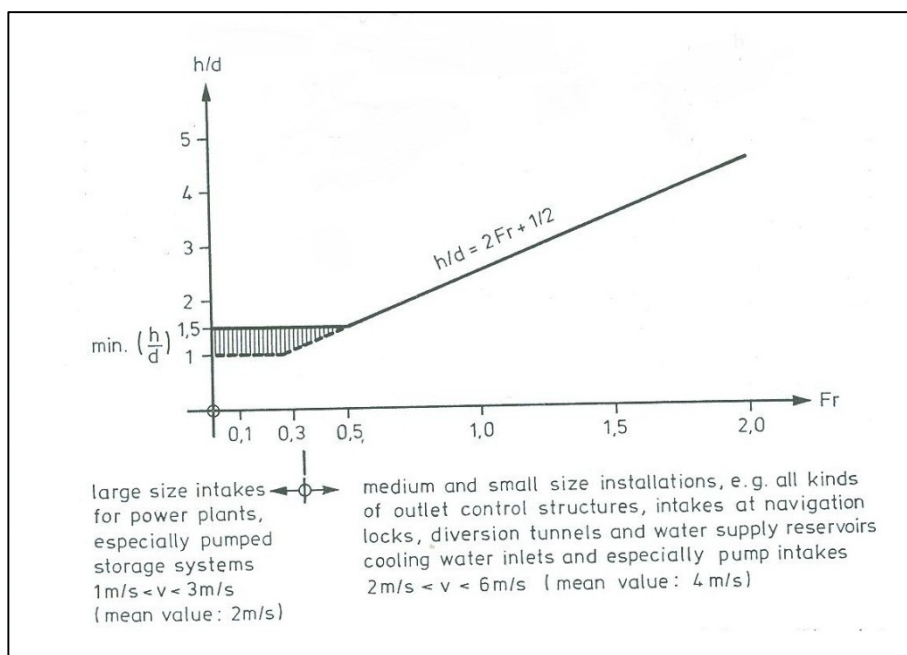


Figure 2.2 Recommended submergence for intakes with proper approach flow conditions, but without use of special devices for vortex suppression (Knauss, 1987)

Yıldırım and Kocabaş (1995) researched critical submergence for an air-entraining vortex by applying potential flow solution and conducted experiments. For experiments, a horizontal rectangular flume was used with vertically oriented intake and analytical analysis performed by considering combination of a point sink and uniform channel flow, which is known as Rankine's half body. To find critical submergence with Rankine's half body, it was assumed that the distance

between the top of the intake and free surface is equal to the radius of an imaginary spherical sink surface which is called as critical spherical sink surface (CSSS) and this distance is considered as the critical submergence, shown in Figure 2.3.

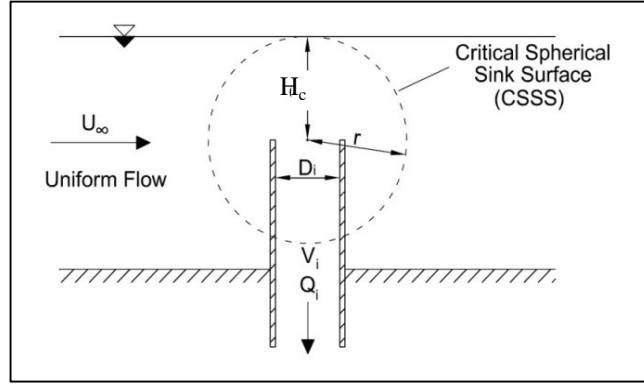


Figure 2.3 Illustration of the critical spherical sink surface (CSSS) (Yıldırım and Kocabaş, 1995)

As a result of the potential flow solution, a formula for critical submergence ratio is found as follows

$$\frac{H_c}{D_i} = 0.354 \left( C_d \frac{V_i}{U_\infty} \right)^{1/2} \quad [2.8]$$

where  $V_i$  = average intake velocity,  $C_d$  = discharge coefficient and  $U_\infty$  = velocity of uniform canal flow. However, the theoretical results differ from the experimental results; therefore, the coefficient at formula (0.354) is increased by 10% and it is modified as 0.4. As an important note, they found that the formula may not work well when  $(S_c/D_i) < 0.5$  and  $(C_d V_i/U_\infty) < 2$ .

To determine the minimum required submergence before double entrance pressure intake like power intakes, a large scale model study was undertaken by Jiming et al. (2000) not only for double entrance but also for single entrance pressure intake. As a result of the experiments, two empirical formulas were produced for symmetrical and non-symmetrical flow conditions as follows

$$\frac{S_c}{a} = 2.39Fr - 0.001 \quad [2.9]$$

for symmetrical approach flow and,

$$\frac{S_c}{a} = 3.17Fr - 0.001 \quad [2.10]$$

for non-symmetrical approach flow, where  $a$  = intake gate height. The above formula of symmetrical flow condition was compared with Gordons' formula and it was observed that Gordon formula gives lower submergences than required submergence especially for intakes with trashracks. Therefore, it was suggested that Gordons' formula should be multiplied with a larger coefficient or a model study of large projects should be conducted.

Yıldırım et al. (2000) worked on the effects of flow-boundary on the critical submergence of intake pipe experimentally and theoretically. Experiments were performed by using horizontal intake pipe in a horizontal rectangular flume with a dead-end wall. Related to the experiments, they concluded

that when the clearance between the intake and dead-end wall is equal to zero, an air-core vortex is obtained in lower critical submergences due to boundary effect of dead-end wall and air entraining vortices become the intermittent type, not continuous. In addition, to apply potential flow solution, the distance between the summit point and center of the intake should be subtracted from the critical submergence because in horizontal intakes, air ingestion occurs from a point close to the summit of the intake and consequently, the center of the critical spherical sink surface and intake center do not coincide. As a result of the study, it was found that potential flow solution gives acceptable results when the distance between the boundaries and intake pipe is smaller than  $S_c$  but it overestimates the critical submergence by about 80% if aforementioned distance is much smaller than  $S_c$ .

Yıldırım and Kocabaş (2002) repeated their study (conducted in 2000) with different critical spherical sink surface approach to reinvestigate the effects of the flow boundaries and blockage of the intake pipe on the critical submergence. The critical spherical sink surface was modified as it has a radius of  $S_c/\sqrt{2}$  while in their previous works, they took this radius as  $S_c$ . Comparison of theoretical results and experimental results shows that new approach gives better prediction of the critical submergence, if the distance between the intake center and impervious dead-end wall is less than or equal to the intake diameter. On other cases, the previous approach gives more accurate results for prediction of  $S_c$ .

Li et al. (2008) set up an experimental model by using a vertical intake arrangement to investigate the formation and evolution of free surface vortex at different development stages. During experiments, six types of vortices were observed as it is mentioned at ARL vortex type classification and in all stages, velocity and circulation distributions of free surface vortex were measured. It was found that the tangential velocity distribution is similar to Rankine's vortex model's tangential velocity distribution and the radial velocity distribution changes little in the formation stages. Related to the experimental results, they found an empirical formula which shows the relation between the critical submergence and the Froude number. The formula is

$$\frac{H_c}{D_i} = \frac{1992.84 + 7.54 * Fr^{7.06}}{573.81 + Fr^{7.06}} \quad [2.11]$$

The formula was tested with former researchers' formulas and it is found that the formula agrees with others when the Froude number is smaller but it changes slightly at larger Froude numbers.

Ahmad et al. (2008) worked on an analytical and experimental study regarding the critical submergence for a 90° horizontal intake in an open channel flow. Based on the potential flow and critical spherical sink surface theories, an analytical equation for the critical submergence was derived. However, the analytical equation did not give satisfactory results when the analytical results compared with experimental results. This situation could be explained with the large boundary effect and omission of viscosity, surface tension, and circulation effects from the derivation of the analytical equation. In the experimental part, a concrete flume and three different intake pipe diameter were used for the two cases of bottom clearance;  $c = 0$  and  $c = D_i/2$ . In the experimental part of the study, by using dimensional analysis and least square technique on the collected data from the experiments, a predictor was derived to find critical submergence for the case of  $c = 0$ :

$$\frac{S_c}{D_i} = 0.354 Fr^{-0.11} \left( \frac{V_i}{U_\infty} \right)^{0.91} \quad [2.12]$$

where  $U_\infty$  = uniform approach flow velocity. Similar procedure yielded the following equation for the case of  $c = D_i/2$ :

$$\frac{S_c}{D_i} = 0.27 Fr^{0.039} \left( \frac{V_i}{U_\infty} \right)^{1.02} \quad [2.13]$$

The predictors give satisfactory results with an error of +20% for  $c = 0$  and +15% for  $c = D_i/2$  when they are compared with the experimental results.

Gürbüzdal (2009) conducted a series of experiments by using horizontal intakes of four different diameters to study on the possible scale effects on the formation of air-entraining vortices. As a governing parameters of the vortex formation, Froude number, Reynolds number and side wall clearance were chosen and at the end of the experimental study, an empirical formula was derived based on these parameter as shown below:

$$\frac{S_c}{D_i} = Fr^{0.865} \left(\frac{b}{D_i}\right)^{-0.565} Re^{0.0424} \quad [2.14]$$

It was stated that Eq. 2.14 is valid for  $0.51 \leq Fr \leq 4.03$ ,  $1.597 \leq b/D_i \leq 5.147$  and  $2.96 \times 10^4 \leq Re \leq 2.89 \times 10^5$ . It was observed that  $S_c/D_i$  becomes independent of  $b/D_i$  for  $b/D_i \geq 6$  and Reynolds number limit, above which  $S_c/D_i$  is not affected by Reynolds number, increases with the rise of Froude number.

Yıldırım et al. (2009) investigated the effects of dimensions and relative positions of two (dual) vertical intake pipes on the critical submergence using both dimensional analysis for the critical submergence and the governing dimensionless variables and the potential flow solution. As a result of experiments, the critical submergence of the dual intakes is larger than a single intake pipes because in dual pipe system, there are more disturbances which trigger vortex initiation. The experimental results are compared with the theoretical results which are obtained from the potential flow solution and the agreement was found good.

Sarkardeh et al. (2010) conducted a study with a horizontal intake in a reservoir to determine the effects of intake head wall slope and the presence of trash rack on the formation of vortices. To avoid the viscous and surface tension effect, the experiments were conducted above the limits which were proposed by other researchers. Four different intake head wall slopes were tested and it was found that as the intake head wall slope increases toward the vertical position, the vortices becomes more unstable and weaker especially for lower Froude numbers. Consequently, the critical submergence decreases as well. In addition, same experiments were repeated with the presence of the trash rack. Related to the experimental results, it was determined that the trash rack reduces the vortex strength especially for strong vortices since it disturbs the flow as well as the vortex formation. By using the results of the experiments, they developed formulas for the critical submergence for the vortex types of 5 and 3 related to ARL vortex type classification:

$$\left(\frac{S_c}{D_i}\right)_5 = 2 \left(\frac{1}{Z}\right)^{0.008} Fr^{0.334} T^{0.369} \quad [2.15]$$

for the type 5 vortex formation and,

$$\left(\frac{S_c}{D_i}\right)_3 = 2.43 \left(\frac{1}{Z}\right)^{0.008} Fr^{0.334} T^{0.369} \quad [2.16]$$

for the type 3 vortex formation, where Z is the intake wall slope and T is the cross-sectional trash rack opening percentage (T=1 for the case of no trash rack).

Taştan and Yıldırım (2010) investigated the effects of dimensionless parameters and boundary friction on air-entraining vortices and the critical submergence of a vertically directed intake for the cases of no-circulation imposed cross-flow and still water. Also, to observe the circulation effect and intake size effect, a guide vane and another intake pipe were tested. To prevent boundary blockage effect on the intake flow and to observe only the effects of Fr, Re and We, the clearances were selected larger than  $H_c$  and no circulation was imposed on the approach flow. They found that for cross-flow, there are certain limiting values of Fr, Re and We and beyond these values  $S_c$  is independent of them. In addition, these values decrease with increase in approach flow. However, it was found difficult to obtain these limiting values for still water, since the approach flow is very small. From both observations, they conclude that these limiting values depend on the flow and the geometrical conditions. From their study about boundary friction effects, they obtained that the

friction effects of boundary sections close to the free surface depend on the ratio of the intake velocity to the approach velocities,  $Fr$ ,  $Re$  and  $We$ . In addition, if the vertical clearance of the uppermost edge of a submerged boundary to the free surface is larger than  $0.1xS_c$ , its frictional effect becomes negligible.

An experimental study was performed by Amiri et al. (2011) to prevent air-entraining vortex formation at power intakes by using horizontal perforated and solid plates and also to examine loss coefficient of the intake due to possible effects of anti-vortex plates. Experiments conducted on a horizontal intake and guide vanes were used in order to increase circulation and obtain a stable air core vortex. Experiments show that when  $Fr$  and the vane angle increase or  $S_c/D_i$  ratio decreases, the circulation number rises. As a result of the experiments, it was found that the dimensions of the perforated plates do not have any effect on the formation of vortices whereas opening percentage of them has a definite effect on elimination of air-entraining vortices (a perforated plate with dimensions of  $1D_i$  in width,  $1.5D_i$  in length and 50% uniform opening is adequate for suppression). In the contrary, dimensions of solid plates have a great importance on prevention of them (a solid plate with  $1.5D_i$  in width and  $2D_i$  in length is sufficient for prevention). In addition, for  $Fr > 1.2$ , intake loss coefficient becomes independent of the submerged depth.

## CHAPTER 3

### MODELLING OF AIR-ENTRAINING VORTICES

#### 3.1 Introductory Remarks

The formation of air-entraining vortices is the consequence of the complex interaction between the geometry of the intake zone and approach channel, the flow velocity and the liquid properties such as surface tension and viscosity. The flow near the intake is quite complex, therefore, it cannot be easily solved by theoretical formulations except use of the idealized shape of the intake zone. Consequently, design of intakes to be free of objectionable air-entraining vortices is based either on past experience or on physical-model studies.

#### 3.2 Dimensionless Parameters

To determine all dimensionless parameters which influence fluid flow, all the variables can be listed under three titles of major modelling elements, based on the dimensional analysis theory.

- Fluid Properties: Density of the fluid ( $\rho$ ), dynamic viscosity of the fluid ( $\mu$ ), and surface tension of the fluid ( $\sigma$ ).
- Flow Properties: Average velocity of the flow at the intake pipe ( $V_i$ ), average circulation imposed to flow ( $\Gamma$ ), and gravitational acceleration ( $g$ ).
- Geometric Properties of the Intake Zone: Diameter of the intake pipe ( $D_i$ ), the distance between the lowest point of the intake and the reservoir bottom ( $c$ ), left-side-wall distance of the reservoir to the intake center line ( $b_1$ ) and right-side-wall distance of the reservoir to the intake center line ( $b_2$ ).

Considering an intake type shown in Figure 3.1, the critical submergence,  $S_c$ , (defined as the one which is sufficient to prevent the formation of air-entraining vortices) may be expressed by the following function:

$$S_c = f_1(\rho, \mu, \sigma, g, V_i, \Gamma, D_i, c, b_1, b_2) \quad [3.1]$$

where  $S_c$  is the vertical distance between the reservoir water level and the top of the intake pipe.

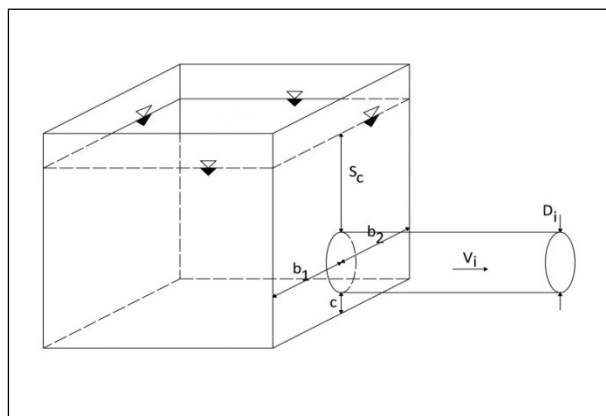


Figure 3.1 Modelling elements for the experimental intake structure

By using dimensional analysis, the following relation is obtained between the dimensionless parameters.

$$\frac{S_c}{D_i} = f_2 \left( \frac{b_1}{D_i}, \frac{b_2}{D_i}, \frac{c}{D_i}, \text{Re}, \text{Fr}, \text{We}, K_o \right) \quad [3.2]$$

where

$$\text{Re} = \text{Intake Reynolds number} = \frac{V_i D_i \rho}{\mu}$$

$$\text{Fr} = \text{Intake Froude number} = \frac{V_i}{\sqrt{g D_i}}$$

$$\text{We} = \text{Intake Weber number} = \frac{\rho V_i^2 D_i}{\sigma}$$

$$K_o = \text{Intake Kolf number} = \frac{\Gamma}{V_i D_i}$$

In the experimental setup used the bottom clearance,  $c$ , is always equal to zero and hence  $c/D_i$  ratio can be removed from Equation 3.2. In addition,  $b_1$  and  $b_2$  can be removed from the equation and written as  $2b/D_i$  since the plexiglass side walls were placed as they had equal distances from the center line of the intake pipe to have symmetrical approach flow toward the intake. Consequently, after these arrangements Equation 3.2 can be written as

$$\frac{S_c}{D_i} = f_2 \left( \frac{2b}{D_i}, \text{Re}, \text{Fr}, \text{We}, K_o \right) \quad [3.3]$$

In a completely similar model, the dimensionless geometric parameters would be the same in the model and the prototype. Equality of  $S_c/D_i$  in the model and the prototype, in general, requires equality of the dimensionless parameters, Fr, Re, We and  $K_o$ , between the model and the prototype and to obtain this equality at the same time is impossible. Therefore, the following discussion about these dimensionless parameters was made to evaluate the importance of these parameters and to enable the designer to decide upon the suitable modelling criteria for his study.

### 3.2.1 Influence of Kolf Number

Circulation depends on the characteristics of the approach flow, the geometry of the intake chamber and the discharge. Since no imposed circulation is applied to the flow and all geometric parameters of the intake pipe, intake zone and approach channel are already in Equation 3.1, the circulation parameter,  $\Gamma$ , could be deleted from this equation. Consequently, Kolf number which is the dimensionless parameter that shows the effect of circulation can be removed from Equation 3.3 and then it becomes

$$\frac{S_c}{D_i} = f_2 \left( \frac{2b}{D_i}, \text{Re}, \text{Fr}, \text{We} \right) \quad [3.4]$$

### 3.2.2 Influence of Weber Number

In literature, Weber number is accepted as it is effective in weak dimple like vortices. Some of researchers like Anwar et al. (1978), Jain et al. (1978) and Padmanabhan and Hecker (1984) stated that the effect of surface tension can be removed from the air-entraining vortex equation if We is greater than  $10^4$ , 120 and 600, respectively. Also, many researcher eliminated surface tension parameter without giving a limit number. Since the limit values proposed by several researchers

cover a wide range and mostly based on experiments conducted in vertical intakes, in this study the analysis related to We is made to show its effect on the formation of air-entraining vortices.

### **3.2.3 Influence of Reynolds Number**

There are different views on the role of Reynolds number in vortex formation in literature. Zielinski and Villemonte (1968), Daggett and Keulegan (1974), Anwar et al. (1978), Jain et al. (1978), and Padmanabhan and Hecker (1984) studied on the formation of vortices and proposed limit values, above which the effect of Reynolds number becomes negligible, as  $1 \times 10^4$ ,  $5 \times 10^4$ ,  $3 \times 10^4$ ,  $5 \times 10^3$  and  $7.7 \times 10^4$ , respectively. In addition, there are many limit values of Reynolds number found by other studies which are not mentioned here. In order to show the effect of the Reynolds number on the formation of air-entraining vortices, this number is also included into the analysis in this study.

### **3.2.4 Influence of Froude Number**

Until now, practically all studies about vortex formation, have emphasized that Froude number is the most important parameter influencing the critical submergence. This acceptance is obvious because air-entraining vortex formation is a free surface phenomenon and affected by gravity. Therefore, model studies performed are mainly based on the Froude similitude. For this reason, the Froude number is going to be the main parameter to be investigated in the formation of air-entraining vortices in this study.

After the evaluation of these parameters affecting air-entraining vortex formation, the final form of the Equation 3.4 remains as it is and experimental works were conducted based on the parameters of Equation 3.4.



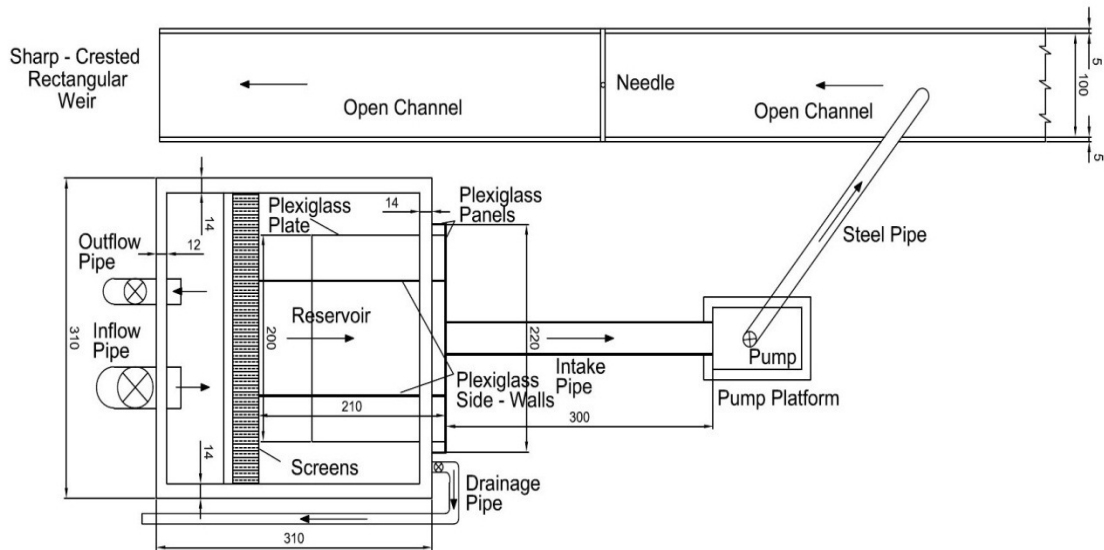
## CHAPTER 4

### EXPERIMENTAL EQUIPMENT AND PROCEDURE

#### 4.1 Experimental Equipment

An experimental concrete reservoir was built to analyze effect of hydraulic parameters on the formation of air-entraining vortices at horizontal intakes. The reservoir, shown in Figures 4.1 – 4.5, is 3.10 m in length and width and 2.20 m in depth and consisting of a dead-volume section, an active reservoir section and an intake section. A diaphragm slab was built to create a dead-volume section and active reservoir section by dividing reservoir into two parts in the horizontal plane and a 90 cm space was left between the slab and the rear wall of the reservoir so that water could reach the active reservoir part while the dead volume is filling. Screens were placed over the end of the slab and fastened to the reservoir side walls to provide energy dissipation of water and uniform motion of water without any waves and circulation in the reservoir. A part of front of the dead-end above the diaphragm slab, 2.20 m in length, 0.30 m in width and 1.20 m in depth, was extended from the reservoir front plane and was made of plexiglass panels to obtain a good observation behind the intake entrance and these panels are attached to each other with waterproofed silicone paste and to the reservoir walls with screws and waterproofed silicone paste. In order to increase its stability, a steel framework was constructed outside of the plexiglass panels. Two plexiglass side walls were placed orthogonally between the extended dead-end and screens and their location could be altered so that the effect of the side wall clearance on the formation of air-entraining vortices could be observed. Plexiglass intake pipes of diameters 30.0 cm, 25.0 cm, 19.4 cm, 14.4 cm, 10.0 cm and 5.0 cm were installed to the extended dead-end for each set of experiments in this order. In order to provide a space for the attachment of the intake pipe, a square hole was opened at the plexiglass dead-end in such a way that the center line of this hole would have an equal distance to the side walls of the reservoir. After mounting the pipe of desired diameter on this hole, a plexiglass plate was placed to the bottom of the reservoir so that the bottom clearance of the pipe would be zero. The intake pipes were connected to a 10.0 kW centrifugal pump which conveys water to a steel pipe 16.5 cm in diameter. Water falls freely from the steel pipe to an open channel which ends with a rectangular sharp-crested weir with 17 cm height and 1 m in width. A point gage was placed to this channel to obtain the water surface elevation with respect to the weir crest to use in the calculation of volumetric flow rate. The calibration of the sharp-crested weir was done by using an acoustic discharge measurement device before the experiments started. The required flow is provided from a large elevated-constant head tank via an inflow pipe 80 cm in diameter. This pipe enters the reservoir below the bottom level of the diaphragm slab in order to fill the dead-volume section first so that the active reservoir section fills and water level rises calmly. In addition, a drainage pipe, to equalize the inflow to outflow, is connected to the front dead-end section. The discharged water from the weir and the drainage pipe was conveyed to the sump below the laboratory and water in the sump is conveyed by another pump to the elevated water tank.

a) Plan view



b) Side view

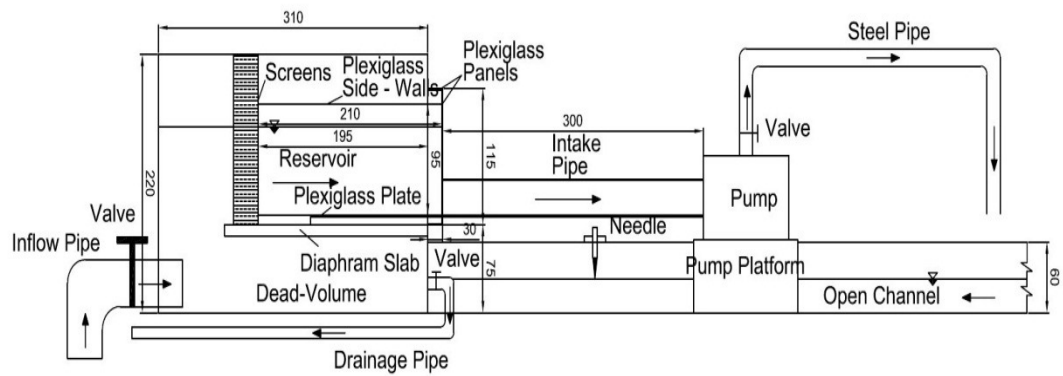


Figure 4.1 Plan (top) view and side view of the physical model (dimensions are given in cm)



Figure 4.2 General view of the experimental setup



Figure 4.3 Experimental setup with intake pipe of  $D_i = 25$  cm



Figure 4.4 Experimental setup with intake pipe of  $D_i = 14.4$  cm



Figure 4.5 Experimental setup with intake pipe of  $D_i = 5$  cm

To test anti – vortex devices in the reservoir, 10 plexiglass plates, shown in Figures 4.6 and 4.7, were prepared. Five of them are 40 cm in length and 5, 10, 15, 20 and 25 cm in width and the rest of them are 50 cm in length and 5, 10, 15, 20 and 25 cm in width. In order to test these plates, a steel bar was connected to the middle of one end of the plate and corners at the other end were cropped to obtain smooth flow around anti – vortex plates. The plates were placed on a pair of needles 2 mm in diameter mounted just over the intake entrance and removed from the reservoir via this steel bar during testing.



Figure 4.6 Anti – vortex plates with 40 cm in length



Figure 4.7 Anti – vortex plates with 50 cm in length

## 4.2 Experimental Procedure

After installation of each intake pipe, the plexiglass side walls were adjusted at required distances into the reservoir and leveling the plexiglass plane at the bottom accordingly, the experimental setup became ready for the experiment. In the experiments six different diameter pipes were used and for each pipe, six different side wall clearances ( $2b = 40, 60, 80, 100, 120$  and  $140$  cm) were tested for a series of discharges. In each experiment, the discharge and water surface level were measured when an air-entraining vortex initiated. In addition, the anti-vortex plates were tested for the highest, one of the middle and one of the lower discharges for each side wall clearance if the air-entraining vortex formation was available. The experimental results of the critical submergence and the related dimensionless parameters are given in Appendix A and the experimental results related to anti-vortex plates are presented in Appendix B.

Before starting the experiment in the reservoir, firstly, the water was pumped from a sump which is below the laboratory to an elevated water tank to obtain a constant head. To start the experiment, the inflow pipe was opened and the reservoir was filled to a level which is above the critical submergence. Then, by turning on the pump and opening the valve on the pumping line, water was conveyed from the reservoir to the open channel. By measuring the water surface elevation from the open channel and using the rectangular weir formula (Rehbock Formula), the discharge was calculated. The desired discharges were obtained by adjusting the valve on the pumping line. The openings of the valve on the pumping line, the inflow pipe valve and the drainage pipe valve were arranged so that the inflow was almost the same as the outflow. Therefore, a constant and calm water surface level was obtained to start observation of the vortex formation steps. Then, by opening the drainage pipe valve at a very small amount, the water level is decreased gradually until observing the formation of swirls, surface depressions and finally air-entraining vortices on the free surface (This process took 30 minutes to 2 hours for different experiments). At this point, the water level and the location of the formation of the air-entraining vortex were noted for that discharge. By changing the opening of the valve on the pumping line and the valve of the inflow pipe, various values of discharges and the dimensionless numbers were obtained for each side wall opening and pipe diameter. This procedure was started with the maximum discharge provided by the pump with fully open valve on the discharge pipe and continued with reduced discharges by closing the valve at small rates until getting the minimum discharge which resulted in air-entraining vortex. However, due to safety of the plexiglass intake pipes with diameters of  $10.0$  cm and  $5.0$  cm, they were tested at lower discharges due to the possibility of cavitation, which causes extreme negative pressure, started at the entrance of the intake pipe at higher discharges due to extreme suction of the pump.

During each set of experiments, the anti-vortex plates were tested for the maximum, one of the middle and one of the lower discharges when the air-entraining vortex just occurred. These aforementioned discharges at which the anti-vortex devices were tested were not always available for all intake pipes and side wall clearances. While the total side wall clearance was  $40$  cm, the plates  $50$  cm in length could not be tested due to the length restriction. At the test of the anti-vortex plates first, an air-entraining vortex was determined at the entrance of the intake pipe and then, the water depth in the reservoir, the discharge and the location of the vortex were noted (This process took 10 minutes for each anti-vortex plate). After that, by placing each plate over the initially located needles just over the pipe entrance, the water surface was observed for the formation and location of the vortices.

## 4.3 Observations

In the experiments, all the vortices formed and dissipated in a very short time. Therefore, they were intermittent type vortices. Except for  $2b = 40$  cm, all the vortices occurred near the intake pipe entrance. Only for  $2b = 40$  cm, the vortices occurred at the boundaries near the plexiglass side walls. The formation steps of the air-entraining vortices in the experiments were as in ARL vortex type classification. While the water level in the reservoir was decreased at a very small amount, the water surface was observed for any vortex formation by naked eye. Weak surface swirl, surface dimple, swirl throughout water column, vortex pulling floating trash, vortex pulling air bubbles and full air

core were observed in this order. First, a weak surface swirl occurred and disappeared. Next, rotational velocity increased at the center of the swirl and a dimple formed. Then, a vortex tail occurred and trash and air bubble ingestion started respectively. When the water level reached to the critical submergence, full air core vortex started to occur at the entrance of the intake. However, all air core vortices were not continuous. They formed and disappeared in a few seconds. If water level was continued to decrease, stronger vortices were formed and their occurrence density increased with the lower water levels.

After observation of a full air core vortex at the entrance of the intake pipe for; the maximum, one of the middle and one of the lower discharge, its location was noted. Then, an anti-vortex plate was placed at the entrance of the intake pipe. Next, water surface was observed for any formation of vortices. The observations were made for three kinds of formations, namely, full air core, air bubble entrance and vortex tail. Also, despite of an anti-vortex plate, if there were any formation of vortex, it was evaluated and its location was noted to compare with the initial location. The same procedure was repeated for other anti-vortex plates.

Some of the pictures taken during experiments are shown in Figures 4.8 – 4.10.



Figure 4.8 A picture showing an air-entraining vortex at the pipe of  $D_i = 5$  cm despite of anti-vortex plate



Figure 4.9 View of an air-entraining vortex forming at higher submergence



Figure 4.10 Vortex formation at the pipe of  $D_i = 25$  cm

## CHAPTER 5

### DISCUSSION OF THE RESULTS

#### 5.1 Introduction

In this chapter, firstly, by using the data collected in the present study, the related graphs were prepared by means of dimensionless parameters as it was mentioned in Equation 3.4;  $S_c/D_i$  versus  $Fr$ ,  $Re$  and  $We$  as a function of  $2b/D_i$  values, for each set of experiments for six different intake pipe diameters. Then, these graphs were analyzed for their variation with the aforementioned dimensionless parameters and the effect of the side wall clearances on the critical submergence ratio. Moreover, curve fitting was applied to the available data by regression analysis to find empirical equations for the critical submergence ratio in terms of different dimensionless parameters. Next, the available data were checked for the possible scale effects. After that, derived equations were compared with the available formulas in the literature. Finally, the use of anti-vortex plates was evaluated. The summary of the present study in terms of related important dimensionless parameters for the critical submergence cases and anti-vortex plate cases are presented in Tables 5.1 and 5.2, respectively. Detailed results of the aforementioned experimental studies are given in Appendix A and Appendix B.

Table 5.1 Summary of the important parameters for which the critical submergence experiments were conducted

$D_i$ (cm)	Range of						Number of Observations
	$Q_i$ (lt/s)	$S_c/D_i$	$Fr$	$Re$	$We$	$2b/D_i$	
30.0	61.57	1.907	0.508	260165	3118	4.667	41
	~	~	~	~	~	~	
	36.79	0.283	0.303	155457	1113	1.333	
25.0	62.55	2.428	0.814	317168	5561	5.600	65
	~	~	~	~	~	~	
	24.34	0.436	0.317	123419	842	1.600	
19.4	62.55	3.325	1.534	408721	11902	7.216	73
	~	~	~	~	~	~	
	21.69	0.644	0.532	141729	1431	2.062	
14.4	62.55	5.243	3.231	550638	29102	9.722	67
	~	~	~	~	~	~	
	21.69	1.069	1.120	190941	3499	2.778	
10.0	51.65	6.650	6.638	654745	59251	12.000	50
	~	~	~	~	~	~	
	21.37	1.880	2.747	270898	10143	4.000	
5.0	14.69	4.420	10.680	372438	38343	16.000	12
	~	~	~	~	~	~	
	6.66	1.900	4.842	168852	7881	8.000	

Table 5.2 Summary of the important parameters for which the experiments related to anti-vortex plates were conducted

$D_i$ (cm)	Range of					Number of Observations
	Fr	$S_c/D_i$	$2b/D_i$	$L_p/D_i$	$W_p/D_i$	
25.0	0.814	1.192	5.600	2.000	1.000	150
	~ 0.357	~ 0.436	~ 2.400	~ 1.600	~ 0.200	
19.4	1.534	3.325	7.216	2.577	1.289	160
	~ 0.743	~ 0.871	~ 2.062	~ 2.062	~ 0.258	
14.4	3.231	5.243	9.722	3.472	1.736	145
	~ 1.566	~ 1.250	~ 2.778	~ 2.778	~ 0.347	
10.0	6.638	6.650	12.000	5.000	2.500	115
	~ 3.085	~ 2.010	~ 4.000	~ 4.000	~ 0.500	
5.0	10.680	4.420	16.000	10.000	5.000	25
		~ 3.620	~ 8.000	~ 8.000	~ 1.000	

## 5.2 The Dimensionless Critical Submergence and the Relevant Dimensionless Parameters

By using the data collected from the present experiments, variation of  $S_c/D_i$  with the related dimensionless parameters, Fr, Re and We, as a function of  $2b/D_i$  was drawn for each intake pipe diameters of  $D_i = 30, 25, 19.4, 14.4, 10$  and  $5$  cm, in Figs 5.1 – 5.18.

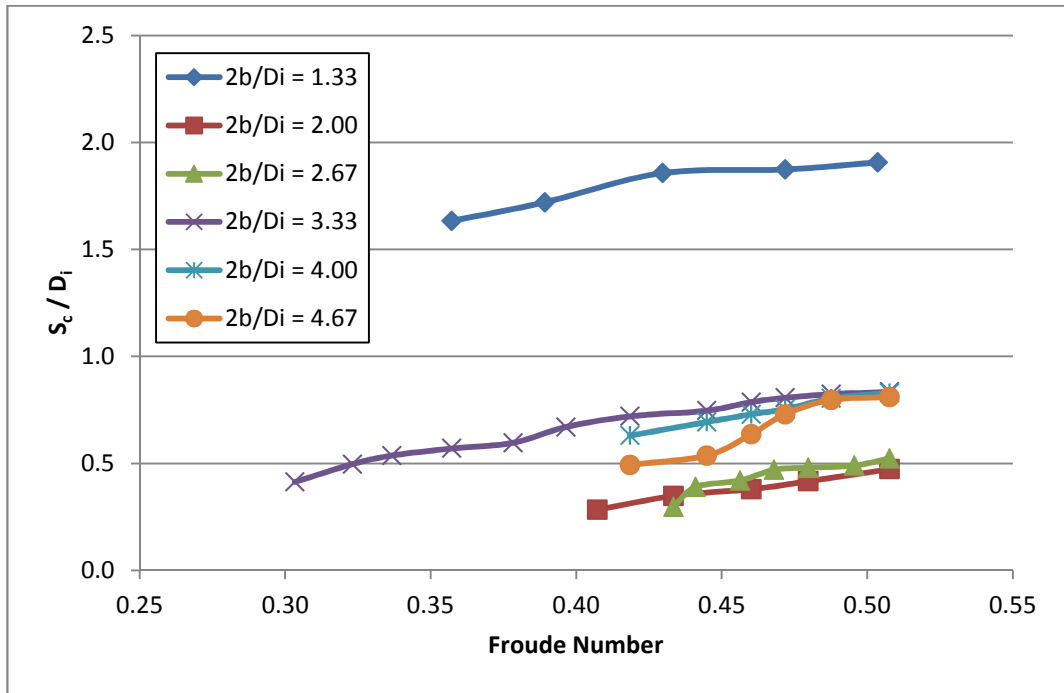


Figure 5.1 Variation of  $S_c/D_i$  with Froude number as a function of  $2b/D_i$  for the pipe of  $D_i = 30$  cm

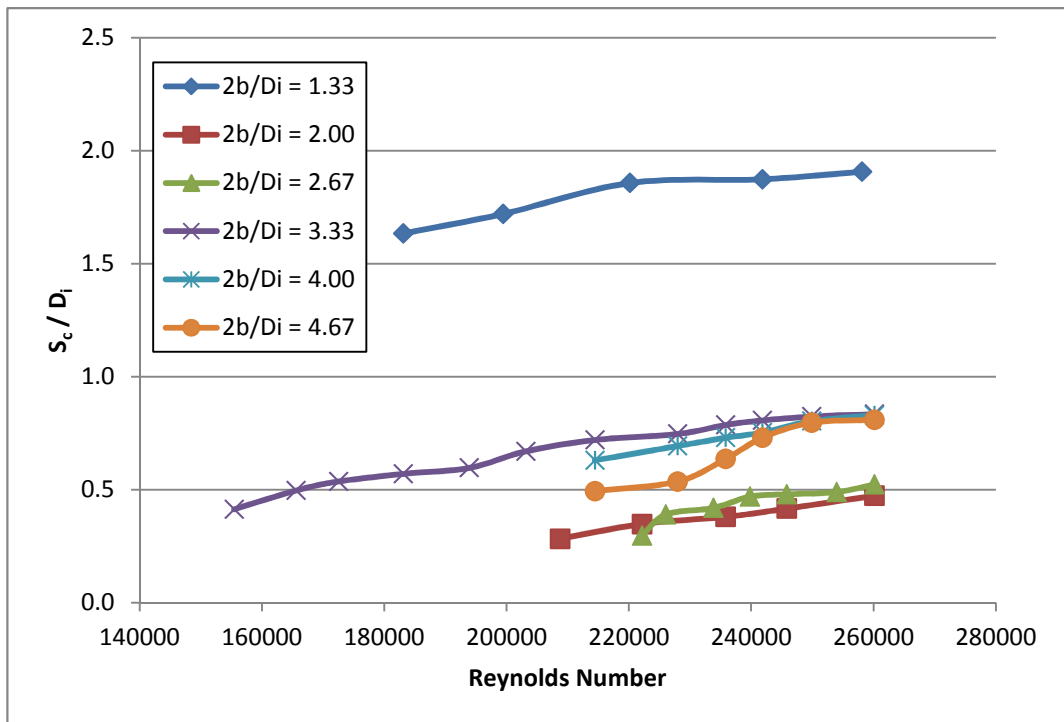


Figure 5.2 Variation of  $S_c/D_i$  with Reynolds number as a function of  $2b/D_i$  for the pipe of  $D_i = 30$  cm

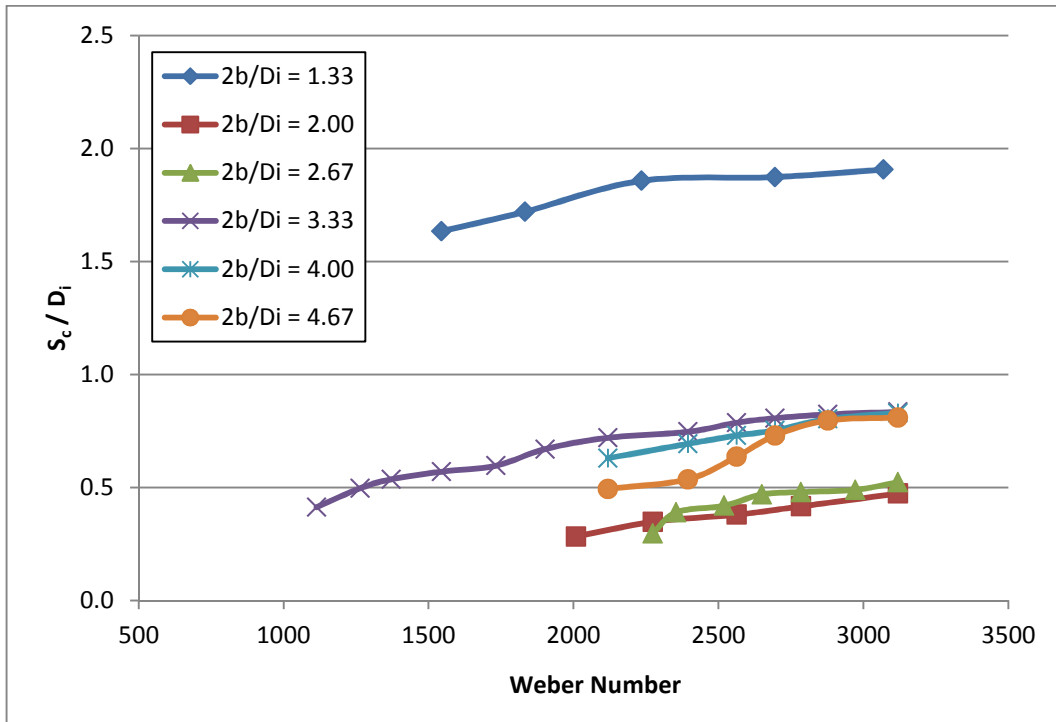


Figure 5.3 Variation of  $S_c/D_i$  with Weber number as a function of  $2b/D_i$  for the pipe of  $D_i = 30$  cm

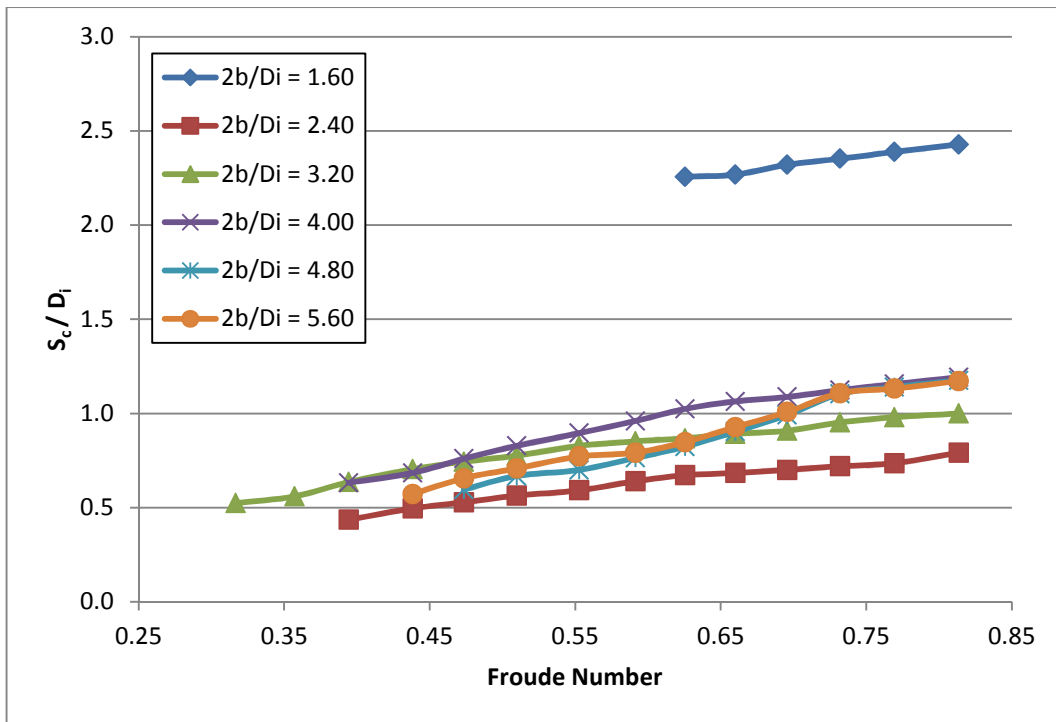


Figure 5.4 Variation of  $S_c/D_i$  with Froude number as a function of  $2b/D_i$  for the pipe of  $D_i = 25$  cm

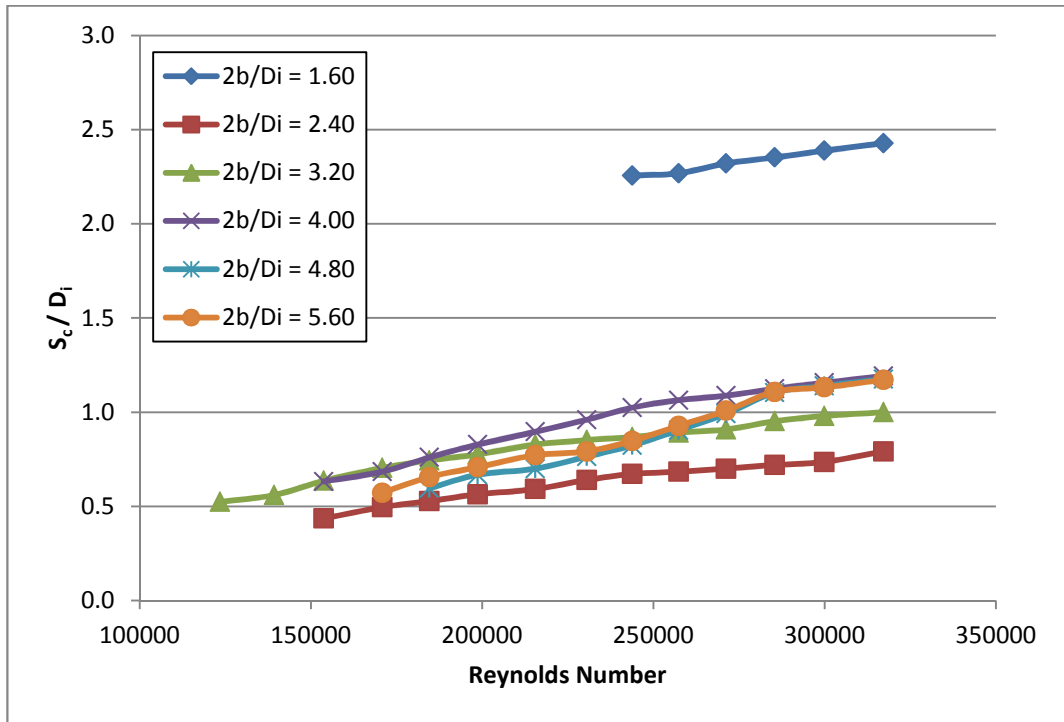


Figure 5.5 Variation of  $S_c/D_i$  with Reynolds number as a function of  $2b/D_i$  for the pipe of  $D_i = 25$  cm

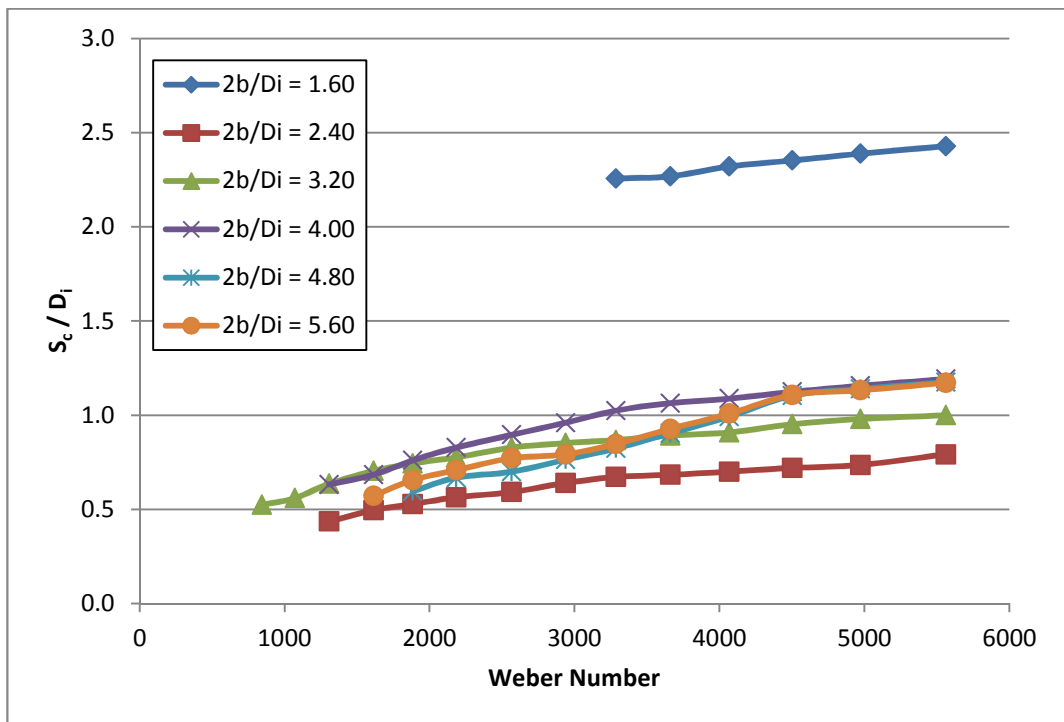


Figure 5.6 Variation of  $S_c/D_i$  with Weber number as a function of  $2b/D_i$  for the pipe of  $D_i = 25$  cm

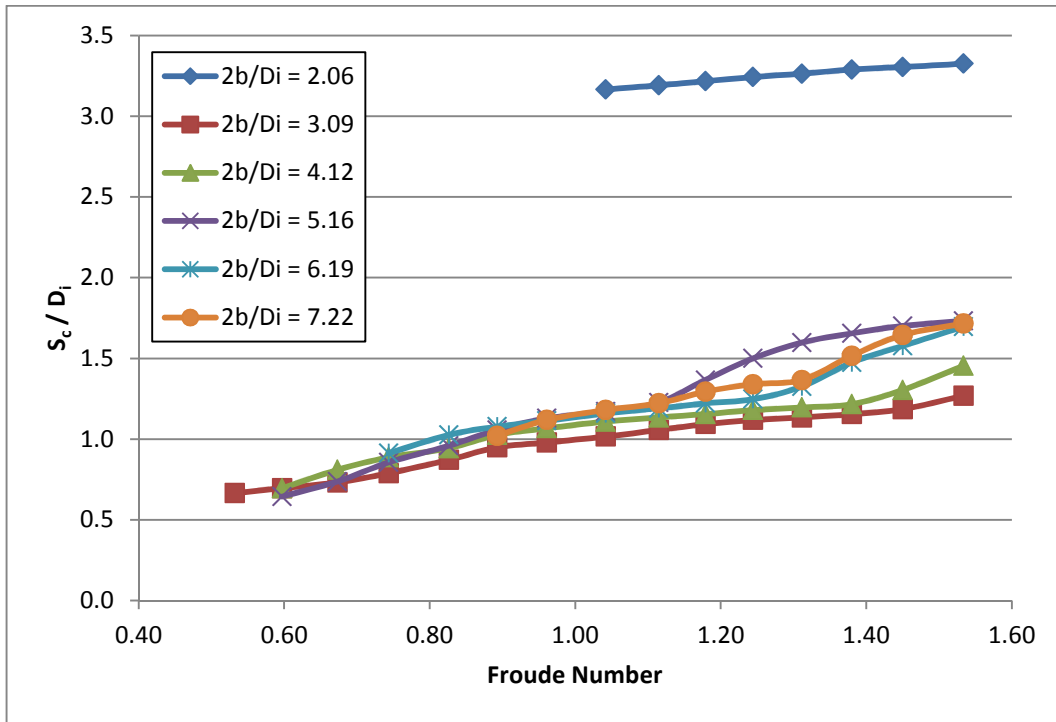


Figure 5.7 Variation of  $S_c/D_i$  with Froude number as a function of  $2b/D_i$  for the pipe of  $D_i = 19.4$  cm

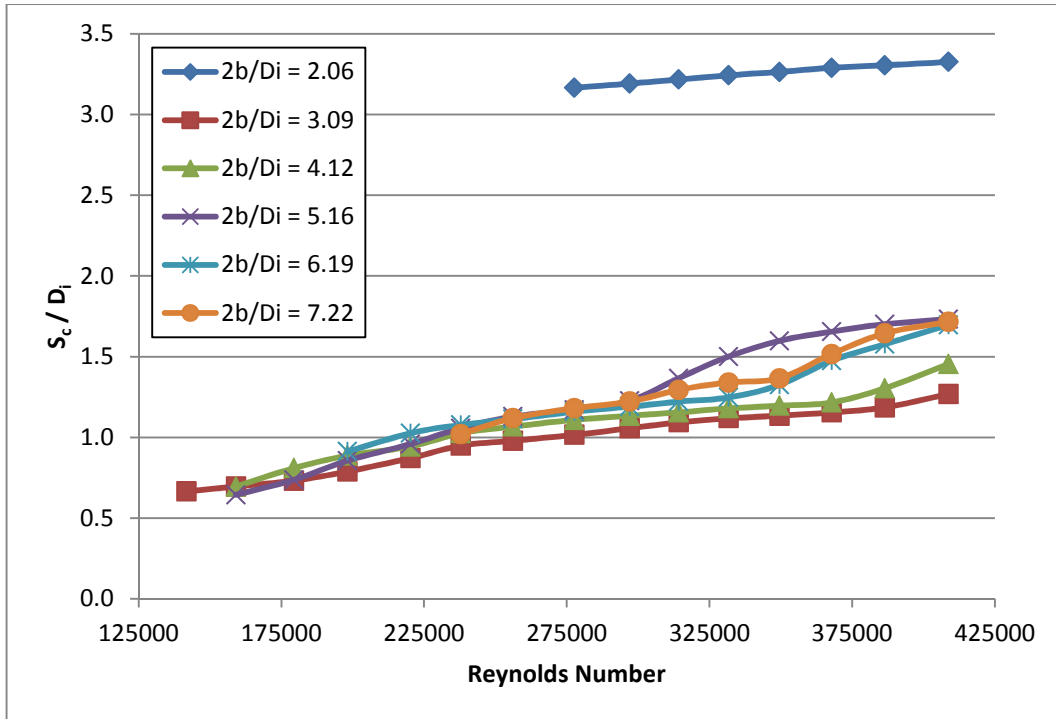


Figure 5.8 Variation of  $S_c/D_i$  with Reynolds number as a function of  $2b/D_i$  for the pipe of  $D_i = 19.4$  cm

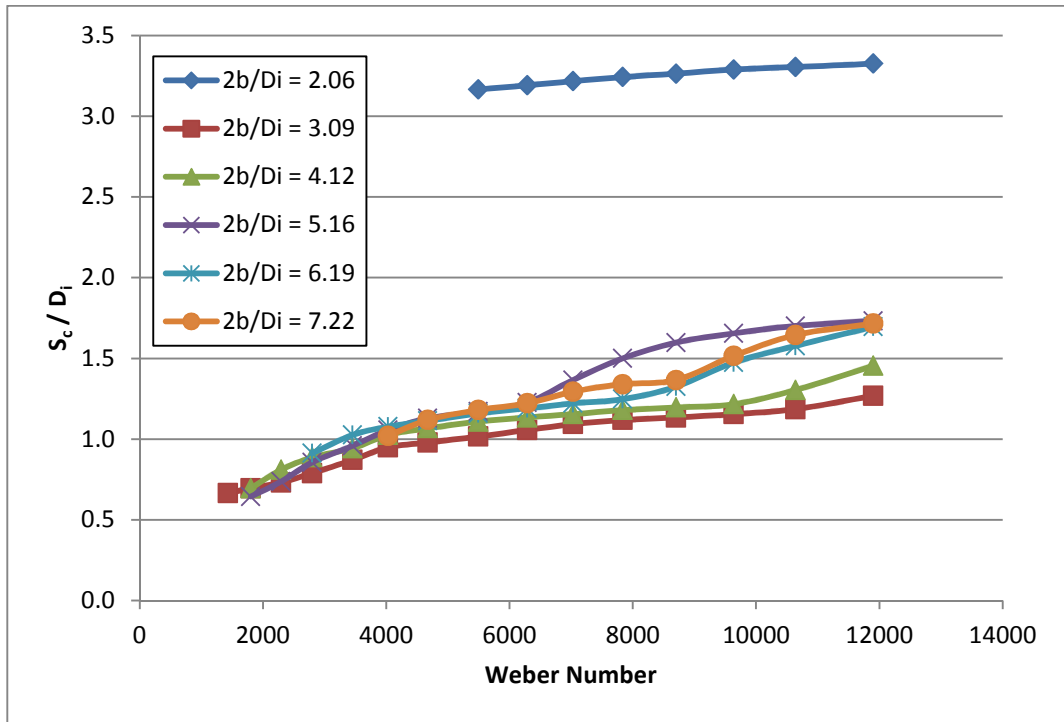


Figure 5.9 Variation of  $S_c/D_i$  with Weber number as a function of  $2b/D_i$  for the pipe of  $D_i = 19.4$  cm

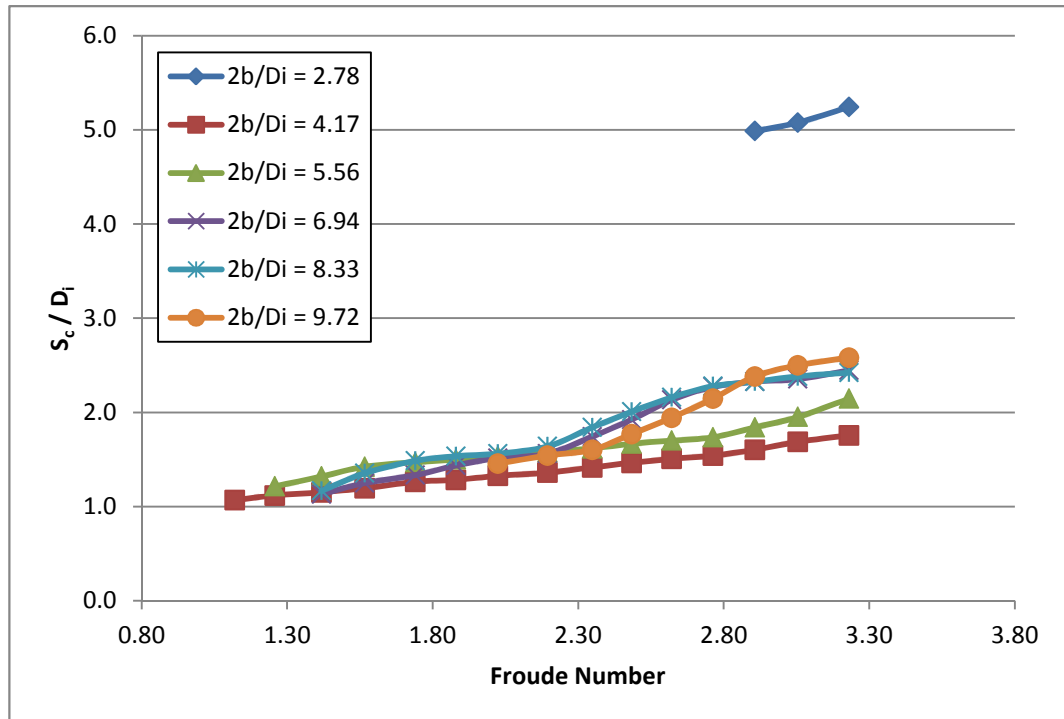


Figure 5.10 Variation of  $S_c/D_i$  with Froude number as a function of  $2b/D_i$  for the pipe of  $D_i = 14.4$  cm

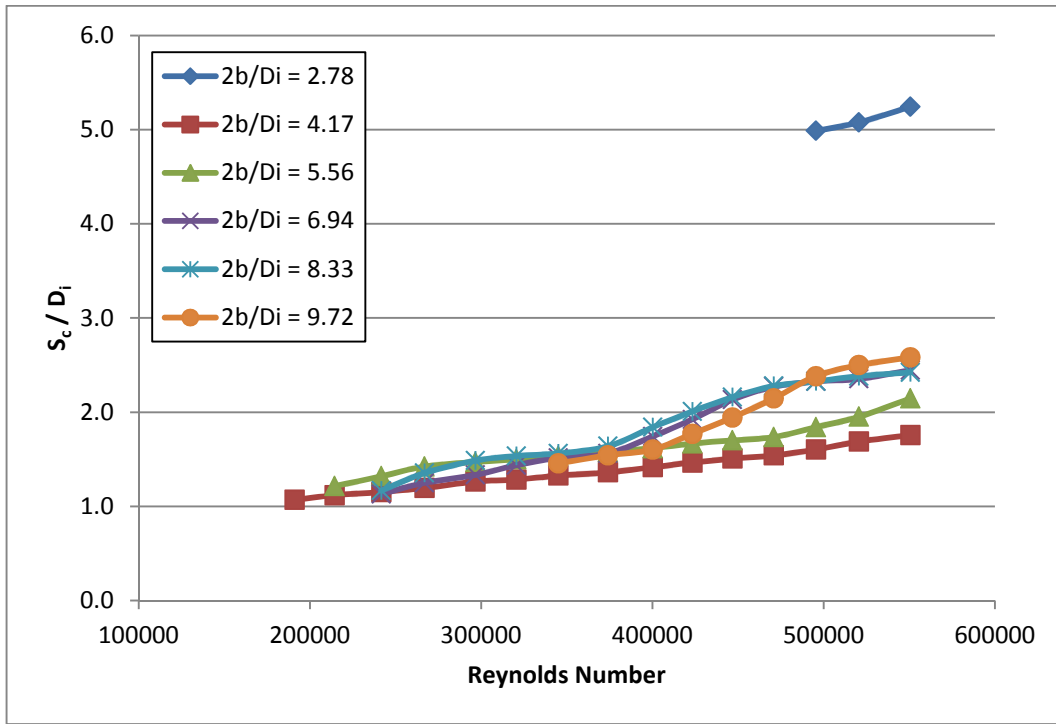


Figure 5.11 Variation of  $S_c/D_i$  with Reynolds number as a function of  $2b/D_i$  for the pipe of  $D_i = 14.4$  cm

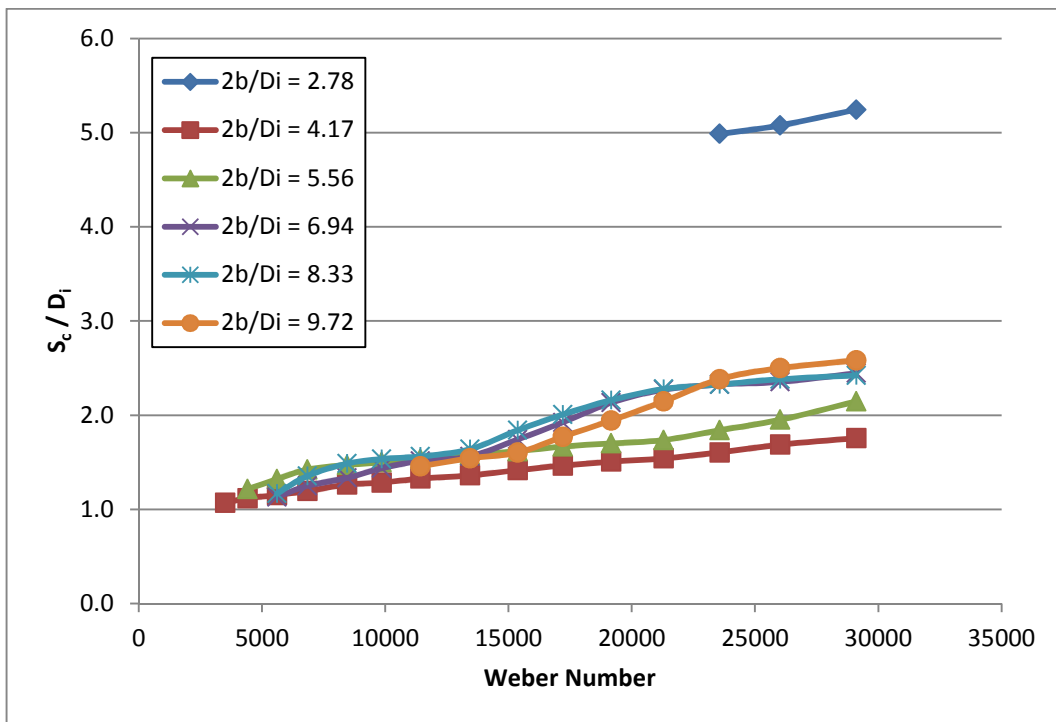


Figure 5.12 Variation of  $S_c/D_i$  with Weber number as a function of  $2b/D_i$  for the pipe of  $D_i = 14.4$  cm

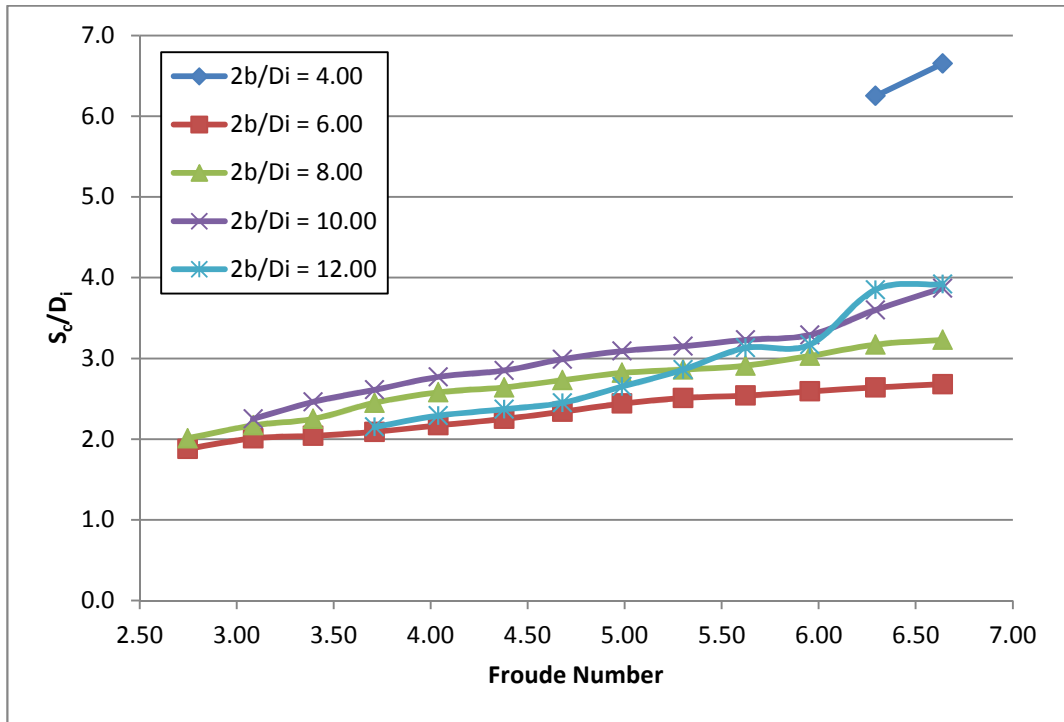


Figure 5.13 Variation of  $S_c/D_i$  with Froude number as a function of  $2b/D_i$  for the pipe of  $D_i = 10$  cm

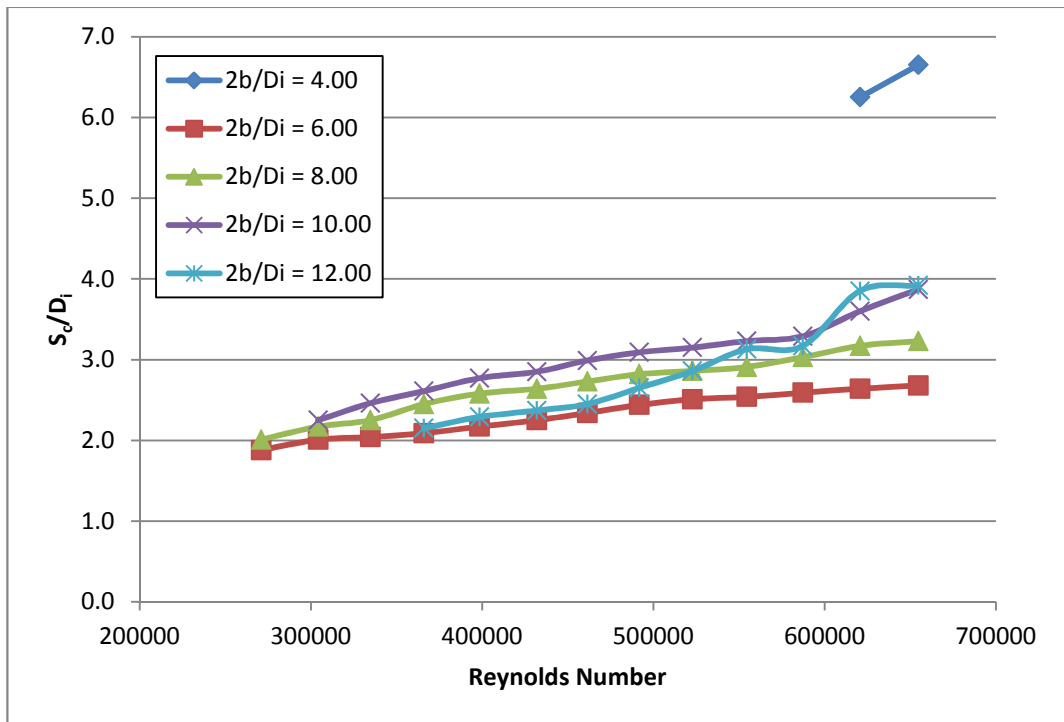


Figure 5.14 Variation of  $S_c/D_i$  with Reynolds number as a function of  $2b/D_i$  for the pipe of  $D_i = 10$  cm

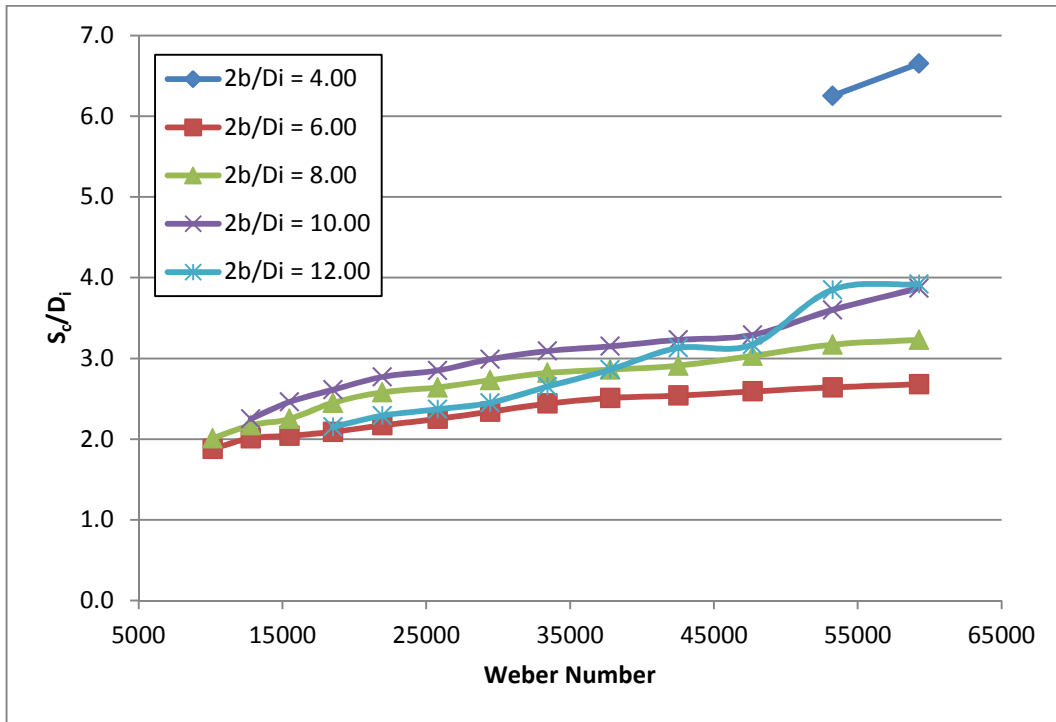


Figure 5.15 Variation of  $S_c/D_i$  with Weber number as a function of  $2b/D_i$  for the pipe of  $D_i = 10$  cm

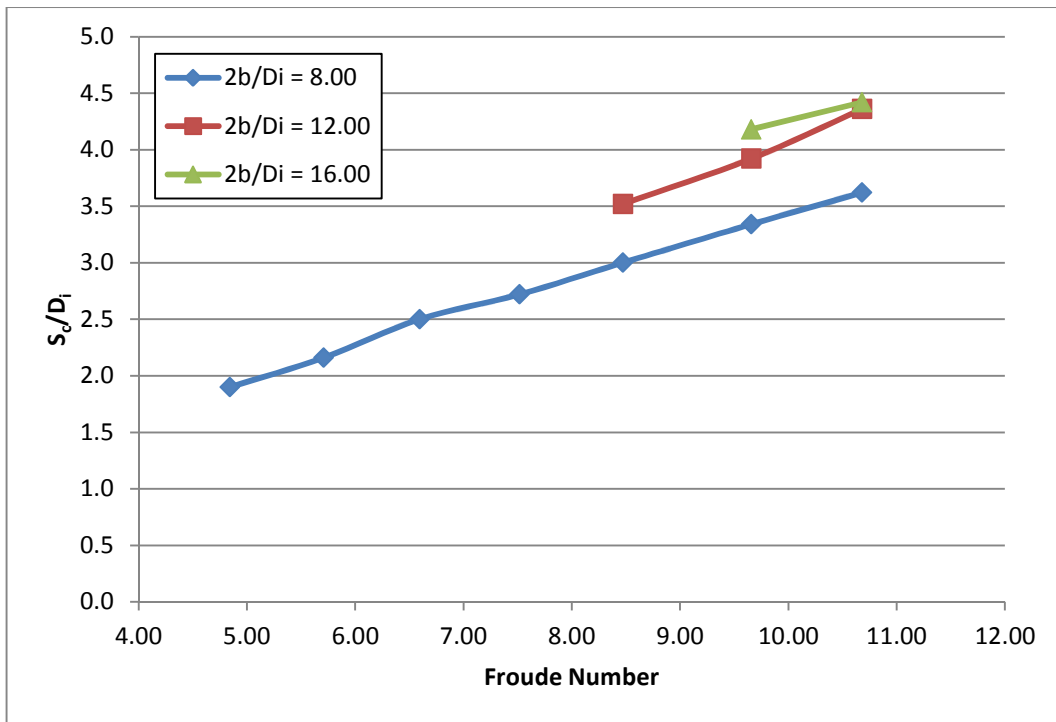


Figure 5.16 Variation of  $S_c/D_i$  with Froude number as a function of  $2b/D_i$  for the pipe of  $D_i = 5$  cm

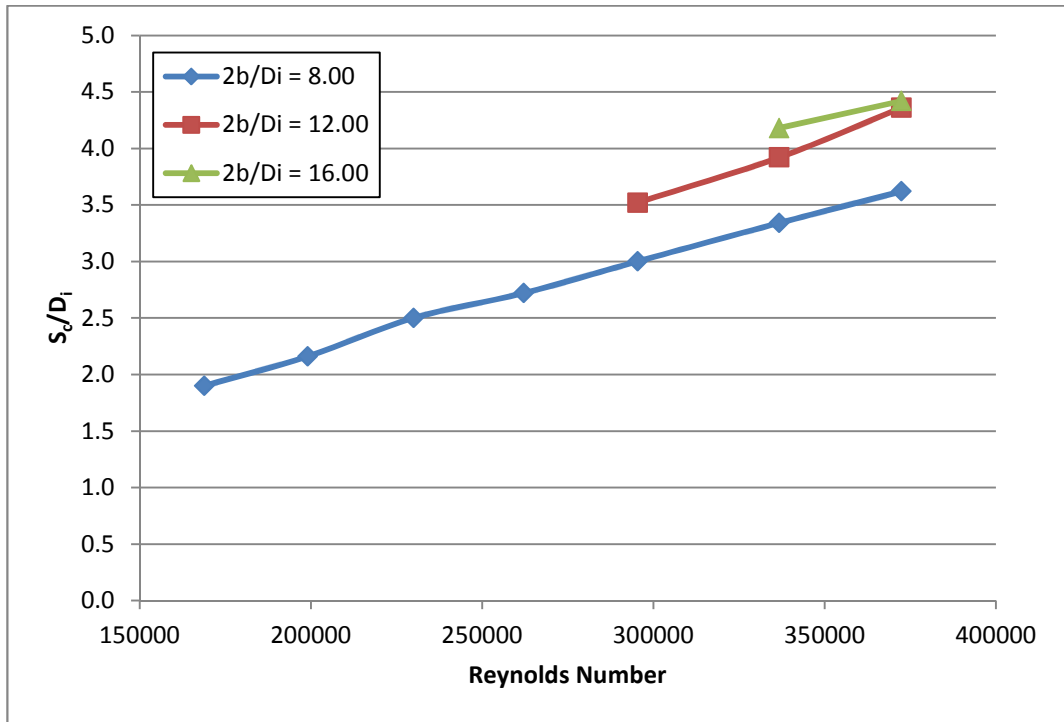


Figure 5.17 Variation of  $S_c/D_i$  with Reynolds number as a function of  $2b/D_i$  for the pipe of  $D_i = 5$  cm

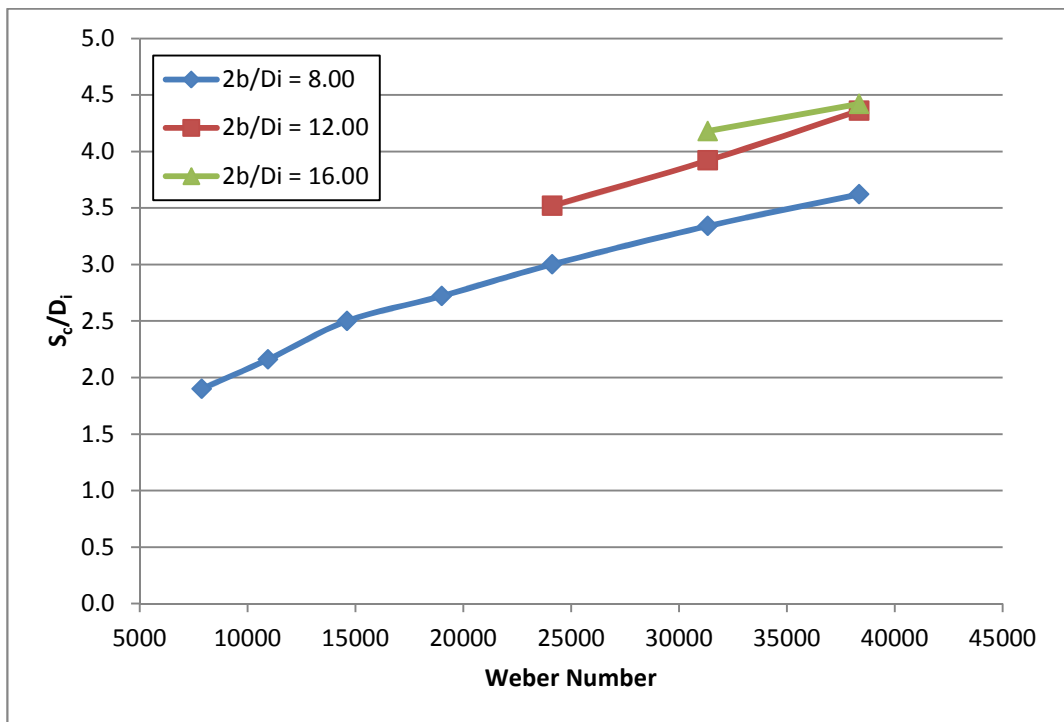


Figure 5.18 Variation of  $S_c/D_i$  with Weber number as a function of  $2b/D_i$  for the pipe of  $D_i = 5$  cm

From these figures the following assessments can be made:

$S_c/D_i$  values increase gradually with increasing Fr, Re and We for a given  $2b/D_i$  value of an intake pipe of known diameter. At the smallest  $2b/D_i$  value ( $2b = 40$  cm) of an intake pipe tested the maximum values of  $S_c/D_i$  are obtained except the intake pipe of  $D_i = 5$  cm. At the next larger and following  $2b/D_i$  values ( $2b = 60$  cm and  $80$  cm except the intake pipe of  $D_i = 5$  cm) the minimum  $S_c/D_i$  values are measured.

For the remaining  $2b/D_i$  values tested the variation of  $S_c/D_i$  with  $2b/D_i$  as a function of Fr, Re and We is not very significant and becomes almost negligible as the related parameter, Fr, Re or We, increases. The data of  $S_c/D_i$  for these intermediate values of  $2b/D_i$  coincide with each other at the maximum values of Fr, Re and We tested. These maximum values of Fr, Re, We and corresponding limit values of  $2b/D_i$  above which  $S_c/D_i$  is independent of  $2b/D_i$ , as a function of intake diameter of  $D_i$  were determined from the data of Figures 5.1 - 5.18 and listed in Table 5.3. From Table 5.3, Figure 5.19 which shows the limit values of  $2b/D_i$  was prepared and plotted. According to Figure 5.19,  $S_c/D_i$  is independent of side wall clearance as long as  $2b/D_i$  values are larger than those stated on the figure for a given intake pipe diameter, and is only function of Fr, Re and We if Fr is larger than those corresponding values given on the figure (the limit values of other parameters; Re and We, are not given on the figure). The area below the curve given in Figure 5.19 belongs to a zone where  $S_c/D_i$  is a function of  $2b/D_i$  and Fr, while in the area above the curve where  $2b/D_i$  is larger than that stated on the curve,  $S_c/D_i$  is independent of  $2b/D_i$  and function of Fr for an intake of known  $D_i$ . This figure also reveals another important information for the intake pipes of larger diameters not tested in this study. From the general trend of the curve, it can be concluded that as the intake pipe diameter gets larger than  $30$  cm, the rate of change of Fr with  $D_i$  gets smaller and maybe approaches to zero at much higher values of  $D_i$ . At the same time, at larger  $D_i$  values, the limit values for Fr and  $2b/D_i$ , above which  $S_c/D_i$  will be independent of  $2b/D_i$ , get smaller than those of the intake pipe of  $D_i = 30$  cm.

Table 5.3 Limit values of  $2b/D_i$  above which  $S_c/D_i$  is independent of  $2b/D_i$  as a function of Fr, Re and We for the intake pipe of diameter of  $D_i$

$D_i$ (cm)	5.0	10.0	14.4	19.4	25.0	30.0
$2b/D_i \geq$	12.00	10.00	6.94	5.16	4.00	3.33
$Fr \geq$	10.68	6.45	3.20	1.53	0.73	0.50
$Re \geq$	373000	635000	545000	409000	284000	258000
$We \geq$	38400	56000	28500	11900	4460	3000

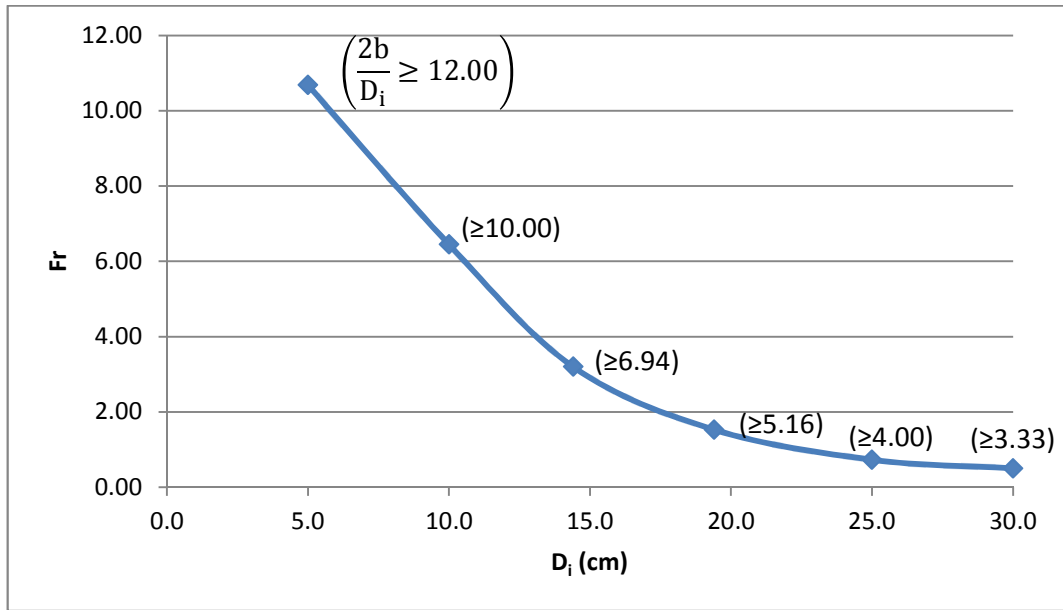


Figure 5.19 Limit values of  $2b/D_i$  above which  $S_c/D_i$  is independent of  $2b/D_i$  and function of  $Fr$ ,  $Re$  and  $We$

Table 5.4 shows  $2b/D_i$  values of the extreme cases which yield the maximum and minimum  $S_c/D_i$  data, as well as intermediate  $S_c/D_i$  data as a function of  $D_i$  and  $2b$  for the intake pipes tested.

Table 5.4  $2b/D_i$  values of the intake pipes of  $D_i$  resulted in maximum, minimum and intermediate  $S_c/D_i$

$D_i$ (cm) \ $2b$ (cm)	5	10	14.4	19.4	25	30
40	8.00	4.00	2.78	2.06	1.60	1.33
60	12.00	6.00	4.17	3.09	2.40	2.00
80	16.00	8.00	5.56	4.12	3.20	2.67
100		10.00	6.94	5.16	4.00	3.33
120		12.00	8.33	6.19	4.80	4.00
140			9.72	7.13	5.60	4.67
2b/D <sub>i</sub> values result in intermediate S <sub>c</sub> /D <sub>i</sub>						
2b/D <sub>i</sub> values result in minimum S <sub>c</sub> /D <sub>i</sub>						
2b/D <sub>i</sub> values result in maximum S <sub>c</sub> /D <sub>i</sub>						

### 5.3 Empirical Equations for Dimensionless Critical Submergence

In Table 5.4,  $2b/D_i$  data of the extreme cases for which the dimensionless critical submergence,  $S_c/D_i$ , was maximum and minimum had been given for the intakes of known diameters as well as those corresponding to the intermediate  $S_c/D_i$  data. In this section, these three groups are treated separately and empirical equations for  $S_c/D_i$  data are provided.

#### 5.3.1 For Extreme Cases

##### 5.3.1.1 The Relationship for the Maximum $S_c/D_i$ Values Measured

The functional relationship for the dimensionless critical submergence as a function of Fr, Re, We and  $2b/D_i$ , stated in Equation 3.4, may be written in the following form

$$\frac{S_c}{D_i} = Fr^{c_1} Re^{c_2} We^{c_3} \left(\frac{2b}{D_i}\right)^{c_4} \quad [5.1]$$

By using the available data of maximum  $S_c/D_i$ , which includes the data of  $2b/D_i = 1.33$  for the pipe of  $D_i = 30$  cm,  $2b/D_i = 1.60$  for the pipe of  $D_i = 25$  cm,  $2b/D_i = 2.06$  for the pipe of  $D_i = 19.4$  cm,  $2b/D_i = 2.78$  for the pipe of  $D_i = 14.4$  cm, and  $2b/D_i = 4.00$  for the pipe of  $D_i = 10$  cm, a regression analysis has been applied with a computer program named DataFit (Oakdale, 2012) to determine the required constants for the empirical equation stated above. Finally, the following equation was obtained with the constants of;  $c_1 = 5.792$ ,  $c_2 = 3.246$ ,  $c_3 = -4.333$  and  $c_4 = -3.489$  and the correlation coefficient of  $R^2 = 0.977$ .

$$\frac{S_c}{D_i} = Fr^{5.792} Re^{3.246} We^{-4.333} \left(\frac{2b}{D_i}\right)^{-3.489} \quad [5.2]$$

The measured  $S_c/D_i$  values and  $S_c/D_i$  values calculated from Equation 5.2 were plotted with respect to each other and presented in Figure 5.20. As it is seen from the figure, all of the data are within  $\pm 5\%$  error lines. It is obvious that there is significant effect of wall clearance on the values of  $S_c/D_i$  presented in this section. If the walls surrounding the intake entrance get closer to each other, the critical submergence ratio increases significantly.

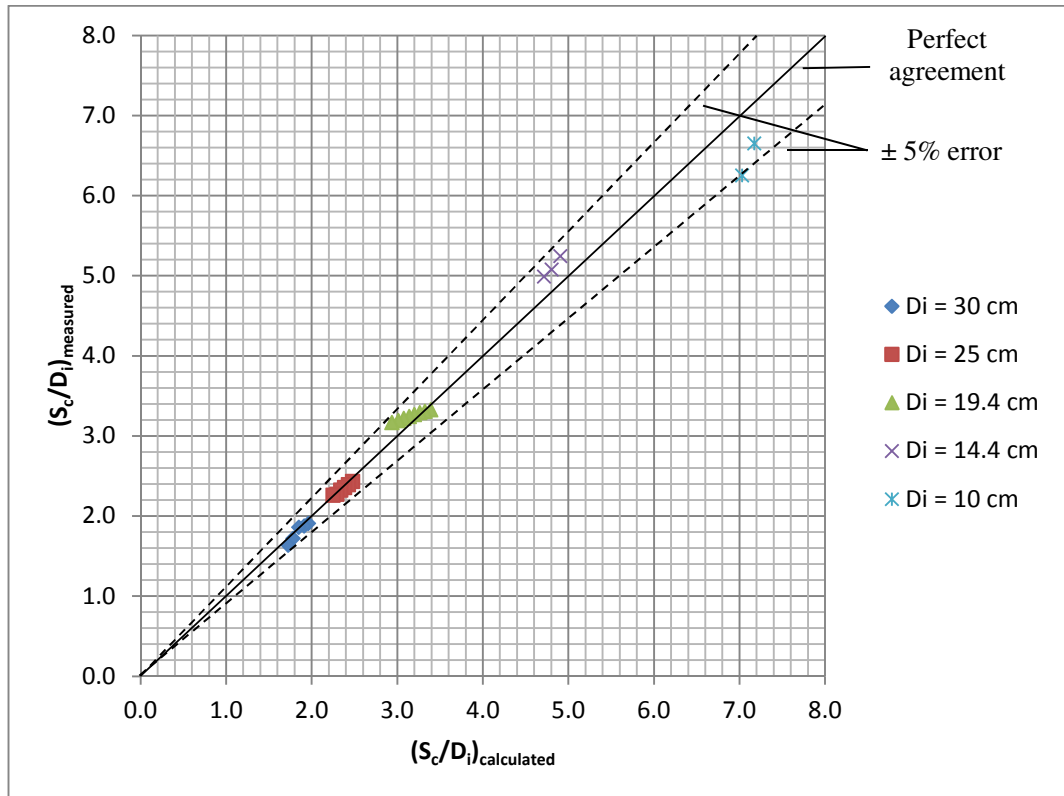


Figure 5.20 Comparison of measured and calculated maximum  $S_c/D_i$  values for the intake pipes tested

### 5.3.1.2 The Relationship for the Minimum $S_c/D_i$ Values Measured

By using the available data of minimum  $S_c/D_i$ , which includes the data of  $2b/D_i = 2.00$  and  $2.67$  for the pipe of  $D_i = 30$  cm,  $2b/D_i = 2.40$  and  $3.20$  for the pipe of  $D_i = 25$  cm,  $2b/D_i = 3.09$  and  $4.12$  for the pipe of  $D_i = 19.4$  cm,  $2b/D_i = 4.17$  and  $5.56$  for the pipe of  $D_i = 14.4$  cm,  $2b/D_i = 6.00$  and  $8.00$  for the pipe of  $D_i = 10$  cm and  $2b/D_i = 8.00$  for the pipe of  $D_i = 5$  cm, a regression analysis has been applied with a computer program named DataFit (Oakdale, 2012) to determine the required constants for the empirical equation stated in Equation 5.1. Finally, the following equation was obtained with the correlation coefficient of  $R^2 = 0.984$ .

$$\frac{S_c}{D_i} = Fr^{0.039} Re^{-0.357} We^{0.425} \left( \frac{2b}{D_i} \right)^{-0.602} \quad [5.3]$$

The measured  $S_c/D_i$  values and  $S_c/D_i$  values calculated from Equation 5.3 were plotted with respect to each other and presented in Figure 5.21. As it is seen from the figure all of the data are within  $\pm 20\%$  error lines. It is obvious that there is significant effect of wall clearance on the values of  $S_c/D_i$  presented in this section.

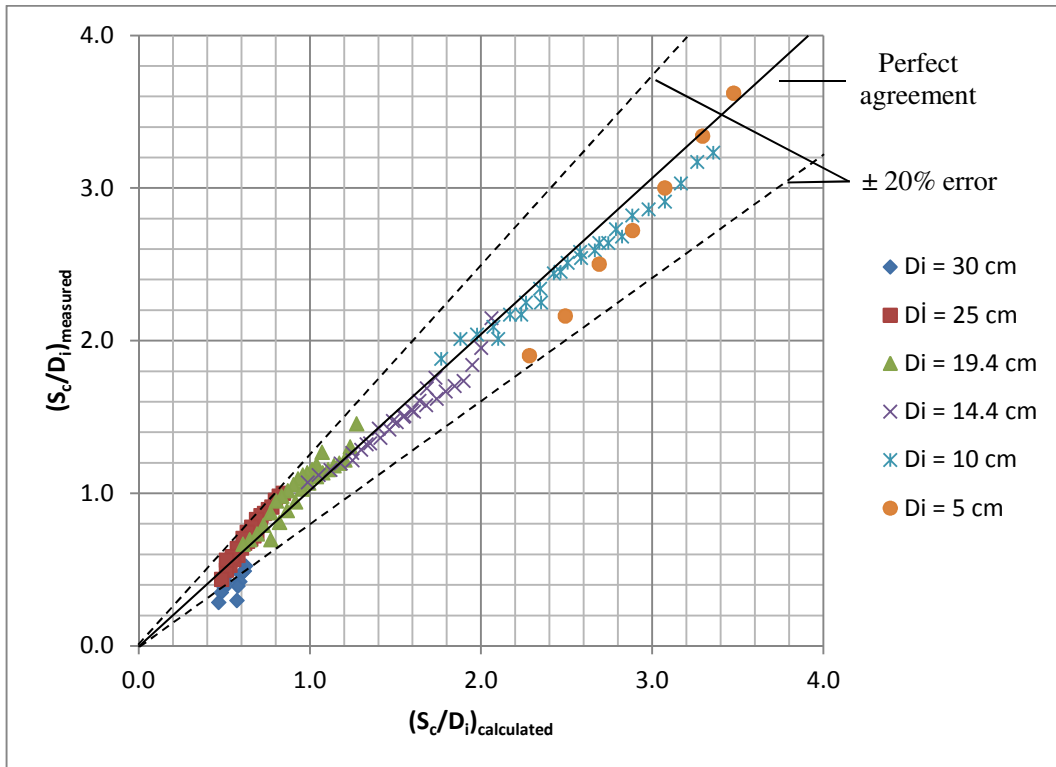


Figure 5.21 Comparison of measured and calculated minimum  $S_c/D_i$  values for the intake pipes tested

### 5.3.2 For Intermediate Values of $S_c/D_i$

When the regression analysis was applied to the remaining data of  $2b/D_i$  listed in Table 5.4, where  $2b/D_i \geq 3.33$  for the pipe of  $D_i = 30$  cm,  $2b/D_i \geq 4.00$  for the pipe of  $D_i = 25$  cm,  $2b/D_i \geq 5.16$  for the pipe of  $D_i = 19.4$  cm,  $2b/D_i \geq 6.94$  for the pipe of  $D_i = 14.4$  cm,  $2b/D_i \geq 10.00$  for the pipe of  $D_i = 10$  cm and  $2b/D_i \geq 12.00$  for the pipe of  $D_i = 5$  cm, Equation 5.1 was obtained in the form of Equation 5.4 with  $R^2 = 0.978$ .

$$\frac{S_c}{D_i} = Fr^{0.336} Re^{-0.229} We^{0.401} \left( \frac{2b}{D_i} \right)^{-0.261} \quad [5.4]$$

The measured  $S_c/D_i$  values and those calculated from Equation 5.4 were plotted and shown in Figure 5.22 with  $\pm 20\%$  error lines with respect to the perfect agreement line. Equation 5.4 is valid for the data taking place below the curve given in Figure 5.19.

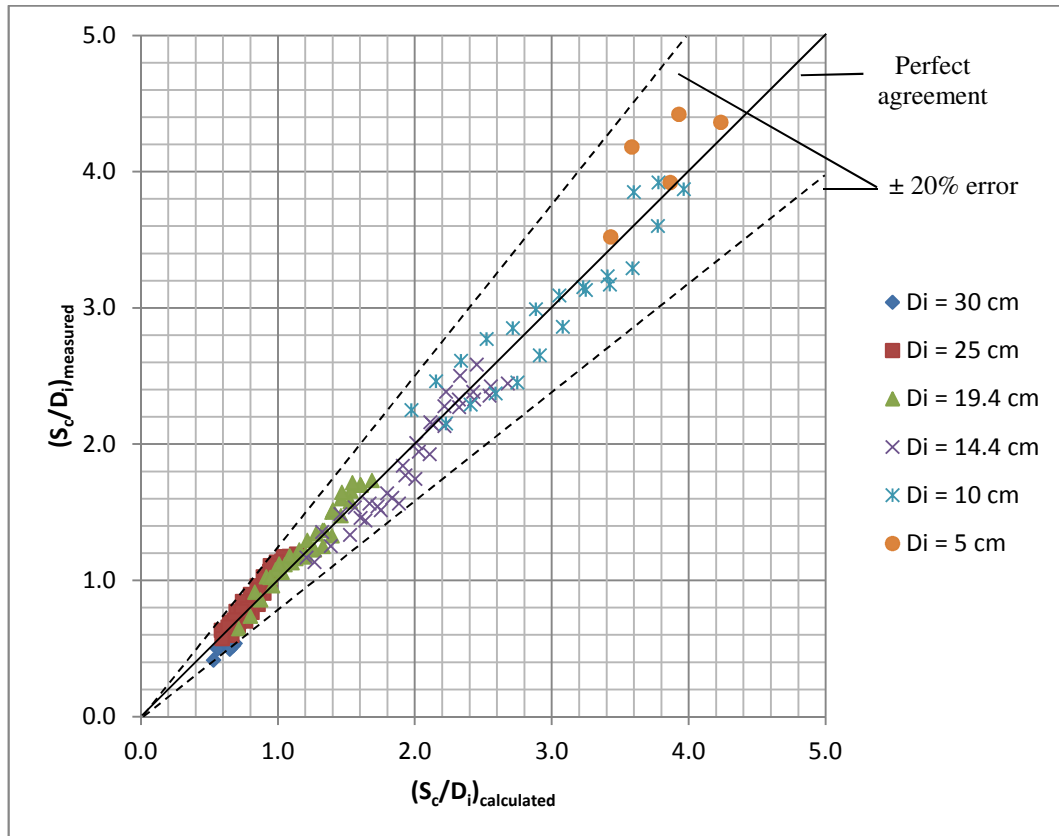


Figure 5.22 Comparison of measured and calculated intermediate  $S_c/D_i$  values for the intake pipes tested

In order to see the effect of  $2b/D_i$ ,  $We$  and  $Re$  on the value of  $S_c/D_i$ , these terms were excluded in a row from Equation 5.4 and the regression analysis was applied to the available intermediate data and the following equations were derived.

$$\frac{S_c}{D_i} = Fr^{0.113} Re^{-0.367} We^{0.550} \quad [5.5]$$

with  $R^2 = 0.972$ ,

$$\frac{S_c}{D_i} = Fr^{0.596} Re^{0.010} \quad [5.6]$$

with  $R^2 = 0.967$ , and

$$\frac{S_c}{D_i} = Fr^{0.639} \quad [5.7]$$

with  $R^2 = 0.964$ .

The variations of the measured and calculated  $S_c/D_i$  values from the above equations are shown in Figures 5.23, 5.24 and 5.25. From these figures and the correlation coefficients given above, it can be concluded that as the related dimensionless terms;  $2b/D_i$ ,  $We$  and  $Re$ , are dropped from the initial general equation, the errors to be obtained in the calculation of  $S_c/D_i$  will increase slightly.

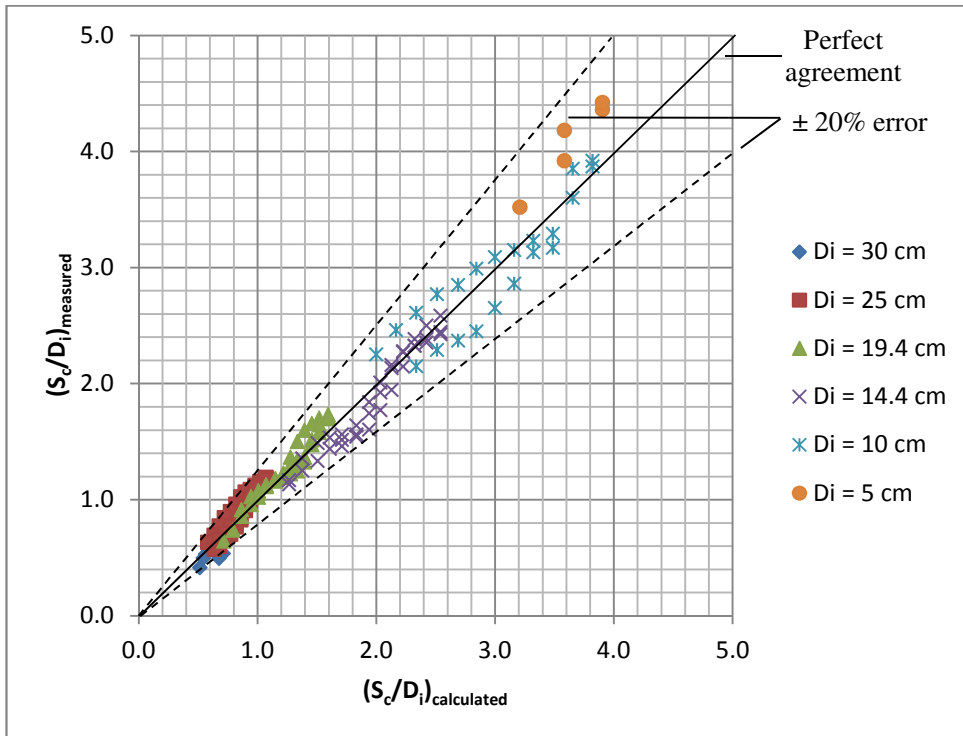


Figure 5.23 Comparison of measured and calculated  $S_c/D_i$  values from the application of Equation [5.5] to the available intermediate data

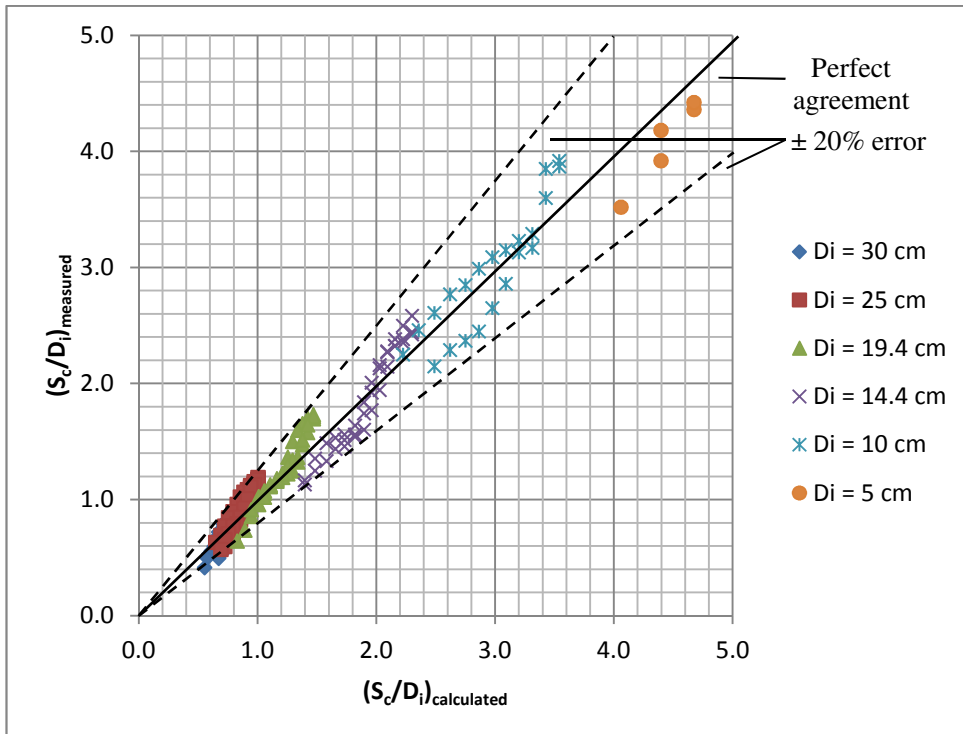


Figure 5.24 Comparison of measured and calculated  $S_c/D_i$  values from the application of Equation [5.6] to the available intermediate data

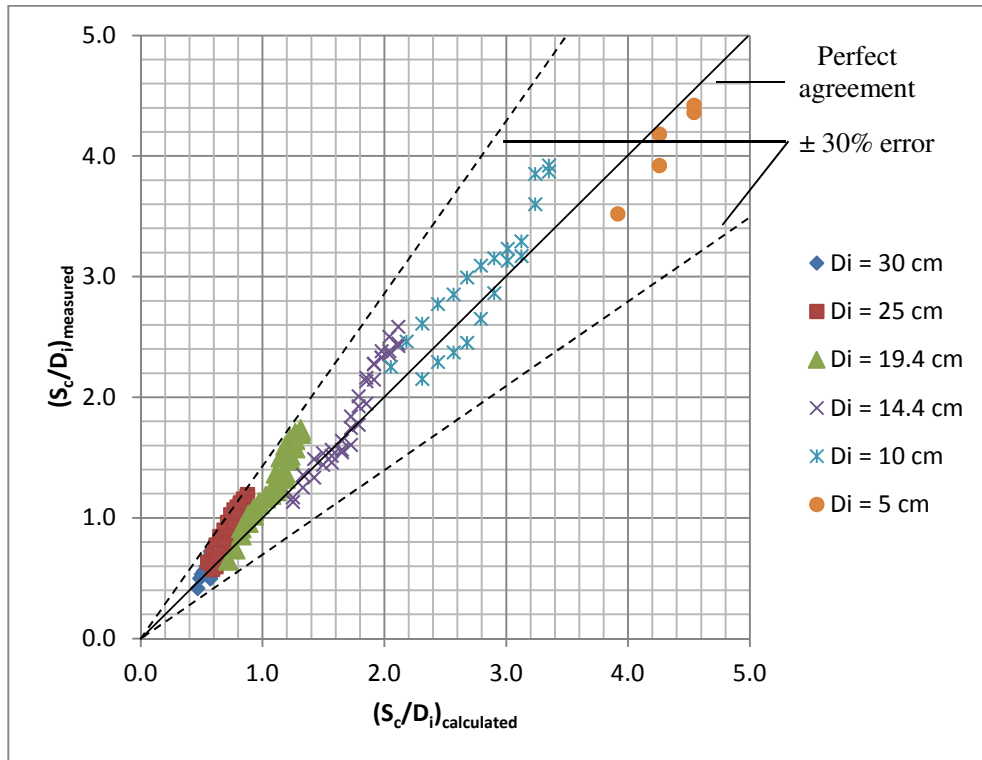


Figure 5.25 Comparison of measured and calculated  $S_c/D_i$  values from the application of Equation [5.7] to the available intermediate data

Finally, if only the data values given on the curve of Figure 5.19 are used;  $S_c/D_i$  values with the  $Fr$  stated on the curve with the corresponding  $Re$  and  $We$  for an intake of known diameter where  $S_c/D_i$  is independent of  $2b/D_i$ , in the regression analysis, the following equations are derived:

$$\frac{S_c}{D_i} = Fr^{0.324} Re^{-0.176} We^{0.282} \quad [5.8]$$

with  $R^2 = 0.997$  as a general equation, and after eliminating  $Re$  and  $We$

$$\frac{S_c}{D_i} = 1.278 Fr^{0.558} \quad [5.9]$$

with  $R^2 = 0.984$  as function of only  $Fr$  which has a range between 0.5 and 10.68.

Figures 5.26 and 5.27 show the variation of the measured and calculated  $S_c/D_i$  values which are obtained from Equations 5.8 and 5.9. As the parameters  $Re$  and  $We$  are excluded from the general equation of  $S_c/D_i$ , Equation 5.8, the correlation coefficient of the new equation, Equation 5.9, decreases slightly.

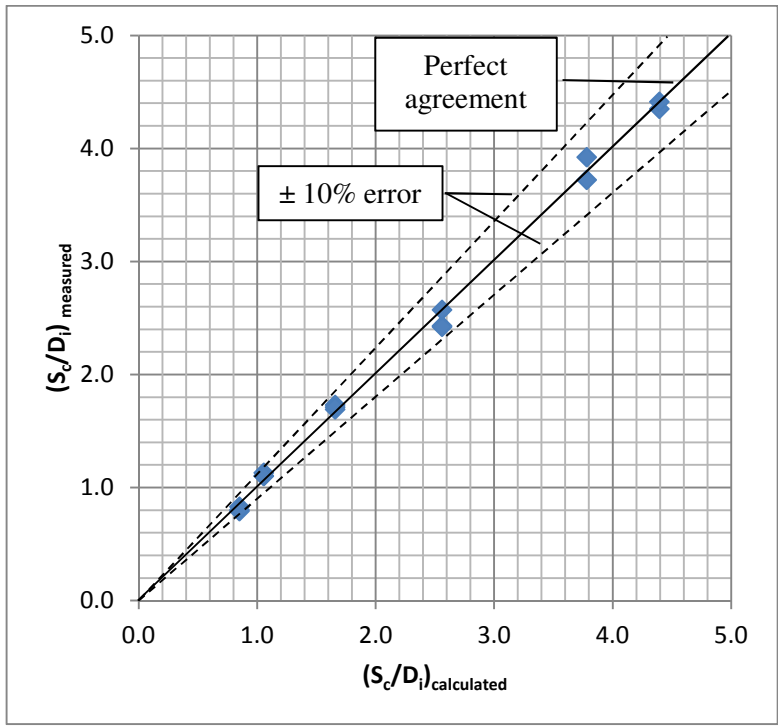


Figure 5.26 Comparison of measured and calculated  $S_c/D_i$  values from the application of Equation [5.8] to the available intermediate data

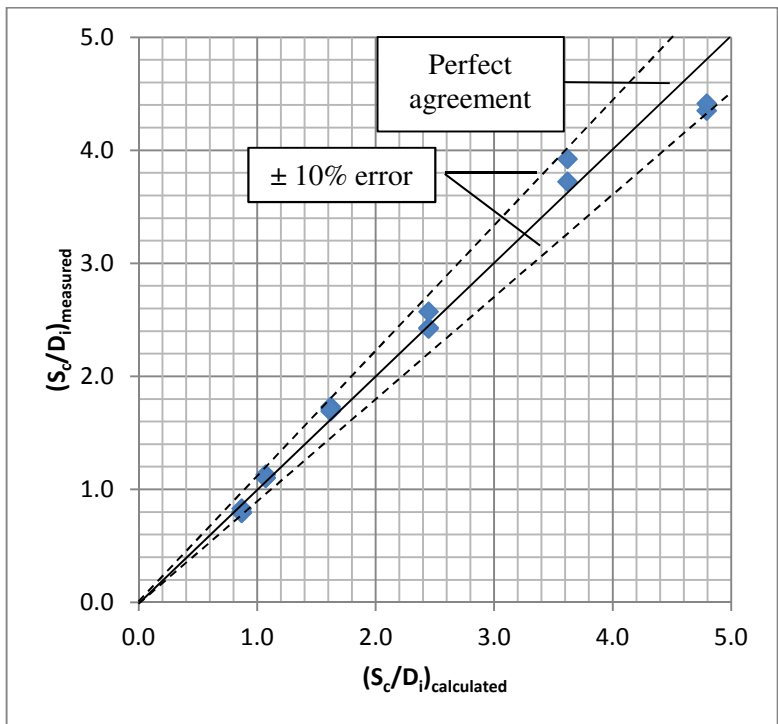


Figure 5.27 Comparison of measured and calculated  $S_c/D_i$  values from the application of Equation [5.9] to the available intermediate data

#### 5.4 Scale Effect on the Value of Dimensionless Critical Submergence

In practice, for complex intake structures, scale model tests are required to determine the critical submergence depths at which air-entraining vortices will form. The length scales of these models should be as large as possible to get more reliable data. Otherwise, one cannot convert the test results directly to the prototype values using the model length scale. Since Froude model law is used in the modeling of vortex problems, due to the neglected other dimensionless terms such as Re and We, there will be scale effects on the test results.

In order to find out the scale effects on the values of  $S_c/D_i$ , the available experimental results were analyzed and the pipe and flow parameters for the same Froude numbers were determined. Among these data, the ones having almost the same  $2b/D_i$  values were selected and presented in Table 5.5. Each pair of data given in Table 5.5 for a known Froude number belongs to two pipes of different diameters. The first pipe which is larger in diameter than the second pipe is considered as the prototype of the second one. In addition to  $S_c/D_i$  values of these pipes, the other parameters; Re, We, model length scale  $L_r = D_m/D_p$ , the ratio of dimensionless critical submergence values for the model and the prototype,  $(S_c/D_i)_r = (S_c/D_i)_m / (S_c/D_i)_p$ , the ratios of the Reynolds numbers,  $(Re)_r = (Re)_m / (Re)_p$ , and the ratios of the Weber numbers,  $(We)_r = (We)_m / (We)_p$ , are listed in Table 5.5.

Table 5.5 Model and prototype data and related scale ratios

D <sub>i</sub> = 30.0 cm (Prototype) versus D <sub>i</sub> = 25.0 cm (Model)										
Fr	Pipe	D <sub>i</sub> (cm)	S <sub>c</sub> /D <sub>i</sub>	2b/D <sub>i</sub>	Re	We	L <sub>r</sub>	(S <sub>c</sub> /D <sub>i</sub> ) <sub>r</sub>	(Re) <sub>r</sub>	(We) <sub>r</sub>
0.35	1	30	0.560	3.33	178500	1450	0.833	0.982	0.762	0.707
	2	25	0.550	3.20	136000	1025				
0.40	1	30	0.675	3.33	204500	1925	0.833	0.956	0.763	0.701
	2	25	0.645	3.20	156000	1350				
0.45	1	30	0.710	4.00	230500	2450	0.833	0.993	0.764	0.704
	2	25	0.705	4.00	176000	1725				
	1	30	0.755	3.33	230500	2450	0.833	0.947	0.764	0.704
	2	25	0.715	3.20	176000	1725				
0.50	1	30	0.805	4.67	256500	3020	0.833	0.807	0.764	0.695
	2	25	0.650	4.80	196000	2100				
	1	30	0.820	4.00	256500	3020	0.833	0.988	0.764	0.695
	2	25	0.810	4.00	196000	2100				
	1	30	0.830	3.33	256500	3020	0.833	0.922	0.764	0.695
	2	25	0.765	3.20	196000	2100				
D <sub>i</sub> = 25.0 cm (Prototype) versus D <sub>i</sub> = 19.4 cm (Model)										
Fr	Pipe	D <sub>i</sub> (cm)	S <sub>c</sub> /D <sub>i</sub>	2b/D <sub>i</sub>	Re	We	L <sub>r</sub>	(S <sub>c</sub> /D <sub>i</sub> ) <sub>r</sub>	(Re) <sub>r</sub>	(We) <sub>r</sub>
0.60	2	25	0.975	4.00	236000	3025	0.776	0.718	0.676	0.598
	3	19.4	0.700	4.12	159500	1810				
	2	25	0.855	3.20	236000	3025	0.776	0.813	0.676	0.598
	3	19.4	0.695	3.09	159500	1810				

Table 5.5 Continued

Fr	Pipe	D <sub>i</sub> (cm)	S <sub>c</sub> /D <sub>i</sub>	2b/D <sub>i</sub>	Re	We	L <sub>r</sub>	(S <sub>c</sub> /D <sub>i</sub> ) <sub>r</sub>	(Re) <sub>r</sub>	(We) <sub>r</sub>
0.70	2	25	1.090	4.00	276000	4125	0.776	0.775	0.678	0.596
	3	19.4	0.845	4.12	187000	2460				
0.70	2	25	0.915	3.20	276000	4125	0.776	0.820	0.678	0.596
	3	19.4	0.750	3.09	187000	2460				
0.80	2	25	1.180	4.00	316000	5400	0.776	0.784	0.676	0.596
	3	19.4	0.925	4.12	213500	3220				
	2	25	0.995	3.20	316000	5400	0.776	0.849	0.676	0.596
	3	19.4	0.845	3.09	213500	3220				
D <sub>i</sub> = 19.4 cm (Prototype) versus D <sub>i</sub> = 14.4 cm (Model)										
Fr	Pipe	D <sub>i</sub> (cm)	S <sub>c</sub> /D <sub>i</sub>	2b/D <sub>i</sub>	Re	We	L <sub>r</sub>	(S <sub>c</sub> /D <sub>i</sub> ) <sub>r</sub>	(Re) <sub>r</sub>	(We) <sub>r</sub>
1.1	3	19.4	1.130	4.12	293000	6180	0.742	0.907	0.679	0.546
	4	14.4	1.025	4.17	199000	3375				
1.2	3	19.4	1.165	4.12	319500	7280	0.742	0.906	0.679	0.598
	4	14.4	1.055	4.17	217000	4350				
1.3	3	19.4	1.190	4.12	346500	8600	0.742	0.899	0.678	0.593
	4	14.4	1.070	4.17	235000	5100				
1.4	3	19.4	1.235	4.12	373000	9900	0.742	0.891	0.678	0.593
	4	14.4	1.100	4.17	253000	5875				
1.5	3	19.4	1.390	4.12	399500	11350	0.742	0.824	0.681	0.581
	4	14.4	1.145	4.17	272000	6600				
D <sub>i</sub> = 10.0 cm (Prototype) versus D <sub>i</sub> = 5.0 cm (Model)										
Fr	Pipe	D <sub>i</sub> (cm)	S <sub>c</sub> /D <sub>i</sub>	2b/D <sub>i</sub>	Re	We	L <sub>r</sub>	(S <sub>c</sub> /D <sub>i</sub> ) <sub>r</sub>	(Re) <sub>r</sub>	(We) <sub>r</sub>
5.00	5	10.0	2.825	8.00	495000	33700	0.500	0.688	0.352	0.249
	6	5.0	1.945	8.00	174000	8400				
5.5	5	10.0	2.885	8.00	545000	40700	0.500	0.724	0.351	0.251
	6	5.0	2.090	8.00	191500	10200				
6.00	5	10.0	3.045	8.00	595000	48400	0.500	0.745	0.351	0.249
	6	5.0	2.270	8.00	209000	12050				
6.50	5	10.0	3.210	8.00	570000	56750	0.500	0.769	0.397	0.250
	6	5.0	2.47	8.00	226500	14200				

To show the effect of  $Fr$ ,  $L_r$ ,  $(Re)_r$  and  $(We)_r$  on  $(S_c/D_i)_r$ , Figures 5.28 – 5.3 were plotted. Figure 5.28 shows the variation of  $(S_c/D_i)_r$  with  $Fr$ , having roughly plotted upper and lower envelope curves covering the all data. This figure reveals that at small values of  $Fr$  up to about 1.8,  $(S_c/D_i)_r$  varies between 0.6 and 1.0. At larger values of  $Fr$ , it may be said that  $(S_c/D_i)_r$  varies between 0.6 and 0.8 even though no data available for  $Fr$  between about 1.0 and 5.0. The variation of  $(S_c/D_i)_r$  with model length scale  $L_r$  is presented in Figure 5.29. From the general trend of the data, it can be concluded that as  $L_r$  decreases,  $(S_c/D_i)_r$  decreases following the envelope curves which are starting from  $L_r = 1.0$  where  $(S_c/D_i)_r = 1.0$ . At larger values of  $L_r$  tested, it may be said that the rate of decrease of  $(S_c/D_i)_r$  gets smaller. For further small values of  $L_r$  at which no experimental data are available, it may be stated that  $(S_c/D_i)_r$  will vary between 0.6 and 0.8.

From the following argument another estimation for the calculation of  $(S_c/D_i)_r$  can be made. If it is assumed that Equation 5.8 is applicable to prototypes as well as models, one can write the following relationship for  $(S_c/D_i)_r$ .

$$\left(\frac{S_c}{D_i}\right)_r = \frac{(S_c/D_i)_m}{(S_c/D_i)_p} = (Fr)_r^{0.324} (Re)_r^{-0.176} (We)_r^{0.282} \quad [5.10]$$

Since  $(Fr)_r = 1$ ,  $(Re)_r = V_r D_r / \nu_r$ ,  $(We)_r = \rho_r V_r^2 D_r / \sigma_r$  and  $\nu_r = 1$ ,  $\rho_r = 1$ ,  $\sigma_r = 1$ , and  $V_r = \sqrt{D_r} = \sqrt{L_r}$ ,

$$\left(\frac{S_c}{D_i}\right)_r = L_r^{0.3} \quad [5.11]$$

If Equation 5.11 is plotted in Figure 5.29 for the zone of  $L_r$  where the test data are available, it is seen that the curve of Equation 5.11 lies between the envelope curves. For a rough calculation of  $(S_c/D_i)_r$ , Equation 5.11 may be used within the zone of  $L_r$  tested in this study. Additional experiments must be conducted at smaller  $L_r$  values to show that Equation 5.11 is applicable or not.

As an example if  $L_r$  is selected as  $\frac{1}{2}$  in a model study and it is assumed that the corresponding  $(S_c/D_i)_r$  is about 0.70 from Figure 5.29, to determine the value of  $(S_c/D_i)_p$ , the measured  $(S_c/D_i)_m$  must be multiplied by a correction coefficient of about 1.43. This coefficient becomes 1.23 if Equation 5.11 is used.

In a similar way to Figure 5.29, Figures 5.30 and 5.31 show the variation of  $(S_c/D_i)_r$  with  $(Re)_r$  and  $(We)_r$  with  $(S_c/D_i)_r$ , respectively. The general trends of the data values of these figures also imply that as  $(Re)_r$  and  $(We)_r$  increase,  $(S_c/D_i)_r$  increase and approach to 1.0 for  $(Re)_r = 1.0$  and  $(We)_r = 1.0$ .

Finally, from the analysis of all these figures, it can be concluded that as the model scale,  $L_r$ , gets smaller, the scale effect on the value of  $(S_c/D_i)_r$  becomes more significant.

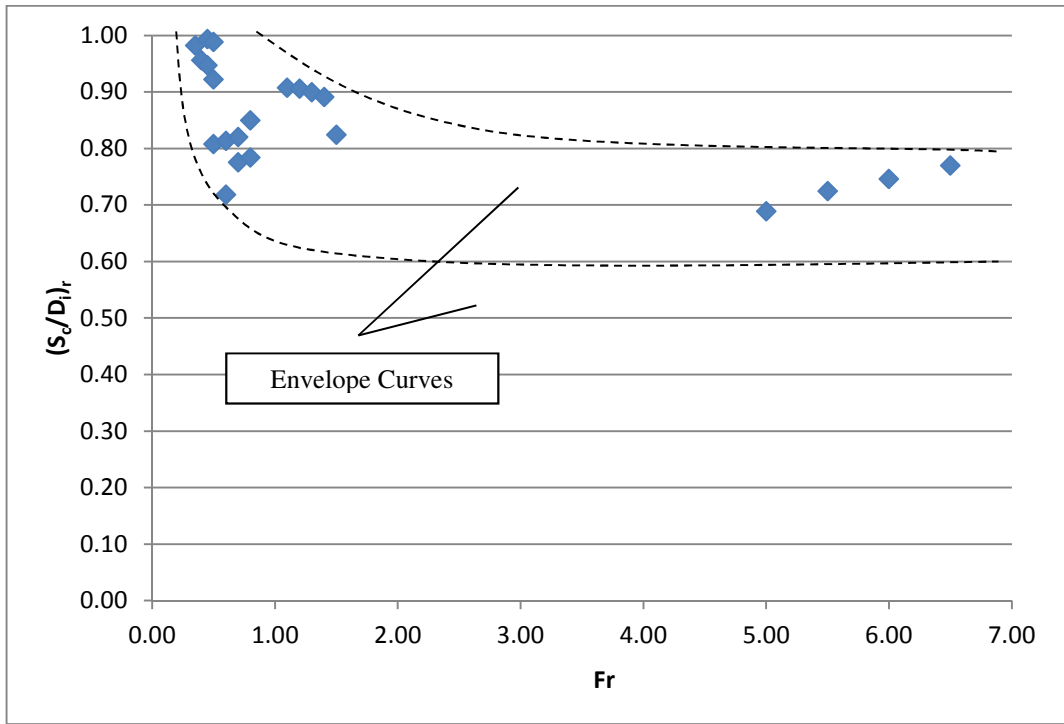


Figure 5.28 Variation of  $(S_c/D_i)_r$  with Froude number

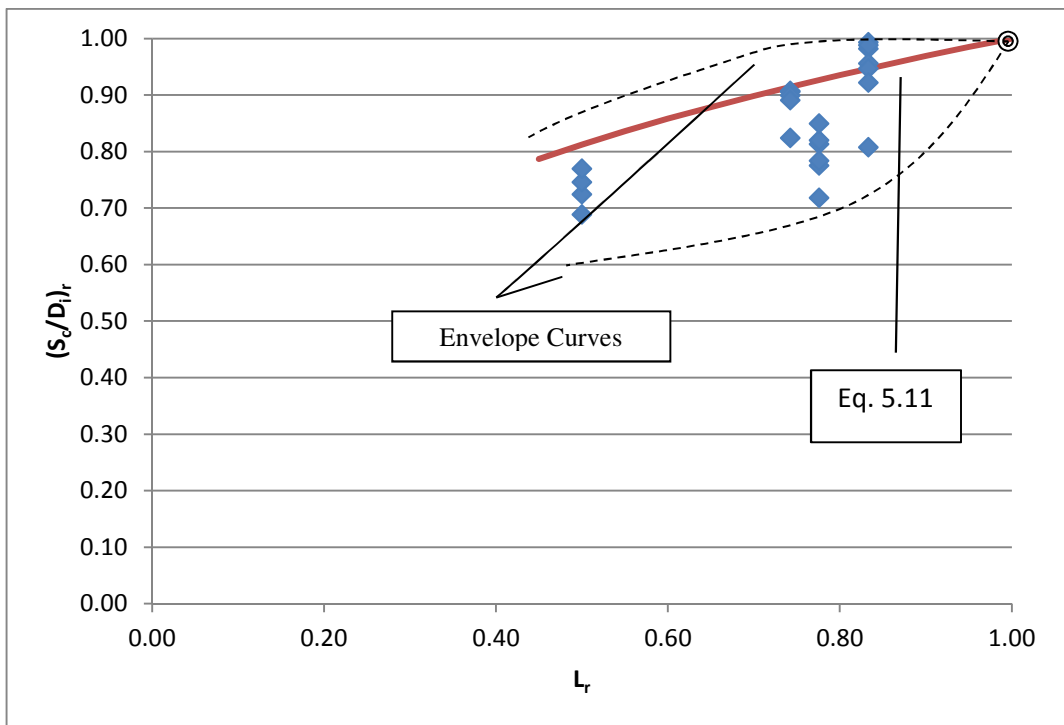


Figure 5.29 Variation of  $(S_c/D_i)_r$  with  $L_r$

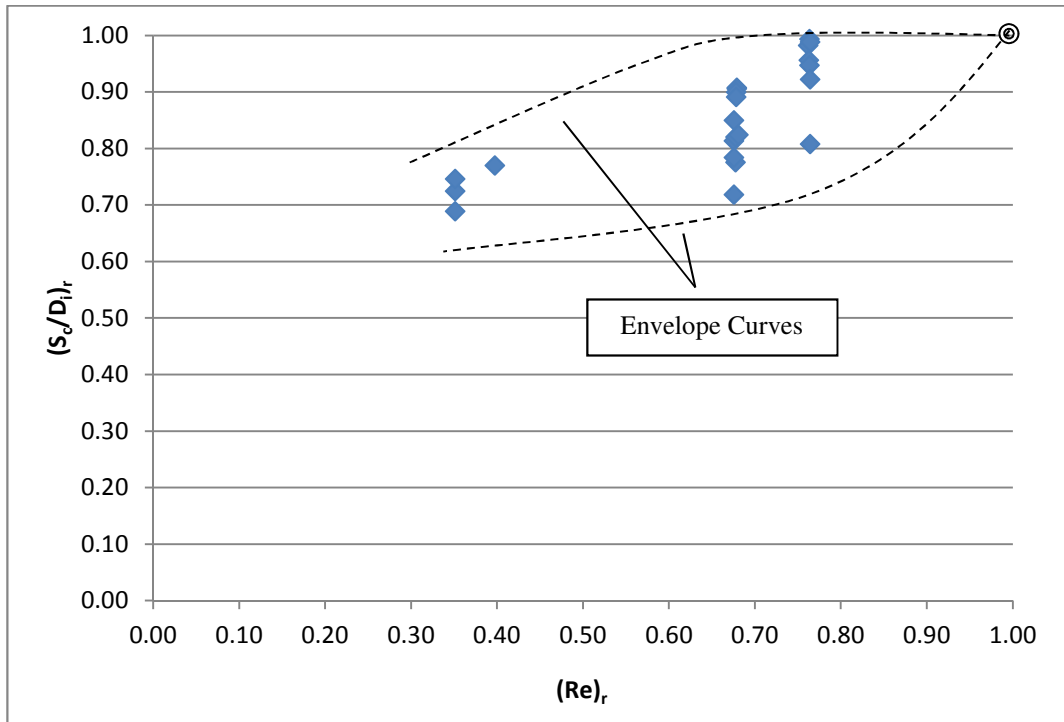


Figure 5.30 Variation of  $(S_c/D_i)_r$  with  $(Re)_r$

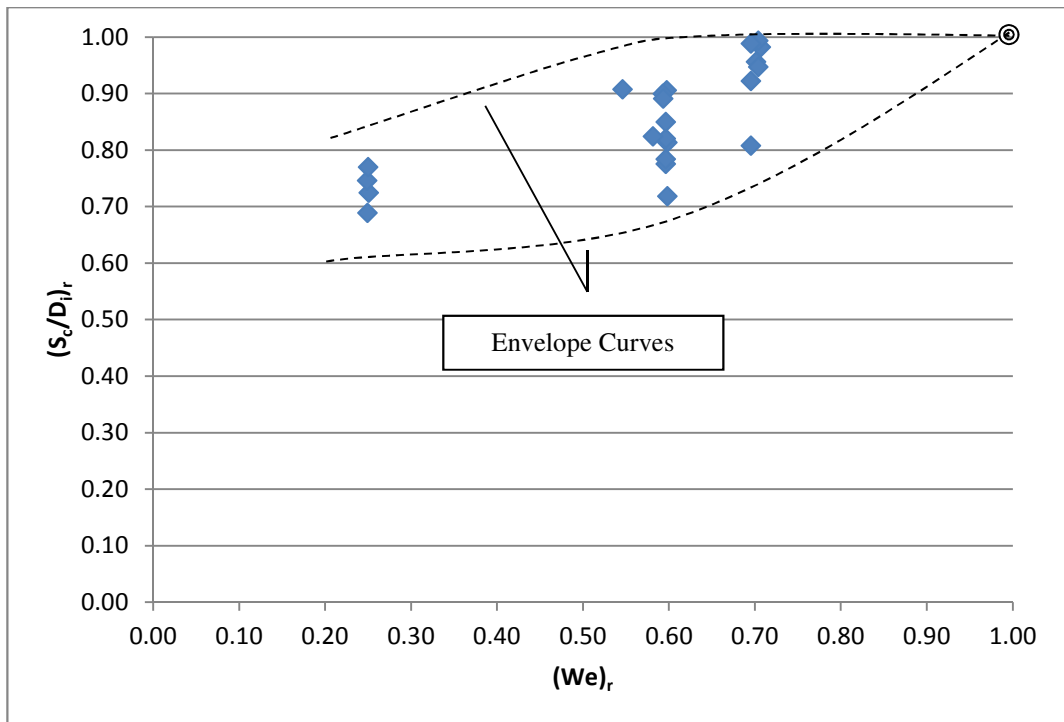


Figure 5.31 Variation of  $(S_c/D_i)_r$  with  $(We)_r$

## 5.5 Comparison of the Proposed Empirical Equations with the Related Relationships Presented in the Literature

### 5.5.1 Gürbüzdal’s Study (2009)

Gürbüzdal conducted similar experiments to those presented in this study with four pipes of different diameters described in the section of “Literature Review”. The experiments were conducted in a similar setup with constant  $2b = 31.5$  cm for a wide range of discharges.  $2b/D_i$  values used in the experiments and maximum Froude numbers tested with each intake pipe used are shown in Figure 5.32 along with the corresponding values of this study which were presented in Figure 5.19. From Figure 5.32, it is clearly seen that the data of Gürbüzdal are below the curve of the present study which was named as “intermediate zone” where  $S_c/D_i$  is function of  $2b/D_i$ , Fr, Re and We. In order to show how well the empirical equation, Equation 5.4 proposed in this study fits the data of Gürbüzdal, Figure 5.33 is plotted. In this figure, the calculated  $S_c/D_i$  values were determined using the required values of Fr, Re, We and  $2b/D_i$  from the data of Gürbüzdal and plotted with respect to those observed by Gürbüzdal as measured  $S_c/D_i$ . Figure 5.33 reveals that there is a good agreement between the proposed equation, Equation 5.4, and Gürbüzdal’s data which lie within  $\pm 20\%$  error lines.

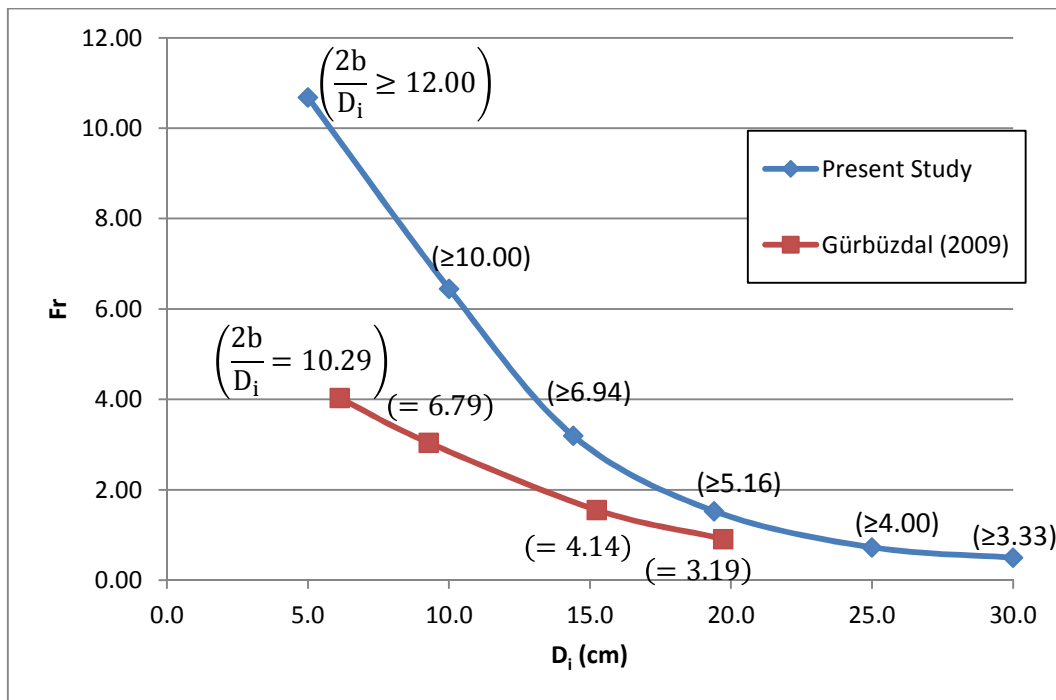


Figure 5.32 For present and Gürbüzdal (2009) study, limit values of  $2b/D_i$  above which  $S_c/D_i$  is independent of  $2b/D_i$  and function of Fr, Re and We

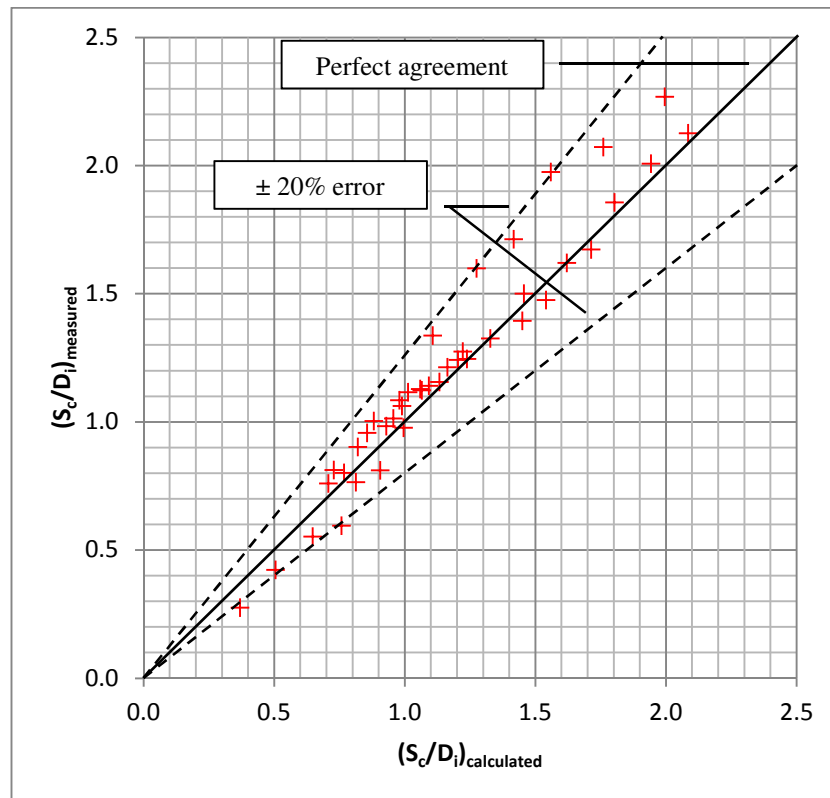


Figure 5.33 Comparison of measured and calculated (from Eq. 5.4) intermediate  $S_c/D_i$  values of Gürbüzdal (2009)

### 5.5.2 Gordon's (1970), Reddy and Pickford's (1972) and Rindels and Gulliver's (1983) Studies

As stated in the section of "Literature Review" Rindels and Gulliver (1983) compiled all the available data on existing installations and presented in Figure 2.1. In order to compare the validity of Equation 5.9 with the available data of  $S_c/D_i$  in literature, Equation 5.9 was plotted in Figure 2.1 and presented as Figure 5.34. The curve of Equation 5.9 lies below all the other curves given in the figure. The agreement between Equation 5.9 and the relations of Gordon (1970) is quite good for the Froude number up to about 0.6. For larger Froude numbers, Equation 5.9 estimates much lower  $S_c/D_i$  values than the others. Large Froude numbers were achieved in the present study by using mostly pipes of small diameters. Whereas, most of the data presented in Figure 5.34 were provided from existing installations. Therefore, the data of the small diameter pipes used in the present study represent only the data of small scale models, from which one cannot directly convert the model data to the prototype values. The scale effects due to neglecting the similarity of  $Re$ ,  $We$  and probably the wall clearance, are the basic reasons for not having good agreement between the model data and prototype data.

As a rough estimation, if it is assumed that the experimental setups tested in this study were models of the prototypes, with a length scale of  $L_r = 1/10$ , from Equation 5.11, the values of  $(S_c/D_i)_r$  is calculated as 0.5, from which  $(S_c/D_i)_p = 2(S_c/D_i)_m$ . This means that, if the validity of Equation 5.11 is assumed for a model of  $L_r = 1/10$ , the critical submergence of the prototype may be selected as twice the corresponding model value. In the light of this information  $(S_c/D_i)$  values of Equation 5.9 can be multiplied by 2 to determine the  $S_c/D_i$  values to be expected in the prototype which are

shown in Figure 5.34 as “corrected Eq. 5.9” for this specific example. As it is seen from the figure, the curve of the “corrected Eq. 5.9” lies above most of the data having vortex problems.

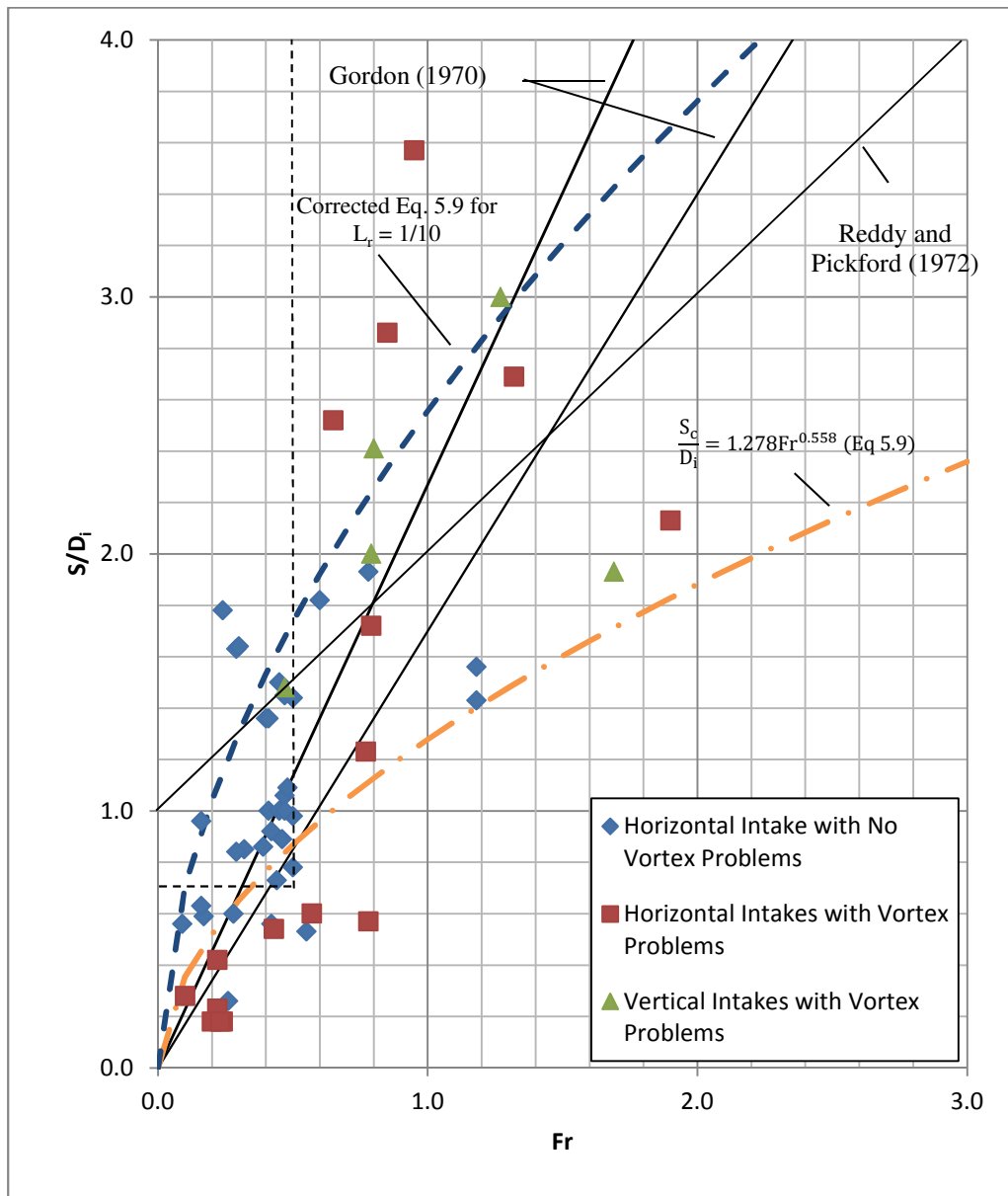


Figure 5.34 Dimensionless plot of data obtained from existing intakes, field installations and model studies (Rindels and Gulliver, 1983) with the relationships proposed by Gordon (1970), Reddy and Pickford (1972), Eq. 5.9 and corrected Eq 5.9 for  $L_r = 1/10$

## 5.6 Effect of Horizontal Plates on Elimination of Vortices

To eliminate the air-entraining vortices forming in front of the intake structure, horizontal plates of different dimensions described earlier were tested in the experiments and the related data and observations made were presented in Tables B.1 – B.62 in Appendix B. In these tables, for an intake pipe of known diameter, the dimensions of the horizontal plates;  $L_p$  as the length and  $W_p$  as the width, and the locations and some other properties of the vortices forming listed. At some of the experiments double vortex formations, designated by “DV”, was observed but they did not appear systematically. Under the title of “Results”, the performances of the tested horizontal plates were stated using the symbols of “S” and “US”. Here in, “US” and “S” stand for; air-entraining vortex is forming and not forming, respectively. In some cases, the horizontal plates completely eliminated air-entraining vortices while in some other cases only the strengths of the vortices were reduced and vortices of types 2 – 3 with “vortex tails” formed. The horizontal plates resulted in vortices having reduced types were also considered as satisfactory.

In each table presented in Appendix B for a given  $Fr$  and  $L_p/D_i$ ,  $D_i$  is fixed and  $L_p$  is either 40 cm or 50 cm, the data and results of 5 experiments conducted by varying the width of the plate are given. Among the test results of 5 horizontal plates of varying widths, the one showing a satisfactory performance and having the minimum width was selected as the plate of optimum dimensions and listed in Table 5.6. Since horizontal plates of larger widths were also eliminating air-entraining vortices, in Table 5.6, the symbol of “ $W_p/D_i$ ” was used in 7<sup>th</sup> column to state the limit values of  $W_p/D_i$ . Therefore, the evaluation of Table B.1 – B.62 are presented for the same  $Fr$  by two sets of data; one for  $L_p = 40$  cm and the other one for  $L_p = 50$  cm, in Table 5.6.

At small values of  $2b/D_i$  of each intake pipe tested, it was observed that in most of the cases, the horizontal plates used did not give satisfactory results. The reason of this situation is mainly due to the strong effect of boundary blockage on the formation of vortices as described earlier. Because of that, for a given intake pipe diameter, the data of small  $2b/D_i$  values were disregarded and only those  $2b/D_i$  values giving intermediate  $S_c/D_i$ , as discussed in “Section 5.2” were considered and presented in Table 5.7 (the data related to intermediate  $S_c/D_i$  values which are used in preparation of Table 5.7 are shown as darker shading in Table 5.6) along with Froude numbers and corresponding  $(L_p/D_i)_{1,2}$  and  $S_c/D_i$ . Table 5.7 reveals that for a given  $D_i$ ,  $2b/D_i$  and  $L_p/D_i$ , there are 2 or 3 values of  $(W_p/D_i) \geq$  one of which is the largest and if it is selected, it can be concluded that the horizontal plate satisfying the values of  $W_p/D_i$  and  $L_p/D_i$  which has a constant  $L_p/W_p$ , can be used as an anti-vortex device covering the range of  $Fr$  tested for  $2b/D_i$ . By applying the process for all the  $2b/D_i$  values given in Table 5.7 for both  $L_p/D_i$  values tested, one can obtain the data tabulated in Table 5.8. From this table, one more selection can be made for  $W_p/D_i$  which will be the largest one, and therefore, satisfy all  $2b/D_i$  values of a given  $D_i$ . These selected  $W_i/D_i$  values with the corresponding  $L_p/W_p$  values were presented in Table 5.8.

Figures 5.35 and 5.36 show the variation of selected  $W_p/D_i$  with  $Fr$  for  $L_p/W_p$  values tested. Except the  $W_p/D_i$  of 3 and 4 which correspond to the largest  $Fr$  investigated, which are hardly encountered in practical applications, these curves show that the horizontal plate having the values of  $W_p/D_i = 2$  and  $L_p/W_p = 2.5$  can be used as an anti – vortex device for the range of  $Fr$  tested.

Table 5.6 Evaluation and summary of the data presented in Tables B.1 - B.62

Observation Number	$D_i$ (cm)	$2b/D_i$	Fr	$S_c/D_i$	$L_p/D_i$	$W_p/D_i \geq$	$L_p/W_p$	Table
1	25.0	2.40	0.814	0.792	1.60	1.00	1.60	B.1
2	25.0	2.40	0.814	0.792	2.00	None	-	
3	25.0	2.40	0.591	0.640	1.60	0.80	2.00	B.2
4	25.0	2.40	0.591	0.640	2.00	0.60	3.33	
5	25.0	2.40	0.394	0.436	1.60	0.60	2.67	B.3
6	25.0	2.40	0.394	0.436	2.00	0.60	3.33	
7	25.0	3.20	0.814	1.000	1.60	0.20	8.00	B.4
8	25.0	3.20	0.814	1.000	2.00	0.20	10.00	
9	25.0	3.20	0.660	0.892	1.60	0.20	8.00	B.5
10	25.0	3.20	0.660	0.892	2.00	0.20	10.00	
11	25.0	3.20	0.357	0.584	1.60	0.60	2.67	B.6
12	25.0	3.20	0.357	0.584	2.00	0.60	3.33	
13	25.0	4.00	0.814	1.192	1.60	0.20	8.00	B.7
14	25.0	4.00	0.814	1.192	2.00	0.20	10.00	
15	25.0	4.00	0.625	1.024	1.60	0.20	8.00	B.8
16	25.0	4.00	0.625	1.024	2.00	0.20	10.00	
17	25.0	4.00	0.473	0.772	1.60	0.60	2.67	B.9
18	25.0	4.00	0.473	0.772	2.00	0.80	2.50	
19	25.0	4.80	0.814	1.176	1.60	0.20	8.00	B.10
20	25.0	4.80	0.814	1.176	2.00	0.20	10.00	
21	25.0	4.80	0.625	0.824	1.60	0.80	2.00	B.11
22	25.0	4.80	0.625	0.824	2.00	0.80	2.50	
23	25.0	4.80	0.473	0.596	1.60	0.60	2.67	B.12
24	25.0	4.80	0.473	0.596	2.00	0.60	3.33	
25	25.0	5.60	0.814	1.172	1.60	0.20	8.00	B.13
26	25.0	5.60	0.814	1.172	2.00	0.20	10.00	
27	25.0	5.60	0.625	0.848	1.60	0.20	8.00	B.14
28	25.0	5.60	0.625	0.848	2.00	0.20	10.00	
29	25.0	5.60	0.473	0.656	1.60	0.80	2.00	B.15
30	25.0	5.60	0.473	0.656	2.00	0.80	2.50	
31	19.4	2.06	1.534	3.325	2.06	None	-	B.16
32	19.4	2.06	1.179	3.216	2.06	0.26	7.99	B.17
33	19.4	3.09	1.534	1.268	2.06	0.26	7.99	B.18
34	19.4	3.09	1.534	1.268	2.58	1.29	2.00	
35	19.4	3.09	1.179	1.093	2.06	0.26	7.99	B.19
36	19.4	3.09	1.179	1.093	2.58	0.26	9.99	
37	19.4	3.09	0.826	0.871	2.06	0.77	2.67	B.20
38	19.4	3.09	0.826	0.871	2.58	0.77	3.33	

Table 5.6 Continued

Observation Number	$D_i$ (cm)	$2b/D_i$	Fr	$S_c/D_i$	$L_p/D_i$	$W_p/D_i \geq$	$L_p/W_p$	Table
39	19.4	4.12	1.534	1.454	2.06	0.26	7.99	B.21
40	19.4	4.12	1.534	1.454	2.58	0.26	9.99	
41	19.4	4.12	1.179	1.155	2.06	1.03	2.00	B.22
42	19.4	4.12	1.179	1.155	2.58	0.26	9.99	
43	19.4	4.12	0.743	0.887	2.06	1.03	2.00	B.23
44	19.4	4.12	0.743	0.887	2.58	0.26	9.99	
45	19.4	5.16	1.534	1.732	2.06	0.26	7.99	B.24
46	19.4	5.16	1.534	1.732	2.58	0.26	9.99	
47	19.4	5.16	1.179	1.366	2.06	0.26	7.99	B.25
48	19.4	5.16	1.179	1.366	2.58	0.26	9.99	
49	19.4	5.16	0.826	0.959	2.06	1.03	2.00	B.26
50	19.4	5.16	0.826	0.959	2.58	1.03	2.50	
51	19.4	6.19	1.534	1.696	2.06	0.26	7.99	B.27
52	19.4	6.19	1.534	1.696	2.58	0.26	9.99	
53	19.4	6.19	1.179	1.222	2.06	0.52	4.00	B.28
54	19.4	6.19	1.179	1.222	2.58	0.26	9.99	
55	19.4	6.19	0.826	1.026	2.06	0.77	2.67	B.29
56	19.4	6.19	0.826	1.026	2.58	1.03	2.50	
57	19.4	7.22	1.534	1.716	2.06	0.26	7.99	B.30
58	19.4	7.22	1.534	1.716	2.58	0.26	9.99	
59	19.4	7.22	1.179	1.294	2.06	0.26	7.99	B.31
60	19.4	7.22	1.179	1.294	2.58	0.26	9.99	
61	19.4	7.22	0.892	1.021	2.06	0.77	2.67	B.32
62	19.4	7.22	0.892	1.021	2.58	1.03	2.50	
63	14.4	2.78	3.231	5.243	2.78	None	-	B.33
64	14.4	4.17	3.231	1.757	2.78	0.69	4.00	B.34
65	14.4	4.17	3.231	1.757	3.47	0.69	5.03	
66	14.4	4.17	2.483	1.465	2.78	1.39	2.00	B.35
67	14.4	4.17	2.483	1.465	3.47	0.35	10.01	
68	14.4	4.17	1.740	1.264	2.78	1.04	2.67	B.36
69	14.4	4.17	1.740	1.264	3.47	1.39	2.50	
70	14.4	5.56	3.231	2.146	2.78	0.69	4.00	B.37
71	14.4	5.56	3.231	2.146	3.47	0.35	10.01	
72	14.4	5.56	2.483	1.667	2.78	1.39	2.00	B.38
73	14.4	5.56	2.483	1.667	3.47	0.35	10.01	
74	14.4	5.56	1.740	1.472	2.78	1.04	2.67	B.39
75	14.4	5.56	1.740	1.472	3.47	1.39	2.50	

Table 5.6 Continued

Observation Number	$D_i$ (cm)	$2b/D_i$	Fr	$S_c/D_i$	$L_p/D_i$	$W_p/D_i \geq$	$L_p/W_p$	Table
76	14.4	6.94	3.231	2.444	2.78	0.35	8.01	B.40
77	14.4	6.94	3.231	2.444	3.47	0.35	10.01	
78	14.4	6.94	2.483	1.924	2.78	0.35	8.01	B.41
79	14.4	6.94	2.483	1.924	3.47	0.35	10.01	
80	14.4	6.94	1.566	1.250	2.78	1.39	2.00	B.42
81	14.4	6.94	1.566	1.250	3.47	1.39	2.50	
82	14.4	8.33	3.231	2.424	2.78	0.69	4.00	B.43
83	14.4	8.33	3.231	2.424	3.47	0.35	10.01	
84	14.4	8.33	2.483	2.007	2.78	0.35	8.01	B.44
85	14.4	8.33	2.483	2.007	3.47	0.35	10.01	
86	14.4	8.33	1.566	1.354	2.78	1.39	2.00	B.45
87	14.4	8.33	1.566	1.354	3.47	1.04	3.33	
88	14.4	9.72	3.231	2.583	2.78	1.74	1.60	B.46
89	14.4	9.72	3.231	2.583	3.47	1.04	3.33	
90	14.4	9.72	2.483	1.771	2.78	0.69	4.00	B.47
91	14.4	9.72	2.483	1.771	3.47	0.35	10.01	
92	10.0	4.00	6.638	6.650	4.00	None	-	B.48
93	10.0	6.00	6.638	2.680	4.00	0.50	8.00	B.49
94	10.0	6.00	6.638	2.680	5.00	0.50	10.00	
95	10.0	6.00	4.986	2.440	4.00	0.50	8.00	B.50
96	10.0	6.00	4.986	2.440	5.00	0.50	10.00	
97	10.0	6.00	3.085	2.010	4.00	2.00	2.00	B.51
98	10.0	6.00	3.085	2.010	5.00	1.50	3.33	
99	10.0	8.00	6.638	3.230	4.00	0.50	8.00	B.52
100	10.0	8.00	6.638	3.230	5.00	0.50	10.00	
101	10.0	8.00	4.986	2.820	4.00	1.50	2.67	B.53
102	10.0	8.00	4.986	2.820	5.00	0.50	10.00	
103	10.0	8.00	3.085	2.170	4.00	0.50	8.00	B.54
104	10.0	8.00	3.085	2.170	5.00	2.00	2.50	
105	10.0	10.00	6.638	3.870	4.00	1.00	4.00	B.55
106	10.0	10.00	6.638	3.870	5.00	1.00	5.00	
107	10.0	10.00	4.986	3.090	4.00	1.50	2.67	B.56
108	10.0	10.00	4.986	3.090	5.00	1.50	3.33	
109	10.0	10.00	3.085	2.250	4.00	2.00	2.00	B.57
110	10.0	10.00	3.085	2.250	5.00	2.00	2.50	
111	10.0	12.00	6.638	3.920	4.00	1.00	4.00	B.58
112	10.0	12.00	6.638	3.920	5.00	1.00	5.00	

Table 5.6 Continued

Observation Number	$D_i$ (cm)	$2b/D_i$	Fr	$S_c/D_i$	$L_p/D_i$	$W_p/D_i \geq$	$L_p/W_p$	Table
113	10.0	12.00	4.986	2.650	4.00	1.50	2.67	B.59
114	10.0	12.00	4.986	2.650	5.00	1.50	3.33	
115	5.0	8.00	10.680	3.620	8.00	3.00	2.67	B.60
116	5.0	12.00	10.680	4.360	8.00	3.00	2.67	B.61
117	5.0	12.00	10.680	4.360	10.00	4.00	2.50	
118	5.0	16.00	10.680	4.420	8.00	3.00	2.67	B.62
119	5.0	16.00	10.680	4.420	10.00	3.00	3.33	

Table 5.7 Evaluation and summary of the data of Table 5.6 for intermediate  $S_c/D_i$

$D_i$ (cm)	$2b/D_i$	Fr	$S_c/D_i$	$(L_p/D_i)_1$	$(W_p/D_i)_1 \geq$	$(L_p/D_i)_2$	$(W_p/D_i)_2 \geq$
25	4.00	0.814	1.192	1.60	0.200	2.00	0.200
		0.625	1.024		0.200		0.200
		0.473	0.772		0.600		0.800
	4.80	0.814	1.176	1.60	0.200	2.00	0.200
		0.625	0.824		0.800		0.800
		0.473	0.596		0.600		0.600
	5.60	0.814	1.172	1.60	0.200	2.00	0.200
		0.625	0.848		0.200		0.200
		0.473	0.656		0.800		0.800
19.4	5.16	1.534	1.732	2.06	0.258	2.58	0.258
		1.179	1.366		0.258		0.258
		0.826	0.959		1.031		1.031
	6.19	1.534	1.696	2.06	0.258	2.58	0.258
		1.179	1.222		0.515		0.258
		0.826	1.026		0.773		1.031
	7.22	1.534	1.716	2.06	0.258	2.58	0.258
		1.179	1.294		0.258		0.258
		0.892	1.021		0.773		1.031

Table 5.7 Continued

$D_i$ (cm)	$2b/D_i$	Fr	$S_c/D_i$	$(L_p/D_i)_1$	$(W_p/D_i)_1 \geq$	$(L_p/D_i)_2$	$(W_p/D_i)_2 \geq$
14.4	6.94	3.231	2.444	2.78	0.347	3.47	0.347
		2.483	1.924		0.347		0.347
		1.566	1.250		1.389		1.389
	8.33	3.231	2.424	2.78	0.694	3.47	0.347
		2.483	2.007		0.470		0.347
		1.566	1.354		1.389		1.042
	9.72	3.231	2.583	2.78	1.736	3.47	1.042
		2.483	1.771		0.694		0.347
	10.0	10.00	6.638	3.870	4.00	1.000	5.00
4.986			3.090	1.500		1.500	
3.085			2.250	2.000		2.000	
12.00		6.638	3.920	4.00	1.000	5.00	1.000
		4.986	2.650		1.500		1.500
5.0		12.00	10.680	4.360	8.00	3.000	10.00
	16.00	10.680	4.420	8.00	3.000	10.00	3.000

Table 5.8 Data related to the selection of the most effective horizontal plate as an anti-vortex device

D <sub>i</sub> (cm)	2b/D <sub>i</sub>	≤ Fr ≤	(L <sub>p</sub> /D <sub>i</sub> ) <sub>1</sub>	(W <sub>p</sub> /D <sub>i</sub> ) <sub>1</sub> ≥	Selected		(L <sub>p</sub> /D <sub>i</sub> ) <sub>2</sub>	(W <sub>p</sub> /D <sub>i</sub> ) <sub>2</sub> ≥	Selected	
					(W <sub>p</sub> /D <sub>i</sub> ) <sub>1</sub>	(L <sub>p</sub> /W <sub>p</sub> ) <sub>1</sub>			(W <sub>p</sub> /D <sub>i</sub> ) <sub>2</sub>	(L <sub>p</sub> /W <sub>p</sub> ) <sub>2</sub>
25	4.00	0.473 - 0.814	1.60	0.600	0.80	2.00	2.00	0.800	0.80	2.50
	4.80			0.800				0.800		
	5.60			0.800				0.800		
19.4	5.16	0.826 - 1.534	2.06	1.031	2.03	2.00	2.58	1.031	1.03	2.50
	6.19			0.773				1.031		
	7.22			0.773				1.031		
14.4	6.94	1.566 - 3.231	2.78	1.389	1.74	2.00	3.47	1.389	1.39	2.50
	8.33			1.389				1.042		
	9.72			1.736				1.042		
10	10.00	3.085 - 6.638	4.00	2.000	2.00	4.00	5.00	2.000	2.00	2.50
	12.00			1.500				1.500		
5	12.00	10.68	8.00	3.000	3.00	8.00	10.00	4.000	4.00	2.50
	16.00			3.000				3.000		

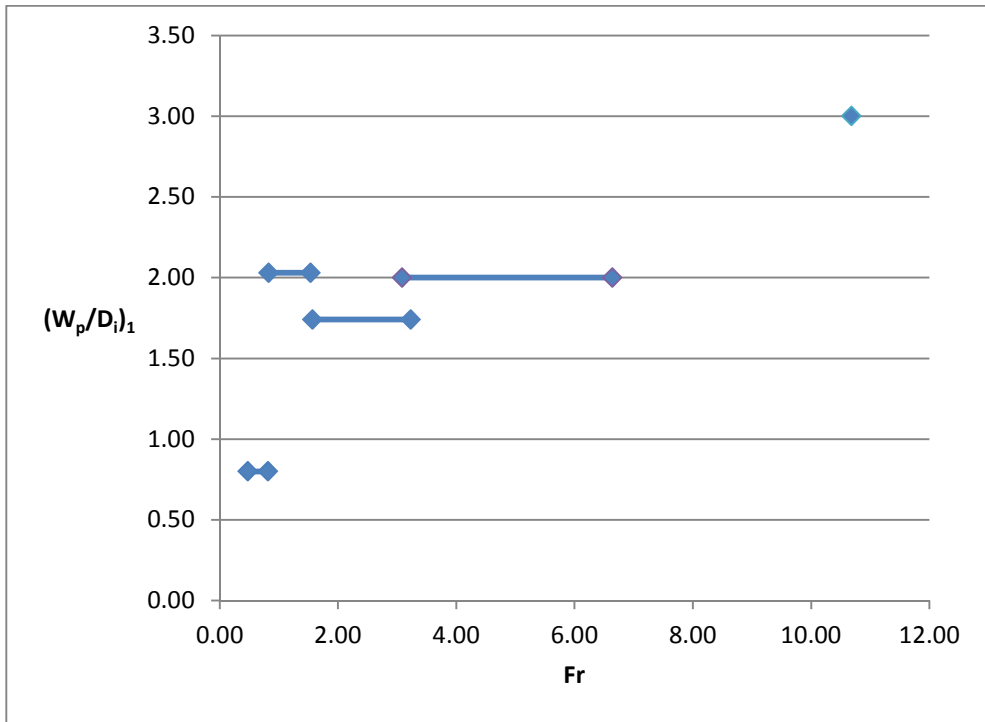


Figure 5.35 Variation of  $(W_p/D_i)_1$  with Fr for  $2.00 \leq L_p/W_p \leq 8.00$

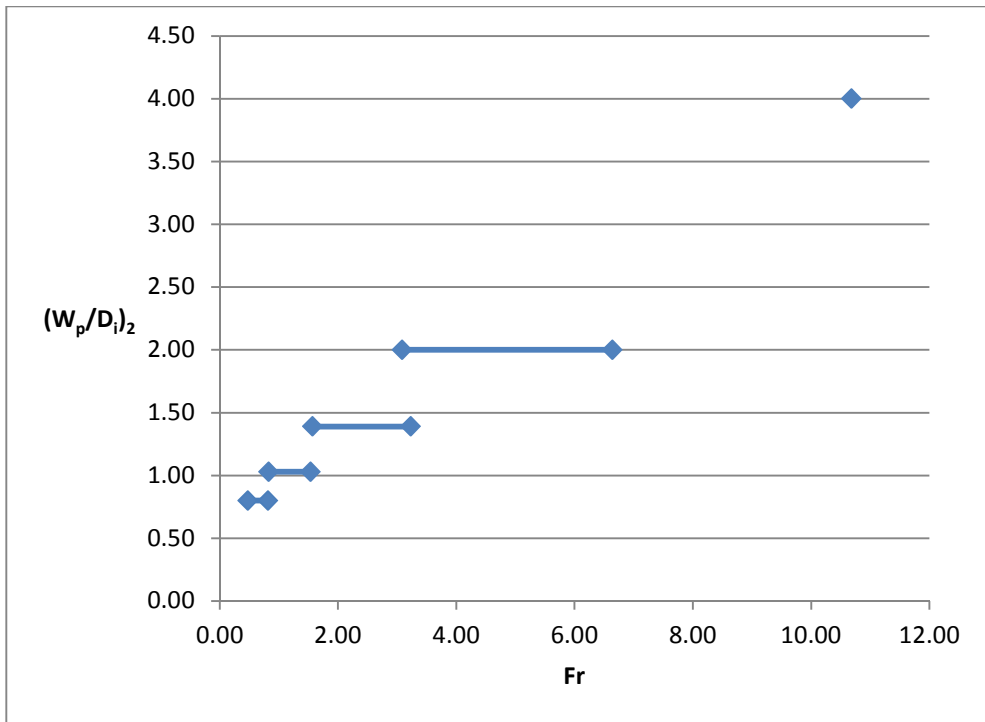


Figure 5.36 Variation of  $(W_p/D_i)_2$  with Fr for  $L_p/W_p = 2.5$



## CHAPTER 6

### CONCLUSION AND RECOMMENDATIONS

In the present study the effects of Froude, Reynolds, Weber numbers and side wall clearance on the formation of air-entraining vortices at horizontal intakes were investigated experimentally. Empirical equations for dimensionless critical submergence depth,  $S_c/D_i$ , were derived from experimental data as a function of relevant dimensionless parameters and the validity of them was checked with other data in the literature. Considering the model – prototype concept, the available data were analyzed and the scale effect on the values of dimensionless critical submergence was investigated. Horizontal plates were tested as anti-vortex devices to observe how much they are effective in reducing the strength of air-entraining vortices. From this experimental study, the following conclusions can be drawn:

1.  $S_c/D_i$  values increase gradually and almost linearly with increasing Fr, Re and We for a given  $2b/D_i$  of an intake pipe of known diameter.
2. At certain small  $2b/D_i$  values of an intake pipe, which are function of pipe diameter, maximum and minimum  $S_c/D_i$  values are obtained due to the strong blockage effect of the walls on the vortex formation.
3. At  $2b/D_i$  values larger than those stated above, the variation of  $S_c/D_i$  that can be called as “intermediate  $S_c/D_i$ ” with  $2b/D_i$  as a function Fr, Re and We is not very significant and becomes almost negligible as Fr, Re and We increase.
4. As a function of intake pipe diameter, there are limit values for Fr, Re, We and  $2b/D_i$  above which  $S_c/D_i$  is independent of  $2b/D_i$  and function of Fr, Re and We.
5. For all three cases described above; yielding maximum, minimum and intermediate  $S_c/D_i$  values as a function of  $2b/D_i$ , and for only limit values of Fr, Re and We, several empirical equations were derived for  $S_c/D_i$  with quite high correlation coefficients.
6. Even though removal of some of the parameters; such as Re, We and  $2b/D_i$  from the initial empirical equations, does not affect the value of  $S_c/D_i$  significantly, the use of simplified empirical equation in model – prototype relation does not give satisfactory results.
7. Due to the significant scale effects,  $S_c/D_i$  values to be obtained from model studies should be multiplied by a correlation coefficient before calculating the corresponding  $S_c/D_i$  values of the prototype directly from the length scale of the model. As the model length scale,  $L_r$ , decreases, the value of the correction coefficient increases.
8. Horizontal solid plates can be used as anti-vortex devices at intake structures to eliminate the air-entraining vortices. Plate length to width ratio about 2.0 – 2.5 and width to the pipe diameter ratio about 2 give satisfactory results.

For future studies, the following recommendations can be made:

1. Similar tests should be conducted, if it is possible, with intake pipes of much larger diameters at a wide range of Froude numbers.
2. Model studies of the available installations should be made at different length scales to provide more data to generalize the scale effects on the values of  $S_c/D_i$ .



## REFERENCES

- Ahmad, Z., Rao, K.V. and Mittal, M.K. (2008), "Critical Submergence for Horizontal Intakes in Open Channel Flows", Department of Civil Engineering, Indian Institute of Technology Roorkee, India.
- Amiri, S.M., Zarrati, A.R., Roshan, R. and Sarkardeh, H. (2011), "Surface Vortex Prevention at Power Intakes by Horizontal Plates", *Water Management*, 2011(WM4), 193-200.
- Anwar, H.O. (1965), "Flow in a Free Vortex", *Water Power* 1965(4), 153-161.
- Anwar, H.O. (1967), "Vortices at Low Head Intakes", *Water Power* 1967(11), 455-457.
- Anwar, H.O. (1968), "Prevention of Vortices at Intakes", *Water Power* 1968(10), 393-401.
- Anwar, H.O., Weller, J.A. and Amphlett, M.B. (1978), "Similarity of Free-Vortex at Horizontal Intake", *J. Hydraulic Res.* 1978(2), 95-105.
- Anwar, H.O. and Amphlett, M.B. (1980), "Vortices at Vertically Inverted Intake", *J. Hydraulic Res.* 1980(2), 123-134.
- Blaisdell F.W. and Donnelly C.A (1958), "Hydraulics of Closed Conduit Spillways Part X.: The Hood Inlet", Tech. Paper No. 20, Series B, University of Minnesota, St. Anthony Falls Hydraulic Laboratory.
- Daggett, L.L. and Keulegan, G.H. (1974), "Similitude in Free-Surface Vortex Formations", *J. Hydraulic Div., ASCE*, HY11, 1565-1581.
- Gordon, J.L. (1970), "Vortices at Intakes", *Water Power* 1970(4), 137-138.
- Gulliver, J.S. and Rindels, A.J. (1983), "An Experimental Study of Critical Submergence to Avoid Free-surface Vortices at Vertical Intakes", Project Report No: 224, University of Minnesota, St. Anthony Falls Hydraulic Laboratory.
- Gürbüzdal, F., (2009), "Scale effects on the formation of vortices at intake structures, M.S. Thesis, Civil Engineering Dept., METU.
- Iversen, H.W. (1953), "Studies of Submergence Requirements of High-Specific Speed Pumps", *ASME*, Vol. 75, 635-641.
- Jain, A.K., Kittur, G.R.R., and Ramachandra, J.G. (1978), "Air Entrainment in Radial Flow Towards Intakes", *J. Hydraulic Div., ASCE*, HY9, 1323-1329.
- Jain, A.K., Kittur, G.R.R., and Ramachandra, J.G. (1978), "Vortex Formation at Vertical Pipe Intakes", *J. Hydraulic Div., ASCE*, HY10, 1429-1448.
- Jiming, M., Yuanbo, L. and Jitang, H. (2000), "Minimum Submergence before Double-Entrance Pressure Intakes", *J. Hydraulic Div., ASCE*, HY10, 628-631.
- Knauss, J. (1987), "Swirling Flow Problems at Intakes", A.A. Balkema, Rotterdam.
- Li H., Chen H., Ma Z. and Zhou Y. (2008) "Experimental and Numerical Investigation of Free Surface Vortex", *J. Hydrodynamics* 2008(4), 485-491.

- Oakdale Engineering web site, <http://www.oakdaleengr.com/download.htm>, last accessed on 27.10.2012.
- Padmanabhan, M. and Hecker, G.E. (1984), "Scale Effects in Pump Sump Models", *J. Hydraulic Engineering*, ASCE, 110, HY11, 1540-1556.
- Reddy, Y.R. and Pickford, J.A. (1972), "Vortices at Intakes in Conventional Sumps", *Water Power* 1972(3), 108-109.
- Sarkardeh, H., Zarrati, A.R., and Roshan, R. (2010), "Effect of Intake Head Wall and Trash Rack on Vortices", *J. Hydraulic Research*, 48:1, 108-112.
- Taştan, K. and Yıldırım, N. (2010), "Effects of Dimensionless Parameters on Air-entraining Vortices", *J. Hydraulic Research*, 48:1, 57-64.
- Yıldırım, N. and Kocabaş, F. (1995), "Critical Submergence for Intakes in Open Channel Flow", *J. Hydraulic Engng.*, ASCE, 121, HY12, 900-905.
- Yıldırım, N., Kocabaş, F. and Gülcan, S.C. (2000), "Flow-Boundary Effects on Critical Submergence of Intake Pipe", *J. Hydraulic Engineering.*, ASCE, 126, HY4, 288-297.
- Yıldırım, N. and Kocabaş, F. (2002), "Prediction of Critical Submergence for an Intake Pipe", *J. Hydraulic Res.* 2002(4), 507-518.
- Yıldırım, N., Taştan, K. and Arslan, M.M. (2009) "Critical Submergence for Dual Pipe Intakes", *J. Hydraulic Research*, 47:2, 242-249.
- Zeigler, E.R. (1976), "Hydraulic Model Vortex Study Grand Coulee Third Powerplant", Engineering and Research Center, U.S Bureau of Reclamation, Denver, Colorado.
- Zielinski, P.B. and Villemonte, J.R. (1968), "Effect of Viscosity on Vortex- Orifice Flow", *J. Hydraulic Div.*, ASCE, HY3, 745-751.

## APPENDIX A

### EXPERIMENTAL RESULTS RELATED TO CRITICAL SUBMERGENCE

This appendix provides detailed data in the form of tables for the experimental results related to the critical submergence for each intake pipe tested. Figure A.1 given below shows the sketch of the model and symbols used in tables and calculations.

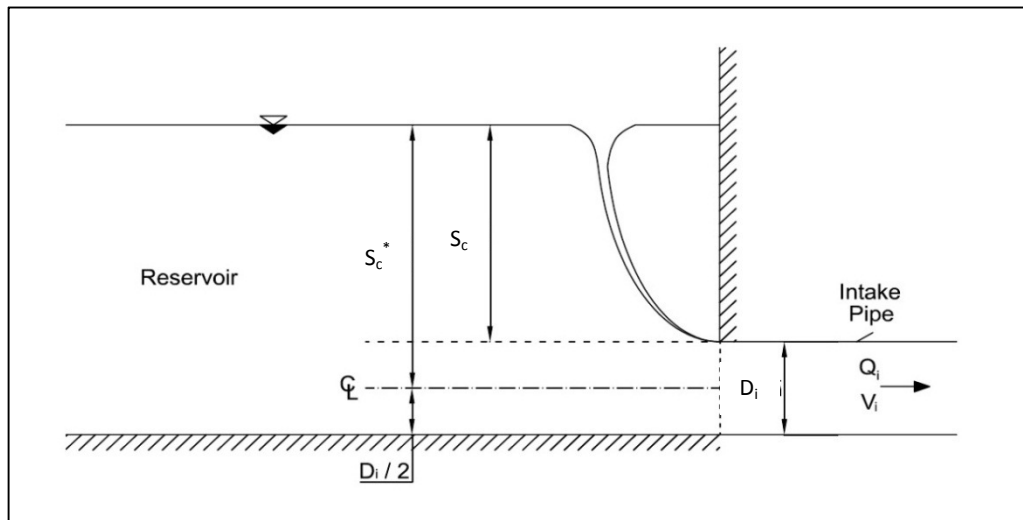


Figure A.1 Simple illustration of the critical submergence concept

In order to obtain dimensionless numbers, the following parameters are used in the related formulas with the given values at 20<sup>o</sup> C:

$$\begin{aligned} \nu &= 1.004\text{E-}6 \text{ (m}^2\text{/s)} \\ \rho &= 9.982\text{E+}2 \text{ (kg/m}^3\text{)} \\ \sigma &= 7.28\text{E-}2 \text{ (N/m)} \end{aligned}$$

It should be noted that  $S_c$  is from summit point of the intake and  $S_c^*$  is from centerline of the intake, herein.

Table A.1 Experimental results related to critical submergence for  $D_i = 30$  cm and  $2b = 40$  cm

Observation	$Q_i$ (l/s)	$S_c$ (cm)	$S_c^*$ (cm)	$S_c / D_i$	$V_i$ (m/s)	Fr	Re	We
1	61.08	57.20	72.20	1.907	0.864	0.504	258095	3069
2	57.23	56.20	71.20	1.873	0.809	0.472	241827	2694
3	52.11	55.70	70.70	1.857	0.737	0.430	220192	2234
4	47.20	51.60	66.60	1.720	0.667	0.389	199445	1833
5	43.33	49.00	64.00	1.633	0.613	0.357	183092	1544

Table A.2 Experimental results related to critical submergence for  $D_i = 30$  cm and  $2b = 60$  cm

Observation	$Q_i$ (l/s)	$S_c$ (cm)	$S_c^*$ (cm)	$S_c / D_i$	$V_i$ (m/s)	Fr	Re	We
1	61.57	14.20	29.20	0.473	0.871	0.508	260165	3118
2	58.18	12.50	27.50	0.417	0.823	0.480	245841	2784
3	55.81	11.40	26.40	0.380	0.789	0.460	235826	2562
4	52.57	10.45	25.45	0.348	0.743	0.433	222136	2273
5	49.40	8.50	23.50	0.283	0.699	0.407	208741	2007

Table A.3 Experimental results related to critical submergence for  $D_i = 30$  cm and  $2b = 80$  cm

Observation	$Q_i$ (l/s)	$S_c$ (cm)	$S_c^*$ (cm)	$S_c / D_i$	$V_i$ (m/s)	Fr	Re	We
1	61.57	15.70	30.70	0.523	0.871	0.508	260165	3118
2	60.10	14.70	29.70	0.490	0.850	0.496	253954	2971
3	58.18	14.40	29.40	0.480	0.823	0.480	245841	2784
4	56.75	14.10	29.10	0.470	0.803	0.468	239798	2649
5	55.34	12.60	27.60	0.420	0.783	0.456	233840	2519
6	53.49	11.70	26.70	0.390	0.756	0.441	226023	2354
7	52.57	8.90	23.90	0.297	0.743	0.433	222136	2273

Table A.4 Experimental results related to critical submergence for  $D_i = 30$  cm and  $2b = 100$  cm

Observation	$Q_i$ (l/s)	$S_c$ (cm)	$S_c^*$ (cm)	$S_c / D_i$	$V_i$ (m/s)	Fr	Re	We
1	61.57	25.05	40.05	0.835	0.871	0.508	260165	3118
2	59.14	24.70	39.70	0.823	0.836	0.488	249897	2877
3	57.23	24.20	39.20	0.807	0.809	0.472	241827	2694
4	55.81	23.60	38.60	0.787	0.789	0.460	235826	2562
5	53.95	22.40	37.40	0.747	0.763	0.445	227967	2394
6	50.75	21.60	36.60	0.720	0.718	0.418	214445	2119
7	48.08	20.10	35.10	0.670	0.680	0.396	203163	1902
8	45.89	17.90	32.90	0.597	0.649	0.378	193909	1732
9	43.33	17.10	32.10	0.570	0.613	0.357	183092	1544
10	40.83	16.10	31.10	0.537	0.577	0.337	172528	1371
11	39.19	14.90	29.90	0.497	0.554	0.323	165598	1263
12	36.79	12.40	27.40	0.413	0.520	0.303	155457	1113

Table A.5 Experimental results related to critical submergence for  $D_i = 30$  cm and  $2b = 120$  cm

Observation	$Q_i$ (l/s)	$S_c$ (cm)	$S_c^*$ (cm)	$S_c / D_i$	$V_i$ (m/s)	Fr	Re	We
1	61.57	24.90	39.90	0.830	0.871	0.508	260165	3118
2	59.14	24.10	39.10	0.803	0.836	0.488	249897	2877
3	57.23	22.60	37.60	0.753	0.809	0.472	241827	2694
4	55.81	21.90	36.90	0.730	0.789	0.460	235826	2562
5	53.95	20.80	35.80	0.693	0.763	0.445	227967	2394
6	50.75	18.90	33.90	0.630	0.718	0.418	214445	2119

Table A.6 Experimental results related to critical submergence for  $D_i = 30$  cm and  $2b = 140$  cm

Observation	$Q_i$ (l/s)	$S_c$ (cm)	$S_c^*$ (cm)	$S_c / D_i$	$V_i$ (m/s)	Fr	Re	We
1	61.57	24.30	39.30	0.810	0.871	0.508	260165	3118
2	59.14	23.90	38.90	0.797	0.836	0.488	249897	2877
3	57.23	21.90	36.90	0.730	0.809	0.472	241827	2694
4	55.81	19.10	34.10	0.637	0.789	0.460	235826	2562
5	53.95	16.10	31.10	0.537	0.763	0.445	227967	2394
6	50.75	14.80	29.80	0.493	0.718	0.418	214445	2119

Table A.7 Experimental results related to critical submergence for  $D_i = 25$  cm and  $2b = 40$  cm

Observation	$Q_i$ (l/s)	$S_c$ (cm)	$S_c^*$ (cm)	$S_c / D_i$	$V_i$ (m/s)	Fr	Re	We
1	62.55	60.70	73.20	2.428	1.274	0.814	317168	5561
2	59.14	59.70	72.20	2.388	1.204	0.769	299877	4972
3	56.28	58.80	71.30	2.352	1.146	0.732	285375	4502
4	53.49	58.00	70.50	2.320	1.089	0.696	271228	4067
5	50.75	56.70	69.20	2.268	1.033	0.660	257334	3661
6	48.08	56.40	68.90	2.256	0.979	0.625	243796	3286

Table A.8 Experimental results related to critical submergence for  $D_i = 25$  cm and  $2b = 60$  cm

Observation	$Q_i$ (l/s)	$S_c$ (cm)	$S_c^*$ (cm)	$S_c / D_i$	$V_i$ (m/s)	Fr	Re	We
1	62.55	19.80	32.30	0.792	1.274	0.814	317168	5561
2	59.14	18.40	30.90	0.736	1.204	0.769	299877	4972
3	56.28	18.00	30.50	0.720	1.146	0.732	285375	4502
4	53.49	17.50	30.00	0.700	1.089	0.696	271228	4067
5	50.75	17.10	29.60	0.684	1.033	0.660	257334	3661
6	48.08	16.80	29.30	0.672	0.979	0.625	243796	3286
7	45.46	16.00	28.50	0.640	0.926	0.591	230511	2938
8	42.49	14.80	27.30	0.592	0.865	0.553	215451	2566
9	39.19	14.10	26.60	0.564	0.798	0.510	198718	2183
10	36.40	13.20	25.70	0.528	0.741	0.473	184571	1883
11	33.69	12.40	24.90	0.496	0.686	0.438	170829	1613
12	30.32	10.90	23.40	0.436	0.617	0.394	153741	1307

Table A.9 Experimental results related to critical submergence for  $D_i = 25$  cm and  $2b = 80$  cm

Observation	$Q_i$ (l/s)	$S_c$ (cm)	$S_c^*$ (cm)	$S_c / D_i$	$V_i$ (m/s)	Fr	Re	We
1	62.55	25.00	37.50	1.000	1.274	0.814	317168	5561
2	59.14	24.50	37.00	0.980	1.204	0.769	299877	4972
3	56.28	23.80	36.30	0.952	1.146	0.732	285375	4502
4	53.49	22.70	35.20	0.908	1.089	0.696	271228	4067
5	50.75	22.30	34.80	0.892	1.033	0.660	257334	3661
6	48.08	21.70	34.20	0.868	0.979	0.625	243796	3286
7	45.46	21.30	33.80	0.852	0.926	0.591	230511	2938
8	42.49	20.70	33.20	0.828	0.865	0.553	215451	2566
9	39.19	19.40	31.90	0.776	0.798	0.510	198718	2183
10	36.40	18.60	31.10	0.744	0.741	0.473	184571	1883
11	33.69	17.60	30.10	0.704	0.686	0.438	170829	1613
12	30.32	15.90	28.40	0.636	0.617	0.394	153741	1307
13	27.45	14.00	26.50	0.560	0.559	0.357	139189	1071
14	24.34	13.10	25.60	0.524	0.496	0.317	123419	842

Table A.10 Experimental results related to critical submergence for  $D_i = 25$  cm and  $2b = 100$  cm

Observation	$Q_i$ (l/s)	$S_c$ (cm)	$S_c^*$ (cm)	$S_c / D_i$	$V_i$ (m/s)	Fr	Re	We
1	62.55	29.80	42.30	1.192	1.274	0.814	317168	5561
2	59.14	28.90	41.40	1.156	1.204	0.769	299877	4972
3	56.28	28.10	40.60	1.124	1.146	0.732	285375	4502
4	53.49	27.20	39.70	1.088	1.089	0.696	271228	4067
5	50.75	26.60	39.10	1.064	1.033	0.660	257334	3661
6	48.08	25.60	38.10	1.024	0.979	0.625	243796	3286
7	45.46	24.00	36.50	0.960	0.926	0.591	230511	2938
8	42.49	22.40	34.90	0.896	0.865	0.553	215451	2566
9	39.19	20.70	33.20	0.828	0.798	0.510	198718	2183
10	36.40	19.00	31.50	0.760	0.741	0.473	184571	1883
11	33.69	17.10	29.60	0.684	0.686	0.438	170829	1613
12	30.32	15.80	28.30	0.632	0.617	0.394	153741	1307

Table A.11 Experimental results related to critical submergence for  $D_i = 25$  cm and  $2b = 120$  cm

Observation	$Q_i$ (l/s)	$S_c$ (cm)	$S_c^*$ (cm)	$S_c / D_i$	$V_i$ (m/s)	Fr	Re	We
1	62.55	29.40	41.90	1.176	1.274	0.814	317168	5561
2	59.14	28.50	41.00	1.140	1.204	0.769	299877	4972
3	56.28	27.60	40.10	1.104	1.146	0.732	285375	4502
4	53.49	24.80	37.30	0.992	1.089	0.696	271228	4067
5	50.75	22.60	35.10	0.904	1.033	0.660	257334	3661
6	48.08	20.60	33.10	0.824	0.979	0.625	243796	3286
7	45.46	19.10	31.60	0.764	0.926	0.591	230511	2938
8	42.49	17.50	30.00	0.700	0.865	0.553	215451	2566
9	39.19	16.70	29.20	0.668	0.798	0.510	198718	2183
10	36.40	14.90	27.40	0.596	0.741	0.473	184571	1883

Table A.12 Experimental results related to critical submergence for  $D_i = 25$  cm and  $2b = 140$  cm

Observation	$Q_i$ (l/s)	$S_c$ (cm)	$S_c^*$ (cm)	$S_c / D_i$	$V_i$ (m/s)	Fr	Re	We
1	62.55	29.30	41.80	1.172	1.274	0.814	317168	5561
2	59.14	28.30	40.80	1.132	1.204	0.769	299877	4972
3	56.28	27.70	40.20	1.108	1.146	0.732	285375	4502
4	53.49	25.20	37.70	1.008	1.089	0.696	271228	4067
5	50.75	23.20	35.70	0.928	1.033	0.660	257334	3661
6	48.08	21.20	33.70	0.848	0.979	0.625	243796	3286
7	45.46	19.80	32.30	0.792	0.926	0.591	230511	2938
8	42.49	19.30	31.80	0.772	0.865	0.553	215451	2566
9	39.19	17.70	30.20	0.708	0.798	0.510	198718	2183
10	36.40	16.40	28.90	0.656	0.741	0.473	184571	1883
11	33.69	14.30	26.80	0.572	0.686	0.438	170829	1613

Table A.13 Experimental results related to critical submergence for  $D_i = 19.4$  cm and  $2b = 40$  cm

Observation	$Q_i$ (l/s)	$S_c$ (cm)	$S_c^*$ (cm)	$S_c / D_i$	$V_i$ (m/s)	Fr	Re	We
1	62.55	64.50	74.20	3.325	2.115	1.534	408721	11902
2	59.14	64.10	73.80	3.304	2.000	1.450	386439	10639
3	56.28	63.80	73.50	3.289	1.903	1.380	367751	9635
4	53.49	63.30	73.00	3.263	1.809	1.311	349520	8704
5	50.75	62.90	72.60	3.242	1.716	1.244	331616	7835
6	48.08	62.40	72.10	3.216	1.626	1.179	314170	7032
7	45.46	61.90	71.60	3.191	1.537	1.115	297050	6287
8	42.49	61.40	71.10	3.165	1.437	1.042	277643	5492

Table A.14 Experimental results related to critical submergence for  $D_i = 19.4$  cm and  $2b = 60$  cm

Observation	$Q_i$ (l/s)	$S_c$ (cm)	$S_c^*$ (cm)	$S_c / D_i$	$V_i$ (m/s)	Fr	Re	We
1	62.55	24.60	34.30	1.268	2.115	1.534	408721	11902
2	59.14	23.00	32.70	1.186	2.000	1.450	386439	10639
3	56.28	22.40	32.10	1.155	1.903	1.380	367751	9635
4	53.49	22.00	31.70	1.134	1.809	1.311	349520	8704
5	50.75	21.70	31.40	1.119	1.716	1.244	331616	7835
6	48.08	21.20	30.90	1.093	1.626	1.179	314170	7032
7	45.46	20.50	30.20	1.057	1.537	1.115	297050	6287
8	42.49	19.70	29.40	1.015	1.437	1.042	277643	5492
9	39.19	19.00	28.70	0.979	1.325	0.961	256080	4672
10	36.40	18.40	28.10	0.948	1.231	0.892	237849	4030
11	33.69	16.90	26.60	0.871	1.139	0.826	220141	3453
12	30.32	15.30	25.00	0.789	1.025	0.743	198120	2796
13	27.45	14.20	23.90	0.732	0.928	0.673	179367	2292
14	24.34	13.50	23.20	0.696	0.823	0.597	159045	1802
15	21.69	12.90	22.60	0.665	0.733	0.532	141729	1431

Table A.15 Experimental results related to critical submergence for  $D_i = 19.4$  cm and  $2b = 80$  cm

Observation	$Q_i$ (l/s)	$S_c$ (cm)	$S_c^*$ (cm)	$S_c / D_i$	$V_i$ (m/s)	Fr	Re	We
1	62.55	28.20	37.90	1.454	2.115	1.534	408721	11902
2	59.14	25.30	35.00	1.304	2.000	1.450	386439	10639
3	56.28	23.60	33.30	1.216	1.903	1.380	367751	9635
4	53.49	23.20	32.90	1.196	1.809	1.311	349520	8704
5	50.75	22.90	32.60	1.180	1.716	1.244	331616	7835
6	48.08	22.40	32.10	1.155	1.626	1.179	314170	7032
7	45.46	22.00	31.70	1.134	1.537	1.115	297050	6287
8	42.49	21.50	31.20	1.108	1.437	1.042	277643	5492
9	39.19	20.70	30.40	1.067	1.325	0.961	256080	4672
10	36.40	19.90	29.60	1.026	1.231	0.892	237849	4030
11	33.69	18.30	28.00	0.943	1.139	0.826	220141	3453
12	30.32	17.20	26.90	0.887	1.025	0.743	198120	2796
13	27.45	15.70	25.40	0.809	0.928	0.673	179367	2292
14	24.34	13.50	23.20	0.696	0.823	0.597	159045	1802

Table A.16 Experimental results related to critical submergence for  $D_i = 19.4$  cm and  $2b = 100$  cm

Observation	$Q_i$ (l/s)	$S_c$ (cm)	$S_c^*$ (cm)	$S_c / D_i$	$V_i$ (m/s)	Fr	Re	We
1	62.55	33.60	43.30	1.732	2.115	1.534	408721	11902
2	59.14	33.00	42.70	1.701	2.000	1.450	386439	10639
3	56.28	32.10	41.80	1.655	1.903	1.380	367751	9635
4	53.49	31.00	40.70	1.598	1.809	1.311	349520	8704
5	50.75	29.10	38.80	1.500	1.716	1.244	331616	7835
6	48.08	26.50	36.20	1.366	1.626	1.179	314170	7032
7	45.46	23.80	33.50	1.227	1.537	1.115	297050	6287
8	42.49	22.70	32.40	1.170	1.437	1.042	277643	5492
9	39.19	21.90	31.60	1.129	1.325	0.961	256080	4672
10	36.40	20.50	30.20	1.057	1.231	0.892	237849	4030
11	33.69	18.60	28.30	0.959	1.139	0.826	220141	3453
12	30.32	16.60	26.30	0.856	1.025	0.743	198120	2796
13	27.45	14.30	24.00	0.737	0.928	0.673	179367	2292
14	24.34	12.50	22.20	0.644	0.823	0.597	159045	1802

Table A.17 Experimental results related to critical submergence for  $D_i = 19.4$  cm and  $2b = 120$  cm

Observation	$Q_i$ (l/s)	$S_c$ (cm)	$S_c^*$ (cm)	$S_c / D_i$	$V_i$ (m/s)	Fr	Re	We
1	62.55	32.90	42.60	1.696	2.115	1.534	408721	11902
2	59.14	30.60	40.30	1.577	2.000	1.450	386439	10639
3	56.28	28.60	38.30	1.474	1.903	1.380	367751	9635
4	53.49	25.70	35.40	1.325	1.809	1.311	349520	8704
5	50.75	24.20	33.90	1.247	1.716	1.244	331616	7835
6	48.08	23.70	33.40	1.222	1.626	1.179	314170	7032
7	45.46	23.10	32.80	1.191	1.537	1.115	297050	6287
8	42.49	22.50	32.20	1.160	1.437	1.042	277643	5492
9	39.19	21.60	31.30	1.113	1.325	0.961	256080	4672
10	36.40	20.90	30.60	1.077	1.231	0.892	237849	4030
11	33.69	19.90	29.60	1.026	1.139	0.826	220141	3453
12	30.32	17.70	27.40	0.912	1.025	0.743	198120	2796

Table A.18 Experimental results related to critical submergence for  $D_i = 19.4$  cm and  $2b = 140$  cm

Observation	$Q_i$ (l/s)	$S_c$ (cm)	$S_c^*$ (cm)	$S_c / D_i$	$V_i$ (m/s)	Fr	Re	We
1	62.55	33.30	43.00	1.716	2.115	1.534	408721	11902
2	59.14	31.90	41.60	1.644	2.000	1.450	386439	10639
3	56.28	29.40	39.10	1.515	1.903	1.380	367751	9635
4	53.49	26.50	36.20	1.366	1.809	1.311	349520	8704
5	50.75	26.00	35.70	1.340	1.716	1.244	331616	7835
6	48.08	25.10	34.80	1.294	1.626	1.179	314170	7032
7	45.46	23.70	33.40	1.222	1.537	1.115	297050	6287
8	42.49	22.90	32.60	1.180	1.437	1.042	277643	5492
9	39.19	21.70	31.40	1.119	1.325	0.961	256080	4672
10	36.40	19.80	29.50	1.021	1.231	0.892	237849	4030

Table A.19 Experimental results related to critical submergence for  $D_i = 14.4$  cm and  $2b = 40$  cm

Observation	$Q_i$ (l/s)	$S_c$ (cm)	$S_c^*$ (cm)	$S_c / D_i$	$V_i$ (m/s)	Fr	Re	We
1	62.55	75.50	82.70	5.243	3.839	3.231	550638	29102
2	59.14	73.10	80.30	5.076	3.630	3.055	520620	26015
3	56.28	71.80	79.00	4.986	3.454	2.907	495442	23560

Table A.20 Experimental results related to critical submergence for  $D_i = 14.4$  cm and  $2b = 60$  cm

Observation	$Q_i$ (l/s)	$S_c$ (cm)	$S_c^*$ (cm)	$S_c / D_i$	$V_i$ (m/s)	Fr	Re	We
1	62.55	25.30	32.50	1.757	3.839	3.231	550638	29102
2	59.14	24.30	31.50	1.688	3.630	3.055	520620	26015
3	56.28	23.10	30.30	1.604	3.454	2.907	495442	23560
4	53.49	22.20	29.40	1.542	3.283	2.763	470882	21282
5	50.75	21.70	28.90	1.507	3.115	2.621	446761	19158
6	48.08	21.10	28.30	1.465	2.951	2.483	423256	17195
7	45.46	20.40	27.60	1.417	2.790	2.348	400192	15372
8	42.49	19.60	26.80	1.361	2.608	2.195	374047	13429
9	39.19	19.10	26.30	1.326	2.405	2.024	344996	11424
10	36.40	18.50	25.70	1.285	2.234	1.880	320435	9855
11	33.69	18.20	25.40	1.264	2.068	1.740	296579	8443
12	30.32	17.20	24.40	1.194	1.861	1.566	266912	6838
13	27.45	16.60	23.80	1.153	1.685	1.418	241647	5605
14	24.34	16.10	23.30	1.118	1.494	1.257	214269	4407
15	21.69	15.40	22.60	1.069	1.331	1.120	190941	3499

Table A.21 Experimental results related to critical submergence for  $D_i = 14.4$  cm and  $2b = 80$  cm

Observation	$Q_i$ (l/s)	$S_c$ (cm)	$S_c^*$ (cm)	$S_c / D_i$	$V_i$ (m/s)	Fr	Re	We
1	62.55	30.90	38.10	2.146	3.839	3.231	550638	29102
2	59.14	28.10	35.30	1.951	3.630	3.055	520620	26015
3	56.28	26.50	33.70	1.840	3.454	2.907	495442	23560
4	53.49	25.00	32.20	1.736	3.283	2.763	470882	21282
5	50.75	24.50	31.70	1.701	3.115	2.621	446761	19158
6	48.08	24.00	31.20	1.667	2.951	2.483	423256	17195
7	45.46	23.30	30.50	1.618	2.790	2.348	400192	15372
8	42.49	22.70	29.90	1.576	2.608	2.195	374047	13429
9	39.19	22.10	29.30	1.535	2.405	2.024	344996	11424
10	36.40	21.60	28.80	1.500	2.234	1.880	320435	9855
11	33.69	21.20	28.40	1.472	2.068	1.740	296579	8443
12	30.32	20.50	27.70	1.424	1.861	1.566	266912	6838
13	27.45	19.00	26.20	1.319	1.685	1.418	241647	5605
14	24.34	17.50	24.70	1.215	1.494	1.257	214269	4407

Table A.22 Experimental results related to critical submergence for  $D_i = 14.4$  cm and  $2b = 100$  cm

Observation	$Q_i$ (l/s)	$S_c$ (cm)	$S_c^*$ (cm)	$S_c / D_i$	$V_i$ (m/s)	Fr	Re	We
1	62.55	35.20	42.40	2.444	3.839	3.231	550638	29102
2	59.14	33.90	41.10	2.354	3.630	3.055	520620	26015
3	56.28	33.50	40.70	2.326	3.454	2.907	495442	23560
4	53.49	32.70	39.90	2.271	3.283	2.763	470882	21282
5	50.75	30.70	37.90	2.132	3.115	2.621	446761	19158
6	48.08	27.70	34.90	1.924	2.951	2.483	423256	17195
7	45.46	25.10	32.30	1.743	2.790	2.348	400192	15372
8	42.49	22.50	29.70	1.563	2.608	2.195	374047	13429
9	39.19	21.80	29.00	1.514	2.405	2.024	344996	11424
10	36.40	20.70	27.90	1.438	2.234	1.880	320435	9855
11	33.69	19.20	26.40	1.333	2.068	1.740	296579	8443
12	30.32	18.00	25.20	1.250	1.861	1.566	266912	6838
13	27.45	16.30	23.50	1.132	1.685	1.418	241647	5605

Table A.23 Experimental results related to critical submergence for  $D_i = 14.4$  cm and  $2b = 120$  cm

Observation	$Q_i$ (l/s)	$S_c$ (cm)	$S_c^*$ (cm)	$S_c / D_i$	$V_i$ (m/s)	Fr	Re	We
1	62.55	34.90	42.10	2.424	3.839	3.231	550638	29102
2	59.14	34.30	41.50	2.382	3.630	3.055	520620	26015
3	56.28	33.50	40.70	2.326	3.454	2.907	495442	23560
4	53.49	32.80	40.00	2.278	3.283	2.763	470882	21282
5	50.75	31.10	38.30	2.160	3.115	2.621	446761	19158
6	48.08	28.90	36.10	2.007	2.951	2.483	423256	17195
7	45.46	26.50	33.70	1.840	2.790	2.348	400192	15372
8	42.49	23.60	30.80	1.639	2.608	2.195	374047	13429
9	39.19	22.50	29.70	1.563	2.405	2.024	344996	11424
10	36.40	22.10	29.30	1.535	2.234	1.880	320435	9855
11	33.69	21.40	28.60	1.486	2.068	1.740	296579	8443
12	30.32	19.50	26.70	1.354	1.861	1.566	266912	6838
13	27.45	16.80	24.00	1.167	1.685	1.418	241647	5605

Table A.24 Experimental results related to critical submergence for  $D_i = 14.4$  cm and  $2b = 140$  cm

Observation	$Q_i$ (l/s)	$S_c$ (cm)	$S_c^*$ (cm)	$S_c / D_i$	$V_i$ (m/s)	Fr	Re	We
1	62.55	37.20	44.40	2.583	3.839	3.231	550638	29102
2	59.14	36.00	43.20	2.500	3.630	3.055	520620	26015
3	56.28	34.30	41.50	2.382	3.454	2.907	495442	23560
4	53.49	30.90	38.10	2.146	3.283	2.763	470882	21282
5	50.75	28.00	35.20	1.944	3.115	2.621	446761	19158
6	48.08	25.50	32.70	1.771	2.951	2.483	423256	17195
7	45.46	23.10	30.30	1.604	2.790	2.348	400192	15372
8	42.49	22.20	29.40	1.542	2.608	2.195	374047	13429
9	39.19	21.00	28.20	1.458	2.405	2.024	344996	11424

Table A.25 Experimental results related to critical submergence for  $D_i = 10$  cm and  $2b = 40$  cm

Observation	$Q_i$ (l/s)	$S_c$ (cm)	$S_c^*$ (cm)	$S_c / D_i$	$V_i$ (m/s)	Fr	Re	We
1	51.65	66.50	71.50	6.650	6.574	6.638	654745	59251
2	48.96	62.50	67.50	6.250	6.231	6.293	620645	53240

Table A.26 Experimental results related to critical submergence for  $D_i = 10$  cm and  $2b = 60$  cm

Observation	$Q_i$ (l/s)	$S_c$ (cm)	$S_c^*$ (cm)	$S_c / D_i$	$V_i$ (m/s)	Fr	Re	We
1	51.65	26.80	31.80	2.680	6.574	6.638	654745	59251
2	48.96	26.40	31.40	2.640	6.231	6.293	620645	53240
3	46.33	25.90	30.90	2.590	5.897	5.955	587305	47674
4	43.75	25.40	30.40	2.540	5.568	5.623	554600	42512
5	41.24	25.10	30.10	2.510	5.249	5.300	522782	37774
6	38.79	24.40	29.40	2.440	4.937	4.986	491724	33419
7	36.40	23.40	28.40	2.340	4.633	4.678	461427	29428
8	34.07	22.50	27.50	2.250	4.336	4.379	431891	25781
9	31.43	21.70	26.70	2.170	4.000	4.040	398424	21940
10	28.87	20.90	25.90	2.090	3.674	3.711	365972	18512
11	26.40	20.40	25.40	2.040	3.360	3.393	334661	15480
12	24.00	20.10	25.10	2.010	3.055	3.085	304238	12793
13	21.37	18.80	23.80	1.880	2.720	2.747	270898	10143

Table A.27 Experimental results related to critical submergence for  $D_i = 10$  cm and  $2b = 80$  cm

Observation	$Q_i$ (l/s)	$S_c$ (cm)	$S_c^*$ (cm)	$S_c / D_i$	$V_i$ (m/s)	Fr	Re	We
1	51.65	32.30	37.30	3.230	6.574	6.638	654745	59251
2	48.96	31.70	36.70	3.170	6.231	6.293	620645	53240
3	46.33	30.30	35.30	3.030	5.897	5.955	587305	47674
4	43.75	29.10	34.10	2.910	5.568	5.623	554600	42512
5	41.24	28.60	33.60	2.860	5.249	5.300	522782	37774
6	38.79	28.20	33.20	2.820	4.937	4.986	491724	33419
7	36.40	27.30	32.30	2.730	4.633	4.678	461427	29428
8	34.07	26.40	31.40	2.640	4.336	4.379	431891	25781
9	31.43	25.80	30.80	2.580	4.000	4.040	398424	21940
10	28.87	24.50	29.50	2.450	3.674	3.711	365972	18512
11	26.40	22.50	27.50	2.250	3.360	3.393	334661	15480
12	24.00	21.70	26.70	2.170	3.055	3.085	304238	12793
13	21.37	20.10	25.10	2.010	2.720	2.747	270898	10143

Table A.28 Experimental results related to critical submergence for  $D_i = 10$  cm and  $2b = 100$  cm

Observation	$Q_i$ (l/s)	$S_c$ (cm)	$S_c^*$ (cm)	$S_c / D_i$	$V_i$ (m/s)	Fr	Re	We
1	51.65	38.70	43.70	3.870	6.574	6.638	654745	59251
2	48.96	36.00	41.00	3.600	6.231	6.293	620645	53240
3	46.33	32.90	37.90	3.290	5.897	5.955	587305	47674
4	43.75	32.30	37.30	3.230	5.568	5.623	554600	42512
5	41.24	31.50	36.50	3.150	5.249	5.300	522782	37774
6	38.79	30.90	35.90	3.090	4.937	4.986	491724	33419
7	36.40	29.90	34.90	2.990	4.633	4.678	461427	29428
8	34.07	28.50	33.50	2.850	4.336	4.379	431891	25781
9	31.43	27.70	32.70	2.770	4.000	4.040	398424	21940
10	28.87	26.10	31.10	2.610	3.674	3.711	365972	18512
11	26.40	24.60	29.60	2.460	3.360	3.393	334661	15480
12	24.00	22.50	27.50	2.250	3.055	3.085	304238	12793

Table A.29 Experimental results related to critical submergence for  $D_i = 10$  cm and  $2b = 120$  cm

Observation	$Q_i$ (l/s)	$S_c$ (cm)	$S_c^*$ (cm)	$S_c / D_i$	$V_i$ (m/s)	Fr	Re	We
1	51.65	39.20	44.20	3.920	6.574	6.638	654745	59251
2	48.96	38.50	43.50	3.850	6.231	6.293	620645	53240
3	46.33	31.70	36.70	3.170	5.897	5.955	587305	47674
4	43.75	31.30	36.30	3.130	5.568	5.623	554600	42512
5	41.24	28.60	33.60	2.860	5.249	5.300	522782	37774
6	38.79	26.50	31.50	2.650	4.937	4.986	491724	33419
7	36.40	24.50	29.50	2.450	4.633	4.678	461427	29428
8	34.07	23.70	28.70	2.370	4.336	4.379	431891	25781
9	31.43	22.90	27.90	2.290	4.000	4.040	398424	21940
10	28.87	21.50	26.50	2.150	3.674	3.711	365972	18512

Table A.30 Experimental results related to critical submergence for  $D_i = 5$  cm and  $2b = 40$  cm

Observation	$Q_i$ (l/s)	$S_c$ (cm)	$S_c^*$ (cm)	$S_c / D_i$	$V_i$ (m/s)	Fr	Re	We
1	14.69	18.10	20.60	3.620	7.479	10.680	372438	38343
2	13.28	16.70	19.20	3.340	6.761	9.655	336690	31336
3	11.65	15.00	17.50	3.000	5.931	8.470	295364	24116
4	10.34	13.60	16.10	2.720	5.264	7.518	262151	18997
5	9.07	12.50	15.00	2.500	4.617	6.594	229953	14617
6	7.85	10.80	13.30	2.160	3.996	5.707	199022	10949
7	6.66	9.50	12.00	1.900	3.391	4.842	168852	7881

Table A.31 Experimental results related to critical submergence for  $D_i = 5$  cm and  $2b = 60$  cm

Observation	$Q_i$ (l/s)	$S_c$ (cm)	$S_c^*$ (cm)	$S_c / D_i$	$V_i$ (m/s)	Fr	Re	We
1	14.69	21.80	24.30	4.360	7.479	10.680	372438	38343
2	13.28	19.60	22.10	3.920	6.761	9.655	336690	31336
3	11.65	17.60	20.10	3.520	5.931	8.470	295364	24116

Table A.32 Experimental results related to critical submergence for  $D_i = 5$  cm and  $2b = 80$  cm

Observation	$Q_i$ (l/s)	$S_c$ (cm)	$S_c^*$ (cm)	$S_c / D_i$	$V_i$ (m/s)	Fr	Re	We
1	14.69	22.10	24.60	4.420	7.479	10.680	372438	38343
2	13.28	20.90	23.40	4.180	6.761	9.655	336690	31336

## APPENDIX B

### EXPERIMENTAL RESULTS RELATED TO ANTI-VORTEX PLATES

This appendix provides detailed data for the experimental results related to anti-vortex plates for each intake pipe, anti-vortex plate and side wall clearance used during experiments. Experimental results are introduced with tables and abbreviations used in the tables are given below with Figure B.1 for better understanding.

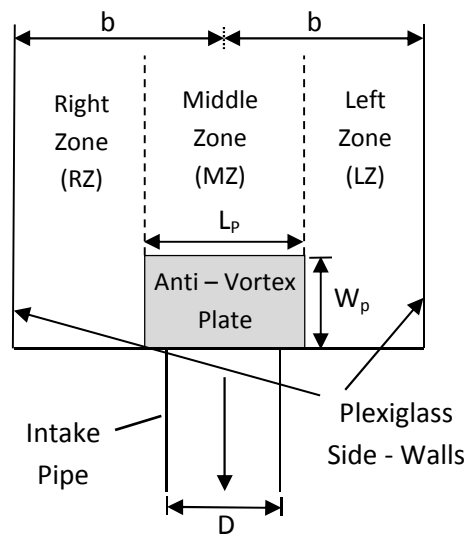


Figure B.1 Plan View of Vortex Zones

DV = Double vortex

$L_p$  = Plate length

LZ = Occurs at left zone

MZ = Occurs at middle zone

NBCTO = Not but close to occurring

NO = Not occurring

O = Occurs

R = Rarely occurs

RZ = Occurs at right zone

S = Satisfactory

US = Unsatisfactory

$W_p$  = Plate width

Table B.1 Experimental results related to the anti – vortex plate for  $D_i = 25.0$  cm,  $Q_i = 62.55$  lt/s and  $2b = 60$  cm

$D_i = 25.0$ cm		$2b = 60$ cm		$Q_i = 62.55$ lt / s		$S_c = 19.80$ cm		Initial Vortex Location: MZ	
$L_p = 40$ cm									
Plate Width $W_p$ (cm)	Full Air - Core	Full Air – Core Location	Air Bubble Entrance	Air Bubble Entrance Location	Vortex Tail	Vortex Tail Location	Result		
5	O	MZ	O	MZ	O	MZ	US		
10	O – DV	MZ	O – DV	MZ	O – DV	MZ	US		
15	NO	-	O	LZ – RZ	O	LZ – RZ	US		
20	NO	-	O – R	LZ – RZ	O	LZ – RZ	US		
25	NO	-	NO	-	O	LZ - RZ	S		
$L_p = 50$ cm									
Plate Width $W_p$ (cm)	Full Air - Core	Full Air – Core Location	Air Bubble Entrance	Air Bubble Entrance Location	Vortex Tail	Vortex Tail Location	Result		
5	O	MZ	O	MZ	O	MZ	US		
10	O – DV	MZ	O – DV	MZ	O – DV	MZ	US		
15	NBCTO	MZ	O	LZ – MZ – RZ	O	LZ – MZ – RZ	US		
20	NBCTO	MZ	O	RZ	O	LZ – RZ	US		
25	NO	-	O	LZ – RZ	O	LZ – RZ	US		

Table B.2 Experimental results related to the anti – vortex plate for  $D_i = 25.0$  cm,  $Q_i = 45.46$  lt/s and  $2b = 60$  cm

$D_i = 25.0$ cm		$2b = 60$ cm		$Q_i = 45.46$ lt / s		$S_c = 16.00$ cm		Initial Vortex Location: MZ	
$L_p = 40$ cm									
Plate Width $W_p$ (cm)	Full Air - Core	Full Air – Core Location	Air Bubble Entrance	Air Bubble Entrance Location	Vortex Tail	Vortex Tail Location	Result		
5	O	MZ	O	MZ	O	MZ	US		
10	O – DV	MZ	O – DV	MZ	O – DV	MZ	US		
15	NO	-	O	LZ – RZ	O	LZ – RZ	US		
20	NO	-	NO	-	O	LZ – RZ	S		
25	NO	-	NO	-	O	LZ - RZ	S		
$L_p = 50$ cm									
Plate Width $W_p$ (cm)	Full Air - Core	Full Air – Core Location	Air Bubble Entrance	Air Bubble Entrance Location	Vortex Tail	Vortex Tail Location	Result		
5	O	MZ	O	MZ	O	MZ	US		
10	O – DV	MZ	O – DV	MZ	O – DV	MZ	US		
15	NO	-	NO	-	O	LZ – RZ	S		
20	NO	-	NO	-	NO	-	S		
25	NO	-	NO	-	NO	-	S		

Table B.3 Experimental results related to the anti – vortex plate for  $D_i = 25.0$  cm,  $Q_i = 30.32$  lt/s and  $2b = 60$  cm

$D_i = 25.0$ cm		$2b = 60$ cm		$Q_i = 30.32$ lt / s		$S_c = 10.90$ cm		Initial Vortex Location: MZ	
$L_p = 40$ cm									
Plate Width $W_p$ (cm)	Full Air - Core	Full Air – Core Location	Air Bubble Entrance	Air Bubble Entrance Location	Vortex Tail	Vortex Tail Location	Result		
5	O	MZ	O	MZ	O	MZ	US		
10	O	MZ	O	MZ	O	MZ	US		
15	NO	-	NO	-	NO	-	S		
20	NO	-	NO	-	NO	-	S		
25	NO	-	NO	-	NO	-	S		
$L_p = 50$ cm									
Plate Width $W_p$ (cm)	Full Air - Core	Full Air – Core Location	Air Bubble Entrance	Air Bubble Entrance Location	Vortex Tail	Vortex Tail Location	Result		
5	O	MZ	O	MZ	O	MZ	US		
10	NBCTO	MZ	O	MZ	O	MZ	US		
15	NO	-	NO	-	NO	-	S		
20	NO	-	NO	-	NO	-	S		
25	NO	-	NO	-	NO	-	S		

Table B.4 Experimental results related to the anti – vortex plate for  $D_i = 25.0$  cm,  $Q_i = 62.55$  lt/s and  $2b = 80$  cm

$D_i = 25.0$ cm		$2b = 80$ cm		$Q_i = 62.55$ lt / s		$S_c = 24.90$ cm		Initial Vortex Location: MZ	
$L_p = 40$ cm									
Plate Width $W_p$ (cm)	Full Air - Core	Full Air – Core Location	Air Bubble Entrance	Air Bubble Entrance Location	Vortex Tail	Vortex Tail Location	Result		
5	NO	-	NO	-	O	MZ	S		
10	NO	-	NO	-	O	MZ	S		
15	NO	-	NO	-	O	LZ – RZ	S		
20	NO	-	NO	-	O	LZ – RZ	S		
25	NO	-	NO	-	NO	-	S		
$L_p = 50$ cm									
Plate Width $W_p$ (cm)	Full Air - Core	Full Air – Core Location	Air Bubble Entrance	Air Bubble Entrance Location	Vortex Tail	Vortex Tail Location	Result		
5	NO	-	NO	-	O	MZ – RZ	S		
10	NO	-	NO	-	O	RZ	S		
15	NO	-	NO	-	O	RZ	S		
20	NO	-	NO	-	NO	-	S		
25	NO	-	NO	-	O	LZ – RZ	S		

Table B.5 Experimental results related to the anti – vortex plate for  $D_i = 25.0$  cm,  $Q_i = 50.75$  lt/s and  $2b = 80$  cm

$D_i = 25.0$ cm		$2b = 80$ cm		$Q_i = 50.75$ lt / s		$S_c = 22.30$ cm		Initial Vortex Location: MZ	
$L_p = 40$ cm									
Plate Width $W_p$ (cm)	Full Air - Core	Full Air – Core Location	Air Bubble Entrance	Air Bubble Entrance Location	Vortex Tail	Vortex Tail Location	Result		
5	NO	-	NO	-	NO	-	S		
10	NO	-	NO	-	O	MZ	S		
15	NO	-	NO	-	NO	-	S		
20	NO	-	NO	-	NO	-	S		
25	NO	-	NO	-	NO	-	S		
$L_p = 50$ cm									
Plate Width $W_p$ (cm)	Full Air - Core	Full Air – Core Location	Air Bubble Entrance	Air Bubble Entrance Location	Vortex Tail	Vortex Tail Location	Result		
5	NO	-	NO	-	O	MZ	S		
10	NO	-	NO	-	O	MZ	S		
15	NO	-	NO	-	NO	-	S		
20	NO	-	NO	-	O – R	LZ – RZ	S		
25	NO	-	NO	-	NO	-	S		

Table B.6 Experimental results related to the anti – vortex plate for  $D_i = 25.0$  cm,  $Q_i = 27.45$  lt/s and  $2b = 80$  cm

$D_i = 25.0$ cm		$2b = 80$ cm		$Q_i = 27.45$ lt / s		$S_c = 14.60$ cm		Initial Vortex Location: MZ	
$L_p = 40$ cm									
Plate Width $W_p$ (cm)	Full Air - Core	Full Air – Core Location	Air Bubble Entrance	Air Bubble Entrance Location	Vortex Tail	Vortex Tail Location	Result		
5	O – R	MZ	O	MZ	O	MZ	US		
10	NBCTO	MZ	O	MZ	O	MZ	US		
15	NO	-	NO	-	O	MZ	S		
20	NO	-	NO	-	NO	-	S		
25	NO	-	NO	-	NO	-	S		
$L_p = 50$ cm									
Plate Width $W_p$ (cm)	Full Air - Core	Full Air – Core Location	Air Bubble Entrance	Air Bubble Entrance Location	Vortex Tail	Vortex Tail Location	Result		
5	NO	-	O	MZ	O	MZ	US		
10	NBCTO	MZ	O	MZ	O	MZ	US		
15	NO	-	NBCTO	MZ	O	MZ	S		
20	NO	-	NO	-	NO	-	S		
25	NO	-	NO	-	NO	-	S		

Table B.7 Experimental results related to the anti – vortex plate for  $D_i = 25.0$  cm,  $Q_i = 62.55$  lt/s and  $2b = 100$  cm

$D_i = 25.0$ cm		$2b = 100$ cm		$Q_i = 62.55$ lt / s		$S_c = 29.80$ cm		Initial Vortex Location: MZ	
$L_p = 40$ cm									
Plate Width $W_p$ (cm)	Full Air - Core	Full Air – Core Location	Air Bubble Entrance	Air Bubble Entrance Location	Vortex Tail	Vortex Tail Location	Result		
5	NO	-	NO	-	O	MZ	S		
10	NO	-	NO	-	O	LZ – MZ – RZ	S		
15	NO	-	NO	-	NO	-	S		
20	NO	-	NO	-	NO	-	S		
25	NO	-	NO	-	NO	-	S		
$L_p = 50$ cm									
Plate Width $W_p$ (cm)	Full Air - Core	Full Air – Core Location	Air Bubble Entrance	Air Bubble Entrance Location	Vortex Tail	Vortex Tail Location	Result		
5	NO	-	NO	-	O – R	MZ	S		
10	NO	-	NO	-	NO	-	S		
15	NO	-	NO	-	NO	-	S		
20	NO	-	NO	-	NO	-	S		
25	NO	-	NO	-	NO	-	S		

Table B.8 Experimental results related to the anti – vortex plate for  $D_i = 25.0$  cm,  $Q_i = 48.08$  lt/s and  $2b = 100$  cm

$D_i = 25.0$ cm		$2b = 100$ cm		$Q_i = 48.08$ lt / s		$S_c = 25.60$ cm		Initial Vortex Location: MZ	
$L_p = 40$ cm									
Plate Width $W_p$ (cm)	Full Air - Core	Full Air – Core Location	Air Bubble Entrance	Air Bubble Entrance Location	Vortex Tail	Vortex Tail Location	Result		
5	NO	-	NO	-	NO	-	S		
10	NO	-	NO	-	O	LZ – MZ	S		
15	NO	-	NO	-	NO	-	S		
20	NO	-	NO	-	NO	-	S		
25	NO	-	NO	-	NO	-	S		
$L_p = 50$ cm									
Plate Width $W_p$ (cm)	Full Air - Core	Full Air – Core Location	Air Bubble Entrance	Air Bubble Entrance Location	Vortex Tail	Vortex Tail Location	Result		
5	NO	-	NO	-	NO	-	S		
10	NO	-	NO	-	NO	-	S		
15	NO	-	NO	-	NO	-	S		
20	NO	-	NO	-	NO	-	S		
25	NO	-	NO	-	NO	-	S		

Table B.9 Experimental results related to the anti – vortex plate for  $D_i = 25.0$  cm,  $Q_i = 36.40$  lt/s and  $2b = 100$  cm

$D_i = 25.0$ cm		$2b = 100$ cm		$Q_i = 36.40$ lt / s		$S_c = 19.30$ cm		Initial Vortex Location: MZ	
$L_p = 40$ cm									
Plate Width $W_p$ (cm)	Full Air - Core	Full Air – Core Location	Air Bubble Entrance	Air Bubble Entrance Location	Vortex Tail	Vortex Tail Location	Result		
5	NO	-	O – R	MZ	O – R	MZ	US		
10	O	MZ	O	MZ	O	MZ	US		
15	NO	-	NBCTO	MZ	O	MZ	S		
20	NO	-	NO	-	NO	-	S		
25	NO	-	NO	-	NO	-	S		
$L_p = 50$ cm									
Plate Width $W_p$ (cm)	Full Air - Core	Full Air – Core Location	Air Bubble Entrance	Air Bubble Entrance Location	Vortex Tail	Vortex Tail Location	Result		
5	NO	-	O – R	MZ	O – R	MZ	US		
10	O	MZ	O	MZ	O	MZ	US		
15	NBCTO	MZ	O	MZ	O	MZ	US		
20	NO	-	NO	-	NO	-	S		
25	NO	-	NO	-	NO	-	S		

Table B.10 Experimental results related to the anti – vortex plate for  $D_i = 25.0$  cm,  $Q_i = 62.55$  lt/s and  $2b = 120$  cm

$D_i = 25.0$ cm		$2b = 120$ cm		$Q_i = 62.55$ lt / s		$S_c = 29.40$ cm		Initial Vortex Location: MZ	
$L_p = 40$ cm									
Plate Width $W_p$ (cm)	Full Air - Core	Full Air – Core Location	Air Bubble Entrance	Air Bubble Entrance Location	Vortex Tail	Vortex Tail Location	Result		
5	NO	-	NO	-	NO	-	S		
10	NO	-	NO	-	NO	-	S		
15	NO	-	NO	-	NO	-	S		
20	NO	-	NO	-	NO	-	S		
25	NO	-	NO	-	NO	-	S		
$L_p = 50$ cm									
Plate Width $W_p$ (cm)	Full Air - Core	Full Air – Core Location	Air Bubble Entrance	Air Bubble Entrance Location	Vortex Tail	Vortex Tail Location	Result		
5	NO	-	NO	-	O – R	LZ - MZ	S		
10	NO	-	NO	-	NO	-	S		
15	NO	-	NO	-	NO	-	S		
20	NO	-	NO	-	NO	-	S		
25	NO	-	NO	-	NO	-	S		

Table B.11 Experimental results related to the anti – vortex plate for  $D_i = 25.0$  cm,  $Q_i = 48.08$  lt/s and  $2b = 120$  cm

$D_i = 25.0$ cm		$2b = 120$ cm		$Q_i = 48.08$ lt / s		$S_c = 20.60$ cm		Initial Vortex Location: MZ	
$L_p = 40$ cm									
Plate Width $W_p$ (cm)	Full Air - Core	Full Air – Core Location	Air Bubble Entrance	Air Bubble Entrance Location	Vortex Tail	Vortex Tail Location	Result		
5	NO	-	O – R	MZ	O	MZ	US		
10	O	MZ	O	MZ	O	MZ	US		
15	O – DV	MZ	O – DV	LZ – MZ	O – DV	LZ – MZ	US		
20	NO	-	NO	-	NO	-	S		
25	NO	-	NO	-	NO	-	S		
$L_p = 50$ cm									
Plate Width $W_p$ (cm)	Full Air - Core	Full Air – Core Location	Air Bubble Entrance	Air Bubble Entrance Location	Vortex Tail	Vortex Tail Location	Result		
5	NO	-	O	MZ	O	MZ	US		
10	O – DV	MZ	O – DV	MZ	O – DV	MZ	US		
15	O – DV	MZ	O – DV	MZ	O – DV	MZ	US		
20	NO	-	NO	-	NO	-	S		
25	NO	-	NO	-	NO	-	S		

Table B.12 Experimental results related to the anti – vortex plate for  $D_i = 25.0$  cm,  $Q_i = 36.40$  lt/s and  $2b = 120$  cm

$D_i = 25.0$ cm		$2b = 120$ cm		$Q_i = 36.40$ lt / s		$S_c = 14.90$ cm		Initial Vortex Location: MZ	
$L_p = 40$ cm									
Plate Width $W_p$ (cm)	Full Air - Core	Full Air – Core Location	Air Bubble Entrance	Air Bubble Entrance Location	Vortex Tail	Vortex Tail Location	Result		
5	NO	-	O	MZ	O	MZ	US		
10	O – R	MZ	O	MZ	O	MZ	US		
15	NO	-	NBCTO	MZ	O	LZ – MZ	S		
20	NO	-	NO	-	NO	-	S		
25	NO	-	NO	-	NO	-	S		
$L_p = 50$ cm									
Plate Width $W_p$ (cm)	Full Air - Core	Full Air – Core Location	Air Bubble Entrance	Air Bubble Entrance Location	Vortex Tail	Vortex Tail Location	Result		
5	O	MZ	O	MZ	O	MZ	US		
10	O	MZ	O	MZ	O	MZ	US		
15	NO	-	NO	-	O	MZ	S		
20	NO	-	NO	-	NO	-	S		
25	NO	-	NO	-	NO	-	S		

Table B.13 Experimental results related to the anti – vortex plate for  $D_i = 25.0$  cm,  $Q_i = 62.55$  lt/s and  $2b = 140$  cm

$D_i = 25.0$ cm		$2b = 140$ cm		$Q_i = 62.55$ lt / s		$S_c = 29.30$ cm		Initial Vortex Location: MZ	
$L_p = 40$ cm									
Plate Width $W_p$ (cm)	Full Air - Core	Full Air – Core Location	Air Bubble Entrance	Air Bubble Entrance Location	Vortex Tail	Vortex Tail Location	Result		
5	NO	-	NO	-	O	RZ	S		
10	NO	-	NO	-	O	RZ	S		
15	NO	-	NO	-	O	MZ – RZ	S		
20	NO	-	NO	-	O	RZ	S		
25	NO	-	NO	-	O	RZ	S		
$L_p = 50$ cm									
Plate Width $W_p$ (cm)	Full Air - Core	Full Air – Core Location	Air Bubble Entrance	Air Bubble Entrance Location	Vortex Tail	Vortex Tail Location	Result		
5	NO	-	NO	-	O	MZ – RZ	S		
10	NO	-	NO	-	O	RZ	S		
15	NO	-	NO	-	O	RZ	S		
20	NO	-	NO	-	O	RZ	S		
25	NO	-	NO	-	O	RZ	S		

Table B.14 Experimental results related to the anti – vortex plate for  $D_i = 25.0$  cm,  $Q_i = 48.08$  lt/s and  $2b = 140$  cm

$D_i = 25.0$ cm		$2b = 140$ cm		$Q_i = 48.08$ lt / s		$S_c = 21.20$ cm		Initial Vortex Location: MZ	
$L_p = 40$ cm									
Plate Width $W_p$ (cm)	Full Air - Core	Full Air – Core Location	Air Bubble Entrance	Air Bubble Entrance Location	Vortex Tail	Vortex Tail Location	Result		
5	NO	-	NO	-	NO	-	S		
10	NO	-	NO	-	O	LZ – MZ	S		
15	NO	-	NO	-	NO	-	S		
20	NO	-	NO	-	NO	-	S		
25	NO	-	NO	-	NO	-	S		
$L_p = 50$ cm									
Plate Width $W_p$ (cm)	Full Air - Core	Full Air – Core Location	Air Bubble Entrance	Air Bubble Entrance Location	Vortex Tail	Vortex Tail Location	Result		
5	NO	-	NO	-	O	MZ	S		
10	NO	-	NO	-	O	LZ – MZ	S		
15	NO	-	NO	-	O	LZ – MZ	S		
20	NO	-	NO	-	NO	-	S		
25	NO	-	NO	-	NO	-	S		

Table B.15 Experimental results related to the anti – vortex plate for  $D_i = 25.0$  cm,  $Q_i = 36.40$  lt/s and  $2b = 140$  cm

$D_i = 25.0$ cm		$2b = 140$ cm		$Q_i = 36.40$ lt / s		$S_c = 16.40$ cm		Initial Vortex Location: MZ	
$L_p = 40$ cm									
Plate Width $W_p$ (cm)	Full Air - Core	Full Air – Core Location	Air Bubble Entrance	Air Bubble Entrance Location	Vortex Tail	Vortex Tail Location	Result		
5	O	MZ	O	MZ	O	MZ	US		
10	O – DV – R	MZ	O – DV	MZ	O – DV	MZ	US		
15	NBCTO	LZ – MZ	O – R	LZ - MZ	O	LZ – MZ	US		
20	NO	-	NO	-	O	LZ – MZ	S		
25	NO	-	NO	-	NO	-	S		
$L_p = 50$ cm									
Plate Width $W_p$ (cm)	Full Air - Core	Full Air – Core Location	Air Bubble Entrance	Air Bubble Entrance Location	Vortex Tail	Vortex Tail Location	Result		
5	O	MZ	O	MZ	O	MZ	US		
10	NBCTO	MZ	O	MZ	O	MZ	US		
15	NO	-	O – DV	LZ - MZ	O – DV	LZ – MZ	US		
20	NO	-	NO	-	O – R	MZ	S		
25	NO	-	NO	-	NO	-	S		

Table B.16 Experimental results related to the anti – vortex plate for  $D_i = 19.4$  cm,  $Q_i = 62.55$  lt/s and  $2b = 40$  cm

$D_i = 19.4$ cm		$2b = 40$ cm		$Q_i = 62.55$ lt / s		$S_c = 64.50$ cm		Initial Vortex Location: LZ	
$L_p = 40$ cm									
Plate Width $W_p$ (cm)	Full Air - Core	Full Air – Core Location	Air Bubble Entrance	Air Bubble Entrance Location	Vortex Tail	Vortex Tail Location	Result		
5	O	LZ – MZ	O	LZ – MZ	O	LZ – MZ	US		
10	O	LZ – MZ	O	LZ – MZ	O	LZ – MZ	US		
15	O	LZ – MZ	O	LZ – MZ	O	LZ – MZ	US		
20	O	LZ – MZ	O	LZ – MZ	O	LZ – MZ	US		
25	O	MZ	O	MZ	O	MZ	US		
$L_p = 50$ cm									
Plate Width $W_p$ (cm)	Full Air - Core	Full Air – Core Location	Air Bubble Entrance	Air Bubble Entrance Location	Vortex Tail	Vortex Tail Location	Result		
5	-	-	-	-	-	-	-		
10	-	-	-	-	-	-	-		
15	-	-	-	-	-	-	-		
20	-	-	-	-	-	-	-		
25	-	-	-	-	-	-	-		

Table B.17 Experimental results related to the anti – vortex plate for  $D_i = 19.4$  cm,  $Q_i = 48.08$  lt/s and  $2b = 40$  cm

$D_i = 19.4$ cm		$2b = 40$ cm		$Q_i = 48.08$ lt / s		$S_c = 62.40$ cm		Initial Vortex Location: LZ	
$L_p = 40$ cm									
Plate Width $W_p$ (cm)	Full Air - Core	Full Air – Core Location	Air Bubble Entrance	Air Bubble Entrance Location	Vortex Tail	Vortex Tail Location	Result		
5	NBCTO	LZ	O	LZ	O	LZ	US		
10	NBCTO	LZ – MZ	O	LZ – MZ	O	LZ – MZ	US		
15	NBCTO	LZ – MZ	O	LZ – MZ	O	LZ – MZ	US		
20	NBCTO	LZ – MZ	NBCTO	LZ – MZ	O	LZ – MZ	S		
25	NBCTO	LZ - MZ	NBCTO	LZ – MZ	O	LZ - MZ	S		
$L_p = 50$ cm									
Plate Width $W_p$ (cm)	Full Air - Core	Full Air – Core Location	Air Bubble Entrance	Air Bubble Entrance Location	Vortex Tail	Vortex Tail Location	Result		
5	-	-	-	-	-	-	-		
10	-	-	-	-	-	-	-		
15	-	-	-	-	-	-	-		
20	-	-	-	-	-	-	-		
25	-	-	-	-	-	-	-		

Table B.18 Experimental results related to the anti – vortex plate for  $D_i = 19.4$  cm,  $Q_i = 62.55$  lt/s and  $2b = 60$  cm

$D_i = 19.4$ cm		$2b = 60$ cm		$Q_i = 62.55$ lt / s		$S_c = 24.60$ cm		Initial Vortex Location: MZ	
$L_p = 40$ cm									
Plate Width $W_p$ (cm)	Full Air - Core	Full Air – Core Location	Air Bubble Entrance	Air Bubble Entrance Location	Vortex Tail	Vortex Tail Location	Result		
5	NO	-	O	MZ – RZ	O	MZ – RZ	US		
10	NO	-	O – R	LZ – RZ	O	LZ – RZ	US		
15	NO	-	O	RZ	O	LZ – RZ	US		
20	NO	-	NO	-	NO	-	S		
25	NO	-	NO	-	NO	-	S		
$L_p = 50$ cm									
Plate Width $W_p$ (cm)	Full Air - Core	Full Air – Core Location	Air Bubble Entrance	Air Bubble Entrance Location	Vortex Tail	Vortex Tail Location	Result		
5	NO	-	O – R	RZ	O	RZ	US		
10	NBCTO	LZ – RZ	O	LZ – MZ – RZ	O	LZ – MZ – RZ	US		
15	NO	-	O	LZ – RZ	O	LZ – RZ	US		
20	NBCTO	LZ – RZ	O	LZ – RZ	O	LZ – RZ	US		
25	NO	-	NO	-	O	LZ - RZ	S		

Table B.19 Experimental results related to the anti – vortex plate for  $D_i = 19.4$  cm,  $Q_i = 48.08$  lt/s and  $2b = 60$  cm

$D_i = 19.4$ cm		$2b = 60$ cm		$Q_i = 48.08$ lt / s		$S_c = 21.20$ cm		Initial Vortex Location: MZ	
$L_p = 40$ cm									
Plate Width $W_p$ (cm)	Full Air - Core	Full Air – Core Location	Air Bubble Entrance	Air Bubble Entrance Location	Vortex Tail	Vortex Tail Location	Result		
5	NO	-	NO	-	O	MZ	S		
10	NO	-	NO	-	O	MZ – RZ	S		
15	NO	-	NO	-	O	LZ – RZ	S		
20	NO	-	NO	-	NO	-	S		
25	NO	-	NO	-	NO	-	S		
$L_p = 50$ cm									
Plate Width $W_p$ (cm)	Full Air - Core	Full Air – Core Location	Air Bubble Entrance	Air Bubble Entrance Location	Vortex Tail	Vortex Tail Location	Result		
5	NO	-	NO	-	O	MZ	S		
10	NO	-	NO	-	O	MZ	S		
15	NO	-	NO	-	O	MZ – RZ	S		
20	NO	-	NO	-	O	MZ – RZ	S		
25	NO	-	NO	-	NO	-	S		

Table B.20 Experimental results related to the anti – vortex plate for  $D_i = 19.4$  cm,  $Q_i = 33.69$  lt/s and  $2b = 60$  cm

$D_i = 19.4$ cm		$2b = 60$ cm		$Q_i = 33.69$ lt / s		$S_c = 16.90$ cm		Initial Vortex Location: MZ	
$L_p = 40$ cm									
Plate Width $W_p$ (cm)	Full Air - Core	Full Air – Core Location	Air Bubble Entrance	Air Bubble Entrance Location	Vortex Tail	Vortex Tail Location	Result		
5	O	MZ	O	MZ	O	MZ	US		
10	NO	-	O – R	MZ	O	MZ – RZ	US		
15	NO	-	NO	-	NO	-	S		
20	NO	-	NO	-	NO	-	S		
25	NO	-	NO	-	NO	-	S		
$L_p = 50$ cm									
Plate Width $W_p$ (cm)	Full Air - Core	Full Air – Core Location	Air Bubble Entrance	Air Bubble Entrance Location	Vortex Tail	Vortex Tail Location	Result		
5	NO	-	O – R	MZ	O	MZ	US		
10	O – DV – R	MZ	O – DV – R	MZ	O – DV – R	MZ	US		
15	NO	-	NO	-	O – R	LZ	S		
20	NO	-	NO	-	NO	-	S		
25	NO	-	NO	-	NO	-	S		

Table B.21 Experimental results related to the anti – vortex plate for  $D_i = 19.4$  cm,  $Q_i = 62.55$  lt/s and  $2b = 80$  cm

$D_i = 19.4$ cm		$2b = 80$ cm		$Q_i = 62.55$ lt / s		$S_c = 28.20$ cm		Initial Vortex Location: MZ	
$L_p = 40$ cm									
Plate Width $W_p$ (cm)	Full Air - Core	Full Air – Core Location	Air Bubble Entrance	Air Bubble Entrance Location	Vortex Tail	Vortex Tail Location	Result		
5	NO	-	NO	-	O	LZ – MZ – RZ	S		
10	NO	-	NO	-	NO	-	S		
15	NO	-	NO	-	NO	-	S		
20	NO	-	NO	-	O	LZ – RZ	S		
25	NO	-	NO	-	O	LZ – RZ	S		
$L_p = 50$ cm									
Plate Width $W_p$ (cm)	Full Air - Core	Full Air – Core Location	Air Bubble Entrance	Air Bubble Entrance Location	Vortex Tail	Vortex Tail Location	Result		
5	NO	-	NO	-	O	LZ – RZ	S		
10	NO	-	NO	-	O	RZ	S		
15	NO	-	NO	-	O	LZ – RZ	S		
20	NO	-	NO	-	O	LZ – RZ	S		
25	NO	-	NO	-	O	LZ – RZ	S		

Table B.22 Experimental results related to the anti – vortex plate for  $D_i = 19.4$  cm,  $Q_i = 48.08$  lt/s and  $2b = 80$  cm

$D_i = 19.4$ cm		$2b = 80$ cm		$Q_i = 48.08$ lt / s		$S_c = 22.40$ cm		Initial Vortex Location: MZ	
$L_p = 40$ cm									
Plate Width $W_p$ (cm)	Full Air - Core	Full Air – Core Location	Air Bubble Entrance	Air Bubble Entrance Location	Vortex Tail	Vortex Tail Location	Result		
5	NO	-	O	MZ	O	MZ	US		
10	O	MZ	O	MZ	O	MZ	US		
15	O – DV	MZ	O – DV	MZ	O – DV	MZ	US		
20	NO	-	NO	-	O	LZ – MZ	S		
25	NO	-	NO	-	NO	-	S		
$L_p = 50$ cm									
Plate Width $W_p$ (cm)	Full Air - Core	Full Air – Core Location	Air Bubble Entrance	Air Bubble Entrance Location	Vortex Tail	Vortex Tail Location	Result		
5	O	MZ	O	MZ	O	MZ	US		
10	O – DV	MZ	O – DV	MZ	O – DV	MZ	US		
15	O – DV	MZ	O – DV	MZ	O – DV	MZ	US		
20	NO	-	NO	-	NO	-	S		
25	NO	-	NO	-	NO	-	S		

Table B.23 Experimental results related to the anti – vortex plate for  $D_i = 19.4$  cm,  $Q_i = 30.32$  lt/s and  $2b = 80$  cm

$D_i = 19.4$ cm		$2b = 80$ cm		$Q_i = 30.32$ lt / s		$S_c = 17.20$ cm		Initial Vortex Location: MZ	
$L_p = 40$ cm									
Plate Width $W_p$ (cm)	Full Air - Core	Full Air – Core Location	Air Bubble Entrance	Air Bubble Entrance Location	Vortex Tail	Vortex Tail Location	Result		
5	NO	-	O	MZ	O	MZ	US		
10	O	MZ	O	MZ	O	MZ	US		
15	NO	-	O – R	MZ	O	MZ	US		
20	NO	-	NO	-	O – R	RZ	S		
25	NO	-	NO	-	NO	-	S		
$L_p = 50$ cm									
Plate Width $W_p$ (cm)	Full Air - Core	Full Air – Core Location	Air Bubble Entrance	Air Bubble Entrance Location	Vortex Tail	Vortex Tail Location	Result		
5	O	MZ	O	MZ	O	MZ	US		
10	O – DV	MZ	O – DV	MZ	O – DV	MZ	US		
15	NO	-	O – DV – R	MZ	O – DV	MZ	US		
20	NO	-	NO	-	NO	-	S		
25	NO	-	NO	-	NO	-	S		

Table B.24 Experimental results related to the anti – vortex plate for  $D_i = 19.4$  cm,  $Q_i = 62.55$  lt/s and  $2b = 100$  cm

$D_i = 19.4$ cm		$2b = 100$ cm		$Q_i = 62.55$ lt / s		$S_c = 33.60$ cm		Initial Vortex Location: MZ	
$L_p = 40$ cm									
Plate Width $W_p$ (cm)	Full Air - Core	Full Air – Core Location	Air Bubble Entrance	Air Bubble Entrance Location	Vortex Tail	Vortex Tail Location	Result		
5	NO	-	NO	-	O	MZ	S		
10	NO	-	NO	-	O	LZ – MZ	S		
15	NO	-	NO	-	O	LZ – MZ	S		
20	NO	-	NO	-	O	LZ – RZ	S		
25	NO	-	NO	-	O	RZ	S		
$L_p = 50$ cm									
Plate Width $W_p$ (cm)	Full Air - Core	Full Air – Core Location	Air Bubble Entrance	Air Bubble Entrance Location	Vortex Tail	Vortex Tail Location	Result		
5	NO	-	NO	-	O	MZ – RZ	S		
10	NO	-	NO	-	O	MZ – RZ	S		
15	NO	-	NO	-	O	MZ – RZ	S		
20	NO	-	NO	-	O	LZ – MZ – RZ	S		
25	NO	-	NO	-	O	LZ – RZ	S		

Table B.25 Experimental results related to the anti – vortex plate for  $D_i = 19.4$  cm,  $Q_i = 48.08$  lt/s and  $2b = 100$  cm

$D_i = 19.4$ cm		$2b = 100$ cm		$Q_i = 48.08$ lt / s		$S_c = 26.50$ cm		Initial Vortex Location: MZ	
$L_p = 40$ cm									
Plate Width $W_p$ (cm)	Full Air - Core	Full Air – Core Location	Air Bubble Entrance	Air Bubble Entrance Location	Vortex Tail	Vortex Tail Location	Result		
5	NO	-	NO	-	NO	-	S		
10	NO	-	NO	-	O	MZ	S		
15	NO	-	NO	-	O	MZ	S		
20	NO	-	NO	-	NO	-	S		
25	NO	-	NO	-	O – R	LZ	S		
$L_p = 50$ cm									
Plate Width $W_p$ (cm)	Full Air - Core	Full Air – Core Location	Air Bubble Entrance	Air Bubble Entrance Location	Vortex Tail	Vortex Tail Location	Result		
5	NO	-	NO	-	NO	-	S		
10	NO	-	NO	-	NO	-	S		
15	NO	-	NO	-	O	MZ	S		
20	NO	-	NO	-	NO	-	S		
25	NO	-	NO	-	NO	-	S		

Table B.26 Experimental results related to the anti – vortex plate for  $D_i = 19.4$  cm,  $Q_i = 33.69$  lt/s and  $2b = 100$  cm

$D_i = 19.4$ cm		$2b = 100$ cm		$Q_i = 33.69$ lt / s		$S_c = 18.60$ cm		Initial Vortex Location: MZ	
$L_p = 40$ cm									
Plate Width $W_p$ (cm)	Full Air - Core	Full Air – Core Location	Air Bubble Entrance	Air Bubble Entrance Location	Vortex Tail	Vortex Tail Location	Result		
5	NO	-	O	MZ	O	MZ	US		
10	O – DV	MZ	O – DV	MZ	O – DV	MZ	US		
15	O – DV	MZ	O – DV	MZ	O – DV	MZ	US		
20	NO	-	NO	-	O	LZ	S		
25	NO	-	NO	-	NO	-	S		
$L_p = 50$ cm									
Plate Width $W_p$ (cm)	Full Air - Core	Full Air – Core Location	Air Bubble Entrance	Air Bubble Entrance Location	Vortex Tail	Vortex Tail Location	Result		
5	NO	-	O	MZ	O	MZ	US		
10	O	MZ	O	MZ	O	MZ	US		
15	NBCTO	MZ	O – DV	MZ	O – DV	MZ	US		
20	NO	-	NO	-	NO	-	S		
25	NO	-	NO	-	NO	-	S		

Table B.27 Experimental results related to the anti – vortex plate for  $D_i = 19.4$  cm,  $Q_i = 62.55$  lt/s and  $2b = 120$  cm

$D_i = 19.4$ cm		$2b = 120$ cm		$Q_i = 62.55$ lt / s		$S_c = 32.90$ cm		Initial Vortex Location: MZ	
$L_p = 40$ cm									
Plate Width $W_p$ (cm)	Full Air - Core	Full Air – Core Location	Air Bubble Entrance	Air Bubble Entrance Location	Vortex Tail	Vortex Tail Location	Result		
5	NO	-	NO	-	NO	-	S		
10	NO	-	NO	-	NO	-	S		
15	NO	-	NO	-	O	LZ – RZ	S		
20	NO	-	NO	-	O	LZ – RZ	S		
25	NO	-	NO	-	O	LZ – RZ	S		
$L_p = 50$ cm									
Plate Width $W_p$ (cm)	Full Air - Core	Full Air – Core Location	Air Bubble Entrance	Air Bubble Entrance Location	Vortex Tail	Vortex Tail Location	Result		
5	NO	-	NO	-	NO	-	S		
10	NO	-	NO	-	NO	-	S		
15	NO	-	NO	-	NO	-	S		
20	NO	-	NO	-	O	RZ	S		
25	NO	-	NO	-	O	RZ	S		

Table B.28 Experimental results related to the anti – vortex plate for  $D_i = 19.4$  cm,  $Q_i = 48.08$  lt/s and  $2b = 120$  cm

$D_i = 19.4$ cm		$2b = 120$ cm		$Q_i = 48.08$ lt / s		$S_c = 23.70$ cm		Initial Vortex Location: MZ	
$L_p = 40$ cm									
Plate Width $W_p$ (cm)	Full Air - Core	Full Air – Core Location	Air Bubble Entrance	Air Bubble Entrance Location	Vortex Tail	Vortex Tail Location	Result		
5	O – R	MZ	O – R	MZ	O	MZ	US		
10	NO	-	NO	-	NO	-	S		
15	NO	-	NO	-	O – R	MZ	S		
20	NO	-	NO	-	O – R	LZ	S		
25	NO	-	NO	-	O – R	LZ	S		
$L_p = 50$ cm									
Plate Width $W_p$ (cm)	Full Air - Core	Full Air – Core Location	Air Bubble Entrance	Air Bubble Entrance Location	Vortex Tail	Vortex Tail Location	Result		
5	NO	-	NO	-	O	MZ	S		
10	NO	-	NO	-	O	MZ	S		
15	NO	-	NO	-	O	MZ	S		
20	NO	-	NO	-	O	MZ	S		
25	NO	-	NO	-	NO	-	S		

Table B.29 Experimental results related to the anti – vortex plate for  $D_i = 19.4$  cm,  $Q_i = 33.69$  lt/s and  $2b = 120$  cm

$D_i = 19.4$ cm		$2b = 120$ cm		$Q_i = 33.69$ lt / s		$S_c = 19.90$ cm		Initial Vortex Location: MZ	
$L_p = 40$ cm									
Plate Width $W_p$ (cm)	Full Air - Core	Full Air – Core Location	Air Bubble Entrance	Air Bubble Entrance Location	Vortex Tail	Vortex Tail Location	Result		
5	O – R	MZ	O – R	MZ	O	MZ	US		
10	NO	-	O	MZ	O	LZ – MZ	US		
15	NO	-	NO	-	O – R	LZ – MZ	S		
20	NO	-	NO	-	O	LZ	S		
25	NO	-	NO	-	NO	-	S		
$L_p = 50$ cm									
Plate Width $W_p$ (cm)	Full Air - Core	Full Air – Core Location	Air Bubble Entrance	Air Bubble Entrance Location	Vortex Tail	Vortex Tail Location	Result		
5	NO	-	O – R	MZ	O – R	MZ	US		
10	O – R	MZ	O	MZ	O	MZ	US		
15	NBCTO	MZ	O	MZ	O	MZ	US		
20	NO	-	NO	-	O	LZ – MZ	S		
25	NO	-	NO	-	O	LZ	S		

Table B.30 Experimental results related to the anti – vortex plate for  $D_i = 19.4$  cm,  $Q_i = 62.55$  lt/s and  $2b = 140$  cm

$D_i = 19.4$ cm		$2b = 140$ cm		$Q_i = 62.55$ lt / s		$S_c = 33.30$ cm		Initial Vortex Location: MZ	
$L_p = 40$ cm									
Plate Width $W_p$ (cm)	Full Air - Core	Full Air – Core Location	Air Bubble Entrance	Air Bubble Entrance Location	Vortex Tail	Vortex Tail Location	Result		
5	NO	-	NO	-	O	LZ – MZ	S		
10	NO	-	NO	-	O	MZ – RZ	S		
15	NO	-	NO	-	NO	-	S		
20	NO	-	NO	-	O	LZ – RZ	S		
25	NO	-	NO	-	O	LZ – RZ	S		
$L_p = 50$ cm									
Plate Width $W_p$ (cm)	Full Air - Core	Full Air – Core Location	Air Bubble Entrance	Air Bubble Entrance Location	Vortex Tail	Vortex Tail Location	Result		
5	NO	-	NO	-	O	MZ – RZ	S		
10	NO	-	NO	-	O	MZ	S		
15	NO	-	NO	-	O	RZ	S		
20	NO	-	NO	-	O	RZ	S		
25	NO	-	NO	-	O	RZ	S		

Table B.31 Experimental results related to the anti – vortex plate for  $D_i = 19.4$  cm,  $Q_i = 48.08$  lt/s and  $2b = 140$  cm

$D_i = 19.4$ cm		$2b = 140$ cm		$Q_i = 48.08$ lt / s		$S_c = 25.10$ cm		Initial Vortex Location: MZ	
$L_p = 40$ cm									
Plate Width $W_p$ (cm)	Full Air - Core	Full Air – Core Location	Air Bubble Entrance	Air Bubble Entrance Location	Vortex Tail	Vortex Tail Location	Result		
5	NO	-	NBCTO	MZ	O	MZ	S		
10	NO	-	NO	-	O	MZ	S		
15	NO	-	NO	-	O	LZ – MZ	S		
20	NO	-	NO	-	NO	-	S		
25	NO	-	NO	-	O	MZ – RZ	S		
$L_p = 50$ cm									
Plate Width $W_p$ (cm)	Full Air - Core	Full Air – Core Location	Air Bubble Entrance	Air Bubble Entrance Location	Vortex Tail	Vortex Tail Location	Result		
5	NO	-	NBCTO	MZ	O	MZ	S		
10	NO	-	NO	-	O	MZ	S		
15	NO	-	NO	-	O	LZ – MZ	S		
20	NO	-	NO	-	O	MZ – RZ	S		
25	NO	-	NO	-	NO	-	S		

Table B.32 Experimental results related to the anti – vortex plate for  $D_i = 19.4$  cm,  $Q_i = 36.40$  lt/s and  $2b = 140$  cm

$D_i = 19.4$ cm		$2b = 140$ cm		$Q_i = 36.40$ lt / s		$S_c = 19.80$ cm		Initial Vortex Location: MZ	
$L_p = 40$ cm									
Plate Width $W_p$ (cm)	Full Air - Core	Full Air – Core Location	Air Bubble Entrance	Air Bubble Entrance Location	Vortex Tail	Vortex Tail Location	Result		
5	NO	-	O – R	MZ	O	MZ	US		
10	O	MZ	O	MZ	O	MZ	US		
15	NO	-	NBCTO	MZ	O	LZ – MZ	S		
20	NO	-	NO	-	O – R	LZ	S		
25	NO	-	NO	-	O – R	RZ	S		
$L_p = 50$ cm									
Plate Width $W_p$ (cm)	Full Air - Core	Full Air – Core Location	Air Bubble Entrance	Air Bubble Entrance Location	Vortex Tail	Vortex Tail Location	Result		
5	O – R	MZ	O – R	MZ	O	MZ	US		
10	NBCTO	MZ	O	MZ	O	MZ	US		
15	NBCTO	MZ	O	MZ	O	LZ	US		
20	NO	-	NO	-	O	LZ – MZ	S		
25	NO	-	NO	-	NO	-	S		

Table B.33 Experimental results related to the anti – vortex plate for  $D_i = 14.4$  cm,  $Q_i = 62.55$  lt/s and  $2b = 40$  cm

$D_i = 14.4$ cm		$2b = 40$ cm		$Q_i = 62.55$ lt / s		$S_c = 75.70$ cm		Initial Vortex Location: LZ	
$L_p = 40$ cm									
Plate Width $W_p$ (cm)	Full Air - Core	Full Air – Core Location	Air Bubble Entrance	Air Bubble Entrance Location	Vortex Tail	Vortex Tail Location	Result		
5	NO	-	O	MZ	O	MZ	US		
10	O	MZ	O	MZ	O	MZ	US		
15	O	MZ	O	MZ	O	MZ	US		
20	O	MZ	O	MZ	O	MZ	US		
25	O	MZ	O	MZ	O	MZ	US		
$L_p = 50$ cm									
Plate Width $W_p$ (cm)	Full Air - Core	Full Air – Core Location	Air Bubble Entrance	Air Bubble Entrance Location	Vortex Tail	Vortex Tail Location	Result		
5	-	-	-	-	-	-	-		
10	-	-	-	-	-	-	-		
15	-	-	-	-	-	-	-		
20	-	-	-	-	-	-	-		
25	-	-	-	-	-	-	-		

Table B.34 Experimental results related to the anti – vortex plate for  $D_i = 14.4$  cm,  $Q_i = 62.55$  lt/s and  $2b = 60$  cm

$D_i = 14.4$ cm		$2b = 60$ cm		$Q_i = 62.55$ lt / s		$S_c = 25.30$ cm		Initial Vortex Location: MZ	
$L_p = 40$ cm									
Plate Width $W_p$ (cm)	Full Air - Core	Full Air – Core Location	Air Bubble Entrance	Air Bubble Entrance Location	Vortex Tail	Vortex Tail Location	Result		
5	NO	-	O – R	LZ	O	LZ – RZ	US		
10	NO	-	NBCTO	LZ	O	LZ	S		
15	NO	-	NBCTO	LZ	O	LZ	S		
20	NO	-	NBCTO	LZ	O	LZ	S		
25	NO	-	NBCTO	LZ	O	LZ	S		
$L_p = 50$ cm									
Plate Width $W_p$ (cm)	Full Air - Core	Full Air – Core Location	Air Bubble Entrance	Air Bubble Entrance Location	Vortex Tail	Vortex Tail Location	Result		
5	NO	-	O – R	MZ	O	MZ – RZ	US		
10	NO	-	NO	-	O	LZ – RZ	S		
15	NO	-	NO	-	O	LZ – RZ	S		
20	NO	-	NO	-	O	LZ – RZ	S		
25	NO	-	NO	-	O	LZ – RZ	S		

Table B.35 Experimental results related to the anti – vortex plate for  $D_i = 14.4$  cm,  $Q_i = 48.08$  lt/s and  $2b = 60$  cm

$D_i = 14.4$ cm		$2b = 60$ cm		$Q_i = 48.08$ lt / s		$S_c = 21.10$ cm		Initial Vortex Location: MZ	
$L_p = 40$ cm									
Plate Width $W_p$ (cm)	Full Air - Core	Full Air – Core Location	Air Bubble Entrance	Air Bubble Entrance Location	Vortex Tail	Vortex Tail Location	Result		
5	NO	-	O	MZ	O	MZ	US		
10	O – R	MZ	O – R	MZ	O – R	MZ	US		
15	O – R	RZ	O – R	RZ	O – R	RZ	US		
20	NO	-	NO	-	NO	-	S		
25	NO	-	NO	-	NO	-	S		
$L_p = 50$ cm									
Plate Width $W_p$ (cm)	Full Air - Core	Full Air – Core Location	Air Bubble Entrance	Air Bubble Entrance Location	Vortex Tail	Vortex Tail Location	Result		
5	NO	-	O	MZ	O	MZ	US		
10	O – R	MZ	O – R	MZ	O	MZ	US		
15	NO	-	NO	-	O	MZ – RZ	S		
20	NO	-	NO	-	O	RZ	S		
25	NO	-	NO	-	O	RZ	S		

Table B.36 Experimental results related to the anti – vortex plate for  $D_i = 14.4$  cm,  $Q_i = 33.69$  lt/s and  $2b = 60$  cm

$D_i = 14.4$ cm		$2b = 60$ cm		$Q_i = 33.69$ lt / s		$S_c = 18.20$ cm		Initial Vortex Location: MZ	
$L_p = 40$ cm									
Plate Width $W_p$ (cm)	Full Air - Core	Full Air – Core Location	Air Bubble Entrance	Air Bubble Entrance Location	Vortex Tail	Vortex Tail Location	Result		
5	O	MZ	O	MZ	O	MZ	US		
10	O	MZ	O	MZ	O	MZ	US		
15	NO	-	NO	-	NO	-	S		
20	NO	-	NO	-	NO	-	S		
25	NO	-	NO	-	NO	-	S		
$L_p = 50$ cm									
Plate Width $W_p$ (cm)	Full Air - Core	Full Air – Core Location	Air Bubble Entrance	Air Bubble Entrance Location	Vortex Tail	Vortex Tail Location	Result		
5	O	MZ	O	MZ	O	MZ	US		
10	O	MZ	O	MZ	O	MZ	US		
15	NBCTO	MZ	O	MZ	O	LZ – MZ – RZ	US		
20	NO	-	NO	-	O	LZ – RZ	S		
25	NO	-	NO	-	O	LZ – RZ	S		

Table B.37 Experimental results related to the anti – vortex plate for  $D_i = 14.4$  cm,  $Q_i = 62.55$  lt/s and  $2b = 80$  cm

$D_i = 14.4$ cm		$2b = 80$ cm		$Q_i = 62.55$ lt / s		$S_c = 30.90$ cm		Initial Vortex Location: MZ	
$L_p = 40$ cm									
Plate Width $W_p$ (cm)	Full Air - Core	Full Air – Core Location	Air Bubble Entrance	Air Bubble Entrance Location	Vortex Tail	Vortex Tail Location	Result		
5	NO	-	O – R	MZ	O	LZ – MZ – RZ	US		
10	NO	-	NO	-	NO	-	S		
15	NO	-	NO	-	O	RZ	S		
20	NO	-	NO	-	NO	-	S		
25	NO	-	NO	-	NO	-	S		
$L_p = 50$ cm									
Plate Width $W_p$ (cm)	Full Air - Core	Full Air – Core Location	Air Bubble Entrance	Air Bubble Entrance Location	Vortex Tail	Vortex Tail Location	Result		
5	NO	-	O	MZ	O	MZ – RZ	US		
10	NO	-	O	MZ	O	MZ – RZ	US		
15	NO	-	NO	-	O	RZ	S		
20	NO	-	NO	-	O	LZ – RZ	S		
25	NO	-	NO	-	O	LZ – RZ	S		

Table B.38 Experimental results related to the anti – vortex plate for  $D_i = 14.4$  cm,  $Q_i = 48.08$  lt/s and  $2b = 80$  cm

$D_i = 14.4$ cm		$2b = 80$ cm		$Q_i = 48.08$ lt / s		$S_c = 24.00$ cm		Initial Vortex Location: MZ	
$L_p = 40$ cm									
Plate Width $W_p$ (cm)	Full Air - Core	Full Air – Core Location	Air Bubble Entrance	Air Bubble Entrance Location	Vortex Tail	Vortex Tail Location	Result		
5	NO	-	O – R	MZ	O	MZ	US		
10	NBCTO	MZ	O	MZ	O	MZ	US		
15	NBCTO	MZ – RZ	O – R	MZ – RZ	O – R	MZ – RZ	US		
20	NO	-	NO	-	O – R	MZ	S		
25	NO	-	NO	-	NO	-	S		
$L_p = 50$ cm									
Plate Width $W_p$ (cm)	Full Air - Core	Full Air – Core Location	Air Bubble Entrance	Air Bubble Entrance Location	Vortex Tail	Vortex Tail Location	Result		
5	NO	-	O – R	MZ	O	MZ	US		
10	NBCTO	MZ	O	MZ	O	MZ	US		
15	NBCTO	MZ	O – DV – R	MZ	O – DV – R	MZ	US		
20	NO	-	NO	-	O	RZ	S		
25	NO	-	NO	-	O	RZ	S		

Table B.39 Experimental results related to the anti – vortex plate for  $D_i = 14.4$  cm,  $Q_i = 33.69$  lt/s and  $2b = 80$  cm

$D_i = 14.4$ cm		$2b = 80$ cm		$Q_i = 33.69$ lt / s		$S_c = 21.20$ cm		Initial Vortex Location: MZ	
$L_p = 40$ cm									
Plate Width $W_p$ (cm)	Full Air - Core	Full Air – Core Location	Air Bubble Entrance	Air Bubble Entrance Location	Vortex Tail	Vortex Tail Location	Result		
5	NO	-	O – R	MZ	O	MZ	US		
10	NO	-	O	MZ	O	MZ	US		
15	NO	-	NO	-	O	MZ	S		
20	NO	-	NO	-	O	RZ	S		
25	NO	-	NO	-	NO	-	S		
$L_p = 50$ cm									
Plate Width $W_p$ (cm)	Full Air - Core	Full Air – Core Location	Air Bubble Entrance	Air Bubble Entrance Location	Vortex Tail	Vortex Tail Location	Result		
5	NO	-	O – R	MZ	O	MZ	US		
10	O – DV	MZ	O – DV	MZ	O – DV	MZ	US		
15	O – DV	MZ	O – DV	MZ	O – DV	MZ	US		
20	NO	-	NO	-	NO	-	S		
25	NO	-	NO	-	NO	-	S		

Table B.40 Experimental results related to the anti – vortex plate for  $D_i = 14.4$  cm,  $Q_i = 62.55$  lt/s and  $2b = 100$  cm

$D_i = 14.4$ cm		$2b = 100$ cm		$Q_i = 62.55$ lt / s		$S_c = 35.20$ cm		Initial Vortex Location: MZ	
$L_p = 40$ cm									
Plate Width $W_p$ (cm)	Full Air - Core	Full Air – Core Location	Air Bubble Entrance	Air Bubble Entrance Location	Vortex Tail	Vortex Tail Location	Result		
5	NO	-	NO	-	O – R	LZ	S		
10	NO	-	NO	-	NO	-	S		
15	NO	-	NO	-	NO	-	S		
20	NO	-	NO	-	NO	-	S		
25	NO	-	NO	-	NO	-	S		
$L_p = 50$ cm									
Plate Width $W_p$ (cm)	Full Air - Core	Full Air – Core Location	Air Bubble Entrance	Air Bubble Entrance Location	Vortex Tail	Vortex Tail Location	Result		
5	NO	-	NO	-	O	RZ	S		
10	NO	-	NO	-	NO	-	S		
15	NO	-	NO	-	O	LZ – RZ	S		
20	NO	-	NO	-	NO	-	S		
25	NO	-	NO	-	NO	-	S		

Table B.41 Experimental results related to the anti – vortex plate for  $D_i = 14.4$  cm,  $Q_i = 48.08$  lt/s and  $2b = 100$  cm

$D_i = 14.4$ cm		$2b = 100$ cm		$Q_i = 48.08$ lt / s		$S_c = 27.70$ cm		Initial Vortex Location: MZ	
$L_p = 40$ cm									
Plate Width $W_p$ (cm)	Full Air - Core	Full Air – Core Location	Air Bubble Entrance	Air Bubble Entrance Location	Vortex Tail	Vortex Tail Location	Result		
5	NO	-	NO	-	O – R	MZ	S		
10	NO	-	NO	-	NO	-	S		
15	NO	-	NO	-	NO	-	S		
20	NO	-	NO	-	NO	-	S		
25	NO	-	NO	-	NO	-	S		
$L_p = 50$ cm									
Plate Width $W_p$ (cm)	Full Air - Core	Full Air – Core Location	Air Bubble Entrance	Air Bubble Entrance Location	Vortex Tail	Vortex Tail Location	Result		
5	NO	-	NO	-	O	MZ	S		
10	NO	-	NO	-	O	MZ	S		
15	NO	-	NO	-	O	LZ – MZ	S		
20	NO	-	NO	-	O	LZ	S		
25	NO	-	NO	-	O	LZ	S		

Table B.42 Experimental results related to the anti – vortex plate for  $D_i = 14.4$  cm,  $Q_i = 30.32$  lt/s and  $2b = 100$  cm

$D_i = 14.4$ cm		$2b = 100$ cm		$Q_i = 30.32$ lt / s		$S_c = 18.00$ cm		Initial Vortex Location: MZ	
$L_p = 40$ cm									
Plate Width $W_p$ (cm)	Full Air - Core	Full Air – Core Location	Air Bubble Entrance	Air Bubble Entrance Location	Vortex Tail	Vortex Tail Location	Result		
5	NO	-	O – R	MZ	O	MZ	US		
10	O	MZ	O	MZ	O	MZ	US		
15	NBCTO	MZ	O – R	MZ	O	MZ	US		
20	NO	-	NO	-	NO	-	S		
25	NO	-	NO	-	NO	-	S		
$L_p = 50$ cm									
Plate Width $W_p$ (cm)	Full Air - Core	Full Air – Core Location	Air Bubble Entrance	Air Bubble Entrance Location	Vortex Tail	Vortex Tail Location	Result		
5	O – R	MZ	O – R	MZ	O	MZ	US		
10	O	MZ	O	MZ	O	MZ	US		
15	NBCTO	MZ	O	MZ	O	MZ	US		
20	NO	-	NO	-	NO	-	S		
25	NO	-	NO	-	NO	-	S		

Table B.43 Experimental results related to the anti – vortex plate for  $D_i = 14.4$  cm,  $Q_i = 62.55$  lt/s and  $2b = 120$  cm

$D_i = 14.4$ cm		$2b = 120$ cm		$Q_i = 62.55$ lt / s		$S_c = 34.90$ cm		Initial Vortex Location: MZ	
$L_p = 40$ cm									
Plate Width $W_p$ (cm)	Full Air – Core	Full Air – Core Location	Air Bubble Entrance	Air Bubble Entrance Location	Vortex Tail	Vortex Tail Location	Result		
5	NBCTO	LZ – MZ	O – R	LZ – MZ	O	LZ – MZ	US		
10	NO	-	NO	-	NO	-	S		
15	NO	-	NO	-	NO	-	S		
20	NO	-	NO	-	NO	-	S		
25	NO	-	NO	-	NO	-	S		
$L_p = 50$ cm									
Plate Width $W_p$ (cm)	Full Air – Core	Full Air – Core Location	Air Bubble Entrance	Air Bubble Entrance Location	Vortex Tail	Vortex Tail Location	Result		
5	NO	-	NO	-	O	RZ	S		
10	NO	-	NO	-	NO	-	S		
15	NO	-	NO	-	NO	-	S		
20	NO	-	NO	-	NO	-	S		
25	NO	-	NO	-	NO	-	S		

Table B.44 Experimental results related to the anti – vortex plate for  $D_i = 14.4$  cm,  $Q_i = 48.08$  lt/s and  $2b = 120$  cm

$D_i = 14.4$ cm		$2b = 120$ cm		$Q_i = 48.08$ lt / s		$S_c = 28.90$ cm		Initial Vortex Location: MZ	
$L_p = 40$ cm									
Plate Width $W_p$ (cm)	Full Air – Core	Full Air – Core Location	Air Bubble Entrance	Air Bubble Entrance Location	Vortex Tail	Vortex Tail Location	Result		
5	NO	-	NO	-	O – R	MZ	S		
10	NO	-	NO	-	NO	-	S		
15	NO	-	NO	-	NO	-	S		
20	NO	-	NO	-	NO	-	S		
25	NO	-	NO	-	NO	-	S		
$L_p = 50$ cm									
Plate Width $W_p$ (cm)	Full Air – Core	Full Air – Core Location	Air Bubble Entrance	Air Bubble Entrance Location	Vortex Tail	Vortex Tail Location	Result		
5	NO	-	NO	-	O – R	MZ	S		
10	NO	-	NO	-	O – R	MZ	S		
15	NO	-	NO	-	NO	-	S		
20	NO	-	NO	-	NO	-	S		
25	NO	-	NO	-	NO	-	S		

Table B.45 Experimental results related to the anti – vortex plate for  $D_i = 14.4$  cm,  $Q_i = 30.32$  lt/s and  $2b = 120$  cm

$D_i = 14.4$ cm		$2b = 120$ cm		$Q_i = 30.32$ lt / s		$S_c = 19.50$ cm		Initial Vortex Location: MZ	
$L_p = 40$ cm									
Plate Width $W_p$ (cm)	Full Air - Core	Full Air – Core Location	Air Bubble Entrance	Air Bubble Entrance Location	Vortex Tail	Vortex Tail Location	Result		
5	NO	-	O	MZ	O	MZ	US		
10	NO	-	O	MZ	O	MZ	US		
15	NBCTO	MZ	O	MZ	O	MZ	US		
20	NO	-	NO	-	O	LZ	S		
25	NO	-	NO	-	O	LZ	S		
$L_p = 50$ cm									
Plate Width $W_p$ (cm)	Full Air - Core	Full Air – Core Location	Air Bubble Entrance	Air Bubble Entrance Location	Vortex Tail	Vortex Tail Location	Result		
5	NO	-	O	MZ	O	MZ	US		
10	O	MZ	O	MZ	O	MZ	US		
15	NO	-	NBCTO	MZ	O	MZ	S		
20	NO	-	NO	-	NO	-	S		
25	NO	-	NO	-	O	RZ	S		

Table B.46 Experimental results related to the anti – vortex plate for  $D_i = 14.4$  cm,  $Q_i = 62.55$  lt/s and  $2b = 140$  cm

$D_i = 14.4$ cm		$2b = 140$ cm		$Q_i = 62.55$ lt / s		$S_c = 37.20$ cm		Initial Vortex Location: MZ	
$L_p = 40$ cm									
Plate Width $W_p$ (cm)	Full Air - Core	Full Air – Core Location	Air Bubble Entrance	Air Bubble Entrance Location	Vortex Tail	Vortex Tail Location	Result		
5	NO	-	O	LZ	O	LZ – MZ	US		
10	NBCTO	LZ	O	LZ	O	LZ	US		
15	O	LZ	O	LZ	O	LZ	US		
20	NBCTO	LZ	O – R	LZ	O – R	LZ	US		
25	NO	-	NO	-	NO	-	S		
$L_p = 50$ cm									
Plate Width $W_p$ (cm)	Full Air - Core	Full Air – Core Location	Air Bubble Entrance	Air Bubble Entrance Location	Vortex Tail	Vortex Tail Location	Result		
5	NO	-	O	LZ	O	LZ – MZ – RZ	US		
10	O – R	MZ	O – R	MZ	O – R	LZ – MZ – RZ	US		
15	NO	-	NO	-	O	MZ	S		
20	NO	-	NO	-	O	MZ – RZ	S		
25	NO	-	NO	-	NO	-	S		

Table B.47 Experimental results related to the anti – vortex plate for  $D_i = 14.4$  cm,  $Q_i = 48.08$  lt/s and  $2b = 140$  cm

$D_i = 14.4$ cm		$2b = 140$ cm		$Q_i = 48.08$ lt / s		$S_c = 25.50$ cm		Initial Vortex Location: MZ	
$L_p = 40$ cm									
Plate Width $W_p$ (cm)	Full Air - Core	Full Air – Core Location	Air Bubble Entrance	Air Bubble Entrance Location	Vortex Tail	Vortex Tail Location	Result		
5	NO	-	O	MZ	O	MZ	US		
10	NO	-	NBCTO	MZ	O	MZ	S		
15	NO	-	NO	-	NO	-	S		
20	NO	-	NO	-	NO	-	S		
25	NO	-	NO	-	NO	-	S		
$L_p = 50$ cm									
Plate Width $W_p$ (cm)	Full Air - Core	Full Air – Core Location	Air Bubble Entrance	Air Bubble Entrance Location	Vortex Tail	Vortex Tail Location	Result		
5	NO	-	NO	-	O	MZ	S		
10	NO	-	NO	-	O	MZ	S		
15	NO	-	NO	-	O	LZ – MZ	S		
20	NO	-	NO	-	NO	-	S		
25	NO	-	NO	-	NO	-	S		

Table B.48 Experimental results related to the anti – vortex plate for  $D_i = 10.0$  cm,  $Q_i = 51.65$  lt/s and  $2b = 40$  cm

$D_i = 10.0$ cm		$2b = 40$ cm		$Q_i = 51.65$ lt / s		$S_c = 66.50$ cm		Initial Vortex Location: RZ	
$L_p = 40$ cm									
Plate Width $W_p$ (cm)	Full Air - Core	Full Air – Core Location	Air Bubble Entrance	Air Bubble Entrance Location	Vortex Tail	Vortex Tail Location	Result		
5	NO	-	O	MZ	O	MZ	US		
10	NO	-	O	MZ	O	MZ	US		
15	O	MZ	O	MZ	O	MZ	US		
20	O	MZ	O	MZ	O	MZ	US		
25	O	MZ	O	MZ	O	MZ	US		
$L_p = 50$ cm									
Plate Width $W_p$ (cm)	Full Air - Core	Full Air – Core Location	Air Bubble Entrance	Air Bubble Entrance Location	Vortex Tail	Vortex Tail Location	Result		
5	-	-	-	-	-	-	-		
10	-	-	-	-	-	-	-		
15	-	-	-	-	-	-	-		
20	-	-	-	-	-	-	-		
25	-	-	-	-	-	-	-		

Table B.49 Experimental results related to the anti – vortex plate for  $D_i = 10.0$  cm,  $Q_i = 51.65$  lt/s and  $2b = 60$  cm

$D_i = 10.0$ cm		$2b = 60$ cm		$Q_i = 51.65$ lt / s		$S_c = 26.80$ cm		Initial Vortex Location: MZ	
$L_p = 40$ cm									
Plate Width $W_p$ (cm)	Full Air - Core	Full Air – Core Location	Air Bubble Entrance	Air Bubble Entrance Location	Vortex Tail	Vortex Tail Location	Result		
5	NO	-	NO	-	O	MZ	S		
10	NO	-	NO	-	O	MZ – RZ	S		
15	NO	-	NO	-	O	RZ	S		
20	NO	-	NO	-	O	LZ – RZ	S		
25	NO	-	NO	-	O	LZ – RZ	S		
$L_p = 50$ cm									
Plate Width $W_p$ (cm)	Full Air - Core	Full Air – Core Location	Air Bubble Entrance	Air Bubble Entrance Location	Vortex Tail	Vortex Tail Location	Result		
5	NO	-	NO	-	O	LZ – MZ – RZ	S		
10	NO	-	NO	-	O	LZ – MZ – RZ	S		
15	NO	-	NO	-	O	LZ – MZ – RZ	S		
20	NO	-	NO	-	O	LZ – MZ – RZ	S		
25	NO	-	NO	-	O	LZ – MZ – RZ	S		

Table B.50 Experimental results related to the anti – vortex plate for  $D_i = 10.0$  cm,  $Q_i = 38.79$  lt/s and  $2b = 60$  cm

$D_i = 10.0$ cm		$2b = 60$ cm		$Q_i = 38.79$ lt / s		$S_c = 24.40$ cm		Initial Vortex Location: MZ	
$L_p = 40$ cm									
Plate Width $W_p$ (cm)	Full Air - Core	Full Air – Core Location	Air Bubble Entrance	Air Bubble Entrance Location	Vortex Tail	Vortex Tail Location	Result		
5	NO	-	NO	-	O	MZ	S		
10	NO	-	NO	-	NO	-	S		
15	NO	-	NO	-	NO	-	S		
20	NO	-	NO	-	NO	-	S		
25	NO	-	NO	-	NO	-	S		
$L_p = 50$ cm									
Plate Width $W_p$ (cm)	Full Air - Core	Full Air – Core Location	Air Bubble Entrance	Air Bubble Entrance Location	Vortex Tail	Vortex Tail Location	Result		
5	NO	-	NO	-	NO	-	S		
10	NO	-	NO	-	O	MZ	S		
15	NO	-	NO	-	NO	-	S		
20	NO	-	NO	-	NO	-	S		
25	NO	-	NO	-	NO	-	S		

Table B.51 Experimental results related to the anti – vortex plate for  $D_i = 10.0$  cm,  $Q_i = 24.00$  lt/s and  $2b = 60$  cm

$D_i = 10.0$ cm		$2b = 60$ cm		$Q_i = 24.00$ lt / s		$S_c = 20.10$ cm		Initial Vortex Location: MZ	
$L_p = 40$ cm									
Plate Width $W_p$ (cm)	Full Air - Core	Full Air – Core Location	Air Bubble Entrance	Air Bubble Entrance Location	Vortex Tail	Vortex Tail Location	Result		
5	O	MZ	O	MZ	O	MZ	US		
10	O – DV	MZ	O – DV	MZ	O – DV	MZ	US		
15	NBCTO	MZ	O	MZ	O	MZ	US		
20	NO	-	NO	-	NO	-	S		
25	NO	-	NO	-	NO	-	S		
$L_p = 50$ cm									
Plate Width $W_p$ (cm)	Full Air - Core	Full Air – Core Location	Air Bubble Entrance	Air Bubble Entrance Location	Vortex Tail	Vortex Tail Location	Result		
5	NO	-	O – R	MZ	O	MZ	US		
10	O – DV	MZ	O – DV	MZ	O – DV	MZ	US		
15	NO	-	NO	-	NO	-	S		
20	NO	-	NO	-	NO	-	S		
25	NO	-	NO	-	NO	-	S		

Table B.52 Experimental results related to the anti – vortex plate for  $D_i = 10.0$  cm,  $Q_i = 51.65$  lt/s and  $2b = 80$  cm

$D_i = 10.0$ cm		$2b = 80$ cm		$Q_i = 51.65$ lt / s		$S_c = 32.30$ cm		Initial Vortex Location: MZ	
$L_p = 40$ cm									
Plate Width $W_p$ (cm)	Full Air - Core	Full Air – Core Location	Air Bubble Entrance	Air Bubble Entrance Location	Vortex Tail	Vortex Tail Location	Result		
5	NO	-	O	MZ	O	MZ	US		
10	NO	-	O – R	MZ	O	MZ	US		
15	NO	-	NO	-	NO	-	S		
20	NO	-	NO	-	NO	-	S		
25	NO	-	NO	-	NO	-	S		
$L_p = 50$ cm									
Plate Width $W_p$ (cm)	Full Air - Core	Full Air – Core Location	Air Bubble Entrance	Air Bubble Entrance Location	Vortex Tail	Vortex Tail Location	Result		
5	NO	-	O	MZ	O	MZ	US		
10	NO	-	O – R	MZ	O	MZ	US		
15	NO	-	NO	-	NO	-	S		
20	NO	-	NO	-	O – R	RZ	S		
25	NO	-	NO	-	O	RZ	S		

Table B.53 Experimental results related to the anti – vortex plate for  $D_i = 10.0$  cm,  $Q_i = 38.79$  lt/s and  $2b = 80$  cm

$D_i = 10.0$ cm		$2b = 80$ cm		$Q_i = 38.79$ lt / s		$S_c = 28.20$ cm		Initial Vortex Location: MZ	
$L_p = 40$ cm									
Plate Width $W_p$ (cm)	Full Air - Core	Full Air – Core Location	Air Bubble Entrance	Air Bubble Entrance Location	Vortex Tail	Vortex Tail Location	Result		
5	O	MZ	O	MZ	O	MZ	US		
10	O	MZ	O	MZ	O	MZ	US		
15	NO	-	NO	-	O	MZ	S		
20	NO	-	NO	-	NO	-	S		
25	NO	-	NO	-	NO	-	S		
$L_p = 50$ cm									
Plate Width $W_p$ (cm)	Full Air - Core	Full Air – Core Location	Air Bubble Entrance	Air Bubble Entrance Location	Vortex Tail	Vortex Tail Location	Result		
5	O	MZ	O	MZ	O	MZ	US		
10	O	MZ	O	MZ	O	MZ	US		
15	O	MZ	O	MZ	O	MZ	US		
20	NO	-	NO	-	NO	-	S		
25	NO	-	NO	-	NO	-	S		

Table B.54 Experimental results related to the anti – vortex plate for  $D_i = 10.0$  cm,  $Q_i = 24.00$  lt/s and  $2b = 80$  cm

$D_i = 10.0$ cm		$2b = 80$ cm		$Q_i = 24.00$ lt / s		$S_c = 21.70$ cm		Initial Vortex Location: MZ	
$L_p = 40$ cm									
Plate Width $W_p$ (cm)	Full Air - Core	Full Air – Core Location	Air Bubble Entrance	Air Bubble Entrance Location	Vortex Tail	Vortex Tail Location	Result		
5	O	MZ	O	MZ	O	MZ	US		
10	O	MZ	O	MZ	O	MZ	US		
15	NBCTO	MZ	O	MZ	O	MZ	US		
20	NO	-	NO	-	O	RZ	S		
25	NO	-	NO	-	O	RZ	S		
$L_p = 50$ cm									
Plate Width $W_p$ (cm)	Full Air - Core	Full Air – Core Location	Air Bubble Entrance	Air Bubble Entrance Location	Vortex Tail	Vortex Tail Location	Result		
5	NO	-	O – R	MZ	O	MZ	US		
10	O	MZ	O	MZ	O	MZ	US		
15	NBCTO	MZ	O	MZ	O	MZ	US		
20	NO	-	NBCTO	MZ – RZ	O	MZ – RZ	S		
25	NO	-	NO	-	NO	-	S		

Table B.55 Experimental results related to the anti – vortex plate for  $D_i = 10.0$  cm,  $Q_i = 51.65$  lt/s and  $2b = 100$  cm

$D_i = 10.0$ cm		$2b = 100$ cm		$Q_i = 51.65$ lt / s		$S_c = 38.70$ cm		Initial Vortex Location: MZ	
$L_p = 40$ cm									
Plate Width $W_p$ (cm)	Full Air - Core	Full Air – Core Location	Air Bubble Entrance	Air Bubble Entrance Location	Vortex Tail	Vortex Tail Location	Result		
5	NO	-	O – R	MZ	O	MZ	US		
10	NO	-	NO	-	O	MZ	S		
15	NO	-	NO	-	O	MZ	S		
20	NO	-	NO	-	NO	-	S		
25	NO	-	NO	-	NO	-	S		
$L_p = 50$ cm									
Plate Width $W_p$ (cm)	Full Air - Core	Full Air – Core Location	Air Bubble Entrance	Air Bubble Entrance Location	Vortex Tail	Vortex Tail Location	Result		
5	NO	-	O – R	MZ	O	MZ	US		
10	NO	-	NO	-	O	MZ	S		
15	NO	-	NO	-	NO	-	S		
20	NO	-	NO	-	NO	-	S		
25	NO	-	NO	-	NO	-	S		

Table B.56 Experimental results related to the anti – vortex plate for  $D_i = 10.0$  cm,  $Q_i = 38.79$  lt/s and  $2b = 100$  cm

$D_i = 10.0$ cm		$2b = 100$ cm		$Q_i = 38.79$ lt / s		$S_c = 30.90$ cm		Initial Vortex Location: MZ	
$L_p = 40$ cm									
Plate Width $W_p$ (cm)	Full Air - Core	Full Air – Core Location	Air Bubble Entrance	Air Bubble Entrance Location	Vortex Tail	Vortex Tail Location	Result		
5	NO	-	O	MZ	O	MZ	US		
10	NO	-	O	MZ	O	MZ	US		
15	NO	-	NO	-	NO	-	S		
20	NO	-	NO	-	NO	-	S		
25	NO	-	NO	-	NO	-	S		
$L_p = 50$ cm									
Plate Width $W_p$ (cm)	Full Air - Core	Full Air – Core Location	Air Bubble Entrance	Air Bubble Entrance Location	Vortex Tail	Vortex Tail Location	Result		
5	NO	-	O	MZ	O	MZ	US		
10	NO	-	O	MZ	O	MZ	US		
15	NO	-	NO	-	NO	-	S		
20	NO	-	NO	-	NO	-	S		
25	NO	-	NO	-	NO	-	S		

Table B.57 Experimental results related to the anti – vortex plate for  $D_i = 10.0$  cm,  $Q_i = 24.00$  lt/s and  $2b = 100$  cm

$D_i = 10.0$ cm		$2b = 100$ cm		$Q_i = 24.00$ lt / s		$S_c = 22.50$ cm		Initial Vortex Location: MZ	
$L_p = 40$ cm									
Plate Width $W_p$ (cm)	Full Air - Core	Full Air – Core Location	Air Bubble Entrance	Air Bubble Entrance Location	Vortex Tail	Vortex Tail Location	Result		
5	NO	-	O	MZ	O	MZ	US		
10	O	MZ	O	MZ	O	MZ	US		
15	NBCTO	MZ	O – R	MZ	O	LZ – MZ	US		
20	NO	-	NO	-	NO	-	S		
25	NO	-	NO	-	NO	-	S		
$L_p = 50$ cm									
Plate Width $W_p$ (cm)	Full Air - Core	Full Air – Core Location	Air Bubble Entrance	Air Bubble Entrance Location	Vortex Tail	Vortex Tail Location	Result		
5	NO	-	O	MZ	O	MZ	US		
10	O	MZ	O	MZ	O	MZ	US		
15	O – R	MZ	O	MZ	O	MZ	US		
20	NO	-	NBCTO	MZ	O	LZ – MZ	S		
25	NO	-	NO	-	O	LZ	S		

Table B.58 Experimental results related to the anti – vortex plate for  $D_i = 10.0$  cm,  $Q_i = 51.65$  lt/s and  $2b = 120$  cm

$D_i = 10.0$ cm		$2b = 120$ cm		$Q_i = 51.65$ lt / s		$S_c = 39.20$ cm		Initial Vortex Location: MZ	
$L_p = 40$ cm									
Plate Width $W_p$ (cm)	Full Air - Core	Full Air – Core Location	Air Bubble Entrance	Air Bubble Entrance Location	Vortex Tail	Vortex Tail Location	Result		
5	NO	-	O – R	MZ	O	MZ	US		
10	NO	-	NO	-	NO	-	S		
15	NO	-	NO	-	NO	-	S		
20	NO	-	NO	-	NO	-	S		
25	NO	-	NO	-	NO	-	S		
$L_p = 50$ cm									
Plate Width $W_p$ (cm)	Full Air - Core	Full Air – Core Location	Air Bubble Entrance	Air Bubble Entrance Location	Vortex Tail	Vortex Tail Location	Result		
5	NO	-	O – R	MZ	O	MZ	US		
10	NO	-	NO	-	NO	-	S		
15	NO	-	NO	-	NO	-	S		
20	NO	-	NO	-	NO	-	S		
25	NO	-	NO	-	NO	-	S		

Table B.59 Experimental results related to the anti – vortex plate for  $D_i = 10.0$  cm,  $Q_i = 38.79$  lt/s and  $2b = 120$  cm

$D_i = 10.0$ cm		$2b = 120$ cm		$Q_i = 38.79$ lt / s		$S_c = 26.50$ cm		Initial Vortex Location: MZ	
$L_p = 40$ cm									
Plate Width $W_p$ (cm)	Full Air - Core	Full Air – Core Location	Air Bubble Entrance	Air Bubble Entrance Location	Vortex Tail	Vortex Tail Location	Result		
5	NO	-	O	MZ	O	MZ	US		
10	NO	-	O	MZ	O	MZ	US		
15	NO	-	NO	-	NO	-	S		
20	NO	-	NO	-	NO	-	S		
25	NO	-	NO	-	NO	-	S		
$L_p = 50$ cm									
Plate Width $W_p$ (cm)	Full Air - Core	Full Air – Core Location	Air Bubble Entrance	Air Bubble Entrance Location	Vortex Tail	Vortex Tail Location	Result		
5	NO	-	O – R	MZ	O	MZ	US		
10	NO	-	O	MZ	O	MZ	US		
15	NO	-	NO	-	O	MZ	S		
20	NO	-	NO	-	NO	-	S		
25	NO	-	NO	-	NO	-	S		



Table B.61 Experimental results related to the anti – vortex plate for  $D_i = 5.0$  cm,  $Q_i = 14.69$  lt/s and  $2b = 60$  cm

$D_i = 5.0$ cm		$2b = 60$ cm		$Q_i = 14.69$ lt / s		$S_c = 21.80$ cm		Initial Vortex Location: MZ	
$L_p = 40$ cm									
Plate Width $W_p$ (cm)	Full Air - Core	Full Air – Core Location	Air Bubble Entrance	Air Bubble Entrance Location	Vortex Tail	Vortex Tail Location	Result		
5	NBCTO	MZ	O	MZ	O	MZ	US		
10	NBCTO	MZ	O	MZ	O	MZ	US		
15	NO	-	NO	-	O	MZ	S		
20	NO	-	NO	-	NO	-	S		
25	NO	-	NO	-	NO	-	S		
$L_p = 50$ cm									
Plate Width $W_p$ (cm)	Full Air - Core	Full Air – Core Location	Air Bubble Entrance	Air Bubble Entrance Location	Vortex Tail	Vortex Tail Location	Result		
5	NBCTO	MZ	O	MZ	O	MZ	US		
10	O	MZ	O	MZ	O	MZ	US		
15	NBCTO	MZ	O	MZ	O	MZ	US		
20	NO	-	NO	-	NO	-	S		
25	NO	-	NO	-	NO	-	S		

Table B.62 Experimental results related to the anti – vortex plate for  $D_i = 5.0$  cm,  $Q_i = 14.69$  lt/s and  $2b = 80$  cm

$D_i = 5.0$ cm		$2b = 80$ cm		$Q_i = 14.69$ lt / s		$S_c = 22.10$ cm		Initial Vortex Location: MZ	
$L_p = 40$ cm									
Plate Width $W_p$ (cm)	Full Air - Core	Full Air – Core Location	Air Bubble Entrance	Air Bubble Entrance Location	Vortex Tail	Vortex Tail Location	Result		
5	NO	-	O	MZ	O	MZ	US		
10	O	MZ	O	MZ	O	MZ	US		
15	NBCTO	MZ	NBCTO	MZ	O	MZ	S		
20	NO	-	NO	-	O	LZ	S		
25	NO	-	NO	-	O	LZ	S		
$L_p = 50$ cm									
Plate Width $W_p$ (cm)	Full Air - Core	Full Air – Core Location	Air Bubble Entrance	Air Bubble Entrance Location	Vortex Tail	Vortex Tail Location	Result		
5	NO	-	O	MZ	O	MZ	US		
10	O	MZ	O	MZ	O	MZ	US		
15	NBCTO	MZ	NBCTO	MZ	O	MZ	S		
20	NO	-	NO	-	O	MZ	S		
25	NO	-	NO	-	NO	-	S		